Rochester Institute of Technology

RIT Scholar Works

Theses

12-1-1983

Linearity of an Electrophotographic Image Reproduction System

Lloyd Clark

Follow this and additional works at: https://scholarworks.rit.edu/theses

Recommended Citation

Clark, Lloyd, "Linearity of an Electrophotographic Image Reproduction System" (1983). Thesis. Rochester Institute of Technology. Accessed from

This Thesis is brought to you for free and open access by RIT Scholar Works. It has been accepted for inclusion in Theses by an authorized administrator of RIT Scholar Works. For more information, please contact ritscholarworks@rit.edu.

LINEARITY OF AN
ELECTROPHOTOGRAPHIC IMAGE REPRODUCTION SYSTEM

by

Lloyd G. Clark

A.A.S. Rochester Institute of Technology

(1978)

A thesis submitted in partial fulfillment of the requirements for the degrees of Bachelor of Science and Master of Science in the School of Photographic Arts and Sciences in the College of Graphic Arts and Photography of the Rochester Institute of Technology.

December, 1983

Signature of the Author Lloyd G. Clark

Imaging and Photographic Science

Accepted by Ronald Francis

Coordinator, M.S. Degree Program

School of Photographic Arts and Sciences
Rochester Institute of Technology
Rochester, New York

CERTIFICATE OF APPROVAL

MASTER'S THESIS

The Master's Thesis of Lloyd G. Clark
has been examined and approved
by the thesis committee as satisfactory
for the thesis requirement for the
Master of Science degree

Burt A. Saunders

Burt A. Saunders, Thesis Advisor

John F. Carson

Professor John F. Carson

Edward L. Gilatti

Edward L. Gliatti

Donald I. Groening

Donald I. Groening

LINEARITY OF AN
ELECTROPHOTOGRAPHIC IMAGE REPRODUCTION SYSTEM

by

Lloyd G. Clark

Submitted to the Imaging and Photographic
Science Division in partial fulfillment
of the requirements for the Bachelor of Science
and Master of Science degrees at the
Rochester Institute of Technology

ABSTRACT

The linearity of image transfer is analyzed for a high resolution electrophotographic film and electrodeveloper combination. The extent of nonlinearities introduced upon transfer through the photoconduction and electrodevelopment stages is conceptualized in terms of inherent physical mechanisms. A spectral shift in narrow band exposing radiation is used to test significance of exponential absorption on linearity of photoconduction transfer. Variations in development electrode spacing and development time test for nonlinearity induced by temporal and spatial frequency dependent depletion of electrodeveloper particles.

As the electrophotographic film employed in the test exhibited low absorption coefficients in all spectral bands, exponential absorption of exposing radiation did not significantly alter linearity of edge image transfer. Results for edge and sinusoidal image transfer indicated nonlinear depletion effects shortly after development initiation. Increased development times reduced adjacency effects for edge distributions and lower harmonic distortions for sinusoidal image distributions. Initial adjacency effects and time rate of change toward linear edge responses are altered by electrode spacing for one electrodevelopment apparatus tested. Reasonable approximations to linear image transfer are obtained as electrodevelopment approaches completion, regardless of electrode spacing or electrodevelopment apparatus employed.

ACKNOWLEDGEMENTS

Successful completion of this thesis owes recognition to support from many sources. Valuable and timely assistance and advice was particularly appreciated from the following:

Mr. Burt A. Saunders, consultant to Coulter Systems Corporation, who kindly consented to act as thesis advisor for the proposal, and gave much of his time and encouragement in its supervision;

Dr. Johan F. Dirks, Senior Scientist at James River Graphics, who thoughtfully provided guidance on technical issues specific to the materials tested in this investigation.

Mr. Roger Summers, Technician for Air Force Wright Aeronautical Laboratory, Mission Avionics, who with skill and patience modified much of the experimental apparatus.

The support of the United States Air Force Wright Aeronautical Laboratory (Work Unit 20040903) is also acknowledged with appreciation.

NOTICE

The tests described herein were performed in-house in the Air Force Wright Aeronautical Laboratory, employing apparatus unique to this facility. Materials specifically identified with James River Graphics, were not originated for use in this investigation. The use of different apparatus and processing conditions than employed at James River Graphics may influence the resulting data. Therefore, the failure of any of the included materials to meet specifications reported elsewhere does not reflect on the quality of the manufacturer's products. No criticism of these materials is implied or intended, nor is any endorsement of the materials by the United States Air Force implied or intended.

TABLE OF CONTENTS

LIST OF TABLES

LIST OF FIGURES

INTRODUCTION

The applicability of the modulation transfer function (MTF) to electrophotographic imaging systems has been the subject of active research in recent years. The requirements of system linearity and shift-invariance for description of image transfer characteristics using this unique transfer function are well known. Imaging systems that produce nonlinear spatial interactions among input points cannot be fully characterized using the ratio of Fourier spectra for input and output signals. Although much research has been aimed at defining approximate linear transfer models for electrophotographic systems, specific process parameters for which these systems provide linear image transfer remain unresolved.

A class of electrophotographic film/electrodevelopment systems known as xerographic processes include a common set of materials and internal mechanisms. The film, consisting of adjacent photoconductive and conductive layers on a substrate, is initially charged to produce a potential across the photoconductive layer. Incident exposure releases charge carriers within the photoconductive layer which subsequently migrate to the surface, thereby reducing the initial potential by a measureable amount. The resulting surface charge distribution forms an electrostatic field distribution above the photoconductor surface. This inherent field distribution exhibits significant intensity only within the photoconductor and above gradients in the image charge distribution. A development electrode, placed at finite spacing above the photoconductor surface, alters the inherent field distribution in the intervening region. A uniform field is also superimposed on the image field distribution by applying a bias voltage to the development electrode. Electrodevelopment commences when a dispersion of electrodeveloper or toner particles is placed in the region between the film and electrode. The image electrostatic fields force the particles to the photoconductor surface, forming an optically dense image distribution. The electrodeveloper particles are then adhered to the photoconductor surface with the application of heat or chemical solvent, producing a permanent image distribution.

The xerographic system can be subdivided into three transfer operations in accordance with internal mechanisms. First, the transfer from image exposure to latent image charge density in the photoconductor layer is defined by a photoconduction mechanism. Second, the transfer from image charge density to optical density associated with deposited toner particles is defined by the electrodevelopment mechanism. The final transfer operation from latent optical density to a permanent density distribution is defined by a fixing mechanism.

Theoretical transfer functions have been derived in attempt to explain image transfer through the xerographic system. These transfer functions are derived using the linear relationship between latent image charge distributions and associated electrostatic field distributions above the photoconductor surface. Neugebauer[1], Schaffert[2], and Kao[3] established the mathematical procedures leading to a Fourier series representation of the image electrostatic field distribution. The mathematical derivations are sound, as the principle of superposition is applicable to electric fields in homogeneous dielectric media. However, Kao recognized that the linear relationship between image charge density and image electrostatic fields provided only an approximation for image transfer through the xerographic system. Linear transfer characteristics associated with photoconduction and electrodevelopment mechanisms may be accounted for in the electrostatic field transfer model.[4,5] When these mechanisms introduce nonlinear spatial interactions, the approximated transfer functions do not adequately characterize image transfer through the xerographic system.

Rushing[6] suggested that a parallel component of electric field forms in the photoconductor layer during the photoconduction process. This component of electric field should drive induced charge carriers from their exposure origins toward image regions of lower exposure, while the charge carriers migrate to the photoconductor surface. In accordance with the distribution of charge carriers with depth in the photoconductor layer, the resulting image charge distribution may be linearly or nonlinearly related to the incident exposure distribution. When the actinic radiation is nonlinearly absorbed with depth in the photoconductor layer, the sum of charge carrier trajectories dictates a nonlinear relationship between incident exposure and resulting charge density distributions.

In the electrodevelopment process, complex interactions between the latent image electric fields and charged electrodeveloper species suggest a localized depletion effect. At the initiation of electrodevelopment, the normal component of image electrostatic fields dictates the rate of particle and ion deposition to the film surface. Except for the case where the electrode spacing equals the photoconductor thickness, the Fourier transformed field distribution dictates initial deposition rates which vary as a function of image spatial frequency. During the course of electrodevelopment, the frequency components which develop at a faster rate should deplete the supply of electrodeveloper in a localized area above the film surface. The frequency components which develop at a slower rate should exhibit a temporary or permanent loss in resulting optical density. When the image electrostatic field distribution exhibits significant intensity variations as a function of spatial frequency content, the localized depletion of electrodeveloper particles should produce a nonlinear transfer from image charge to optical density distributions.

Neugebauer[7] maintained that the Fourier series representation for the image electrostatic field distribution characterizes the frequency transfer function from incident to effective exposure. The only requirement cited was for the incident exposure modulation, which could not exceed the dynamic range for the macroscopic Hurter and Driffield curve. Questioning the applicability of the electrostatic field spectrum as the system transfer function, Witte and Szczepanik[8] obtained empirical transfer functions for a relatively low resolution xerographic system.

The resulting transfer functions were claimed to be reasonable approximations to Kao's electrostatic field spectrum. However, the approximate concordance between their results and the linear field spectrum model may have been fostered by the low resolution materials and processing techniques employed.

The interaction of photogenerated charge carriers with lateral field components produces only small amounts of lateral image spread. For a 10 micron photoconductor thickness, photoconduction effects (excluding exposure spread) produce less than 3 micron spread in the surface charge distribution.[9] Nonlinear photoconduction should produce deviations from an otherwise linear spread within this 3 micron range. As detection of these nonlinearities is currently limited to the final image density distribution, the electrodeveloper dispersion should be limited to particles less than one micron in diameter. The large toner particles (>10 microns) employed in Witte and Szczepaniks' experiment may well have masked a nonlinear photoconduction mechanism. In terms of electrodevelopment, the concentrated toner dispersions and magnetic brush toning methods employed probably minimized any localized depletion effects. Furthermore, larger toner particles exhibit proportionately greater charge per particle, which should have increased their mobility relative to ions in the dispersion. This would explain the lack of permanent depletion associated with ion deposition to the image charge.

In the present investigation, a high resolution electrophotographic film and electrodeveloper combination was employed to test for the significance of photoconduction and electrodevelopment nonlinearities.

This system included a film photoconductor layer similar in thickness to that employed for Rushing's calculations revealing nonlinear image charge distributions. The electrodeveloper included a relatively low concentration of submicron diameter toner particles dispersed in a liquid solvent. The low concentration and small size (low mobility) of toner particles would allow the effects of nonlinear depletion to be observed in the resulting imagery.

It was not feasible to measure the individual photoconduction and electrodevelopment mechanisms at the microscopic level. However, these mechanisms were related to parameters which could be controlled on apparatus designed for routine image reproduction. As the linearity of the photoconduction mechanism depends on the absorption distribution in the film photoconductor layer, a film exhibiting different absorption coefficients as a function of wavelength was employed to test this mechanism. The associated experimental parameter was a spectral shift in exposing wavelength. The electrodevelopment depletion mechanism should be related to the relative rates of particle and ion deposition as a function of image frequency components. The development electrode spacing was employed as an experimental parameter, altering the relative field intensity as a function of spatial frequency in the image distribution. As the frequency dependent rates of deposition change during the electrodevelopment process, the nonlinear depletion mechanism was also tested as a function of development time.

Ingelstam[10] discussed the fundamental difference between edge effects produced on silver halide films and edge effects produced on xerographic films. The chemical adjacency effects observed when silver halide films are processed in certain developer formulations, are represented as nonlinear interactions among the input image components. This phenomenon was contrasted against the inherent edge effect associated with the distribution of electrostatic fields for xerographic film systems. A development electrode placed above a xerographic film, at a distance greater than the photoconductor thickness, dictates enhanced field intensity for a certain range of image spatial frequencies. In the spatial domain, an edge charge distribution therefore exhibits enhanced normal field intensity to either side of the edge center. As the charge density and field distributions are related by a linear operator, this enhanced field distribution is symmetrical with respect to the edge center. This inherent edge effect should be linearly related to an incident edge exposure, unless the photoconduction and electrodevelopment mechanisms introduce significant adjacency effects.

The development adjacency effects observed for silver halide films are considered advantageous for detecting image detail, especially on low contrast aerial imagery. The disadvantage of processing silver halide films for enhanced adjacency effects is the nonlinearity of the development mechanism, which prohibits characterization of image transfer with a unique transfer function. As the edge effect associated with the xerographic image field distribution is a linear phenomenon, exposure and processing parameters may be adjusted to retain a linear edge enhancement.

In this investigation, a subset of photoconduction and electrodevelopment mechanisms were studied with the intent to determine subsystem parameters controlling linearity of image transfer. Exposure and development parameters were tested at levels suitable for a continuous tone, continuous processing xerographic reproduction system. The parameter levels were chosen in attempt to note a transition range between linear and nonlinear image transfer for a high resolution xerographic system. An underlying goal was to determine combinations of exposure and electrodevelopment parameter levels that provide both enhancement of image detail and linearity of image transfer through the system.

I. THEORETICAL BASIS

A. System Identification

To establish a baseline for the assessment of transfer characteristics for an electrophotographic film system, some general system transfer properties are reviewed. Systems are catagorized according to linearity, presence of dynamic elements (memory), and temporal or shifting dependence. In accordance with these catagories, a system is said to be either linear or nonlinear, either having or void of dynamic elements, and either shift invariant or shift dependent. Thus, three independent properties are defined for all systems. Testing a system to determine one of these properties cannot be adequately accomplished without a priori knowledge or assumptions for the other two properties. Specifically, imaging systems are said to have dynamic elements. In testing for linearity of an electrophotographic imaging system, the assumption of shift invariance was established in this study.

An explicit relationship between input and output functions for a system is described using a mathematical operator. Linear systems are said to preserve the principle of superposition, i.e. the sums and proportionality of input functions are maintained upon transfer through the system. Nonlinear systems violate this superposition principle, as they introduce higher order interactions among the input functions upon transfer through the system. A general representation for the system operator is a polynomial series of transfer functions or functionals, which can be applied to both linear and nonlinear systems.[11]

When the input and output signals are represented as weighted series of delta functions in the spatial domain, an appropriate system operator is the Volterra series:[12]

$$y(x)=\int_{-\infty}^{\infty} h_1(x)u(x-\alpha_1)d\alpha_1+\int_{-\infty}^{\infty}\int_{-\infty}^{\infty} h_2(\alpha_1,\alpha_2)u(x-\alpha_1)u(x-\alpha_2)d\alpha_1\alpha_2$$

$$+\int_{-\infty}^{\infty}\int_{-\infty}^{\infty}\int_{-\infty}^{\infty} h_3(\alpha_1,\alpha_2,\alpha_3)u(x-\alpha_1)u(x-\alpha_2)u(x-\alpha_3)d\alpha_1 d\alpha_2 d\alpha_3$$

$$+ \text{ higher order terms.}$$

This functional series includes linear and higher order impulse response functions (kernals) that describe the respective linear and interaction terms among input delta functions. Only the first term, recognized as the convolution integral, is required to characterize linear system transfer. By definition, the first order impulse response, $h_1(x)$, dictates a fixed relationship between each input value and multiple values in the output distribution.

Representing the input and output spatial distributions as delta functions at discrete intervals allows the Volterra series to be approximated by the multidimensional Taylor series:[13]

$$y(x)=\sum_{i=1}^{n} a_i u_i+\sum_{i=1}^{n}\sum_{j=1}^{n} a_{ij}u_i u_j+\sum_{i=1}^{n}\sum_{j=1}^{n}\sum_{k=1}^{n} a_{ijk}u_i u_j u_k+\ldots$$

The first term represents linear relationships between each input delta function and neighboring delta functions at successive increments to either side of the input function. The higher order terms represent spatial interactions between each input delta function and all other delta functions of the input distribution.

Fourier transformation of the input and output distributions produces series of orthogonal exponential terms for each distribution. For a linear system, a unique system operator is characterized using the ratio of output to input Fourier spectra. The discrete notation for the complex frequency transfer function is written:

$$H(nw) = \sum_{n=-\infty}^{\infty} b_n e^{-inwx} \Big/ \sum_{n=-\infty}^{\infty} a_n e^{-inwx} = \sum_{n=-\infty}^{\infty} c_n e^{-inwx} \ ;$$

where a_n and b_n represent coefficients of the input and output frequency components, and c_n represents the ratio of output to input coefficients for respective terms in each series.

For nonlinear systems a polynomial series can be used to determine linear and higher order interactions for input frequency components transferred through the system. Examples for second and higher order series operating on a single frequency input are given in the literature[14]. For the single frequency sinusoidal input, a nonlinear operator series distributes the energy or amplitude of the input between the input and harmonic terms at integer multiples of the input frequency. Clay[15] has shown that the order of each operator series term corresponds to the order of the harmonic terms in the output frequency summation. Higher order transfer series operating on multiple input frequency terms produce interaction terms as well as harmonics of the input frequency components. Examples for polynomial series operating on multiple input frequency components have been illustrated by Swing.[16]

B. Experimental Determination of Linearity

Simonds[17] illustrated the use of a multidimensional Taylor series to describe nonlinear adjacency effects produced upon chemical development of silver halide film. The spatial interactions between input exposure points at discrete intervals were accurately represented by higher order terms in a discrete approximation to the Volterra series (functional operator). In characterizing the functional operator for a nonlinear development process applied to an edge input distribution, an important observation was noted. Assuming an input edge distribution symmetrical with respect to the edge center, a functional operator including higher order interaction terms was required to characterize transfer to an asymmetrical output distribution. This correlation between nonlinear spatial interactions and asymmetry in the response distribution can be employed as a system identification tool.

In attempting to determine linearity or nonlinearity of a system based on the symmetry of edge response functions, certain constraints must be observed. First, the input edge distribution must be symmetrical with respect to the edge center such that a clear distinction between output symmetry or asymmetry can be associated with linearity or nonlinearity, respectively. Second, the system subject to evaluation must be free of phase distortions. Although phase distortion in the system transfer effects an asymmetrical response to an edge input distribution, it is fully characterized using the complex notation for a linear system operator.[18]

Assessment of input distribution symmetry can be accomplished by visual examination of a measured edge exposure distribution. In this investigation, no attempts were made to compute the operator function or functional. The shape of the output distribution, including the degree of asymmetry, was employed to assess transfer characteristics as a function of experimental parameter variations.

For analysis of the transfer operator in the frequency domain, sinusoidal input exposure distributions were employed. Although a variety of methods are available for generating approximately sinusoidal exposure distributions, pure sinusoidal exposure inputs remain a mathematical idealization. Approximately sinusoidal target distributions include finite amplitude at harmonics of the fundamental frequency. Upon nonlinear transformation of the approximate sinusoidal image, input energy in both fundamental and harmonic terms are redistributed. As the input harmonic terms occur at integer multiples of the fundamental frequency, energy redistributed to interaction frequency terms will be confounded with energy redistributed between fundamental and harmonic terms. It is therefore impracticable to accurately determine the coefficients of a nonlinear operator series, given a harmonically distorted input sinusoid and the resulting output frequency spectrum.

Although it is impracticable to extract the nonlinear operator for the case described, this does not exclude a relative measure of nonlinearity for an input sinusoid exhibiting little harmonic distortion. When the input harmonics are small (<10% of fundamental amplitude) significant increases in harmonic distortion content suggest nonlinear image transfer. The specification for small input harmonic amplitudes argues for an increase in harmonic distortion caused by nonlinear transfer, as opposed to amplitude distortion noted in linear system transfer. Assuming amplitude distortion to be negligible, a measure of enhancement for harmonic amplitudes may be used to denote relative amounts of nonlinearity for various system transfer conditions.

A harmonic distortion factor can be computed from the ratio of harmonic distortions for output vs. input frequency spectra. The harmonic distortion for each spectrum is computed using the modulus of harmonic frequency terms normalized to the fundamental frequency response:

$$HDF_i = ((C_i{}^*C_i)/(C_f{}^*C_f))^{1/2}$$

where C_i denotes the coefficient of the i^{th} harmonic, and C_f denotes the coefficient of the fundamental in the (discrete) signal spectrum:

$$g(kT) = 1/N \sum_{n=0}^{N-1} C_n(n/NT)\ \exp(i2\pi nk/N) \quad ;\ k=0,1,\ldots N-1.$$

The harmonic distortion factor may be computed for all harmonics within the system passband.

C. Effects of Electrophotographic Mechanisms on Image Transfer

The linearity or nonlinearity of image transfer through the photoconduction and electrodevelopment stages were assessed in terms of associated physical mechanisms. No attempts were made to determine theoretical transfer operators and resulting image distributions for various input distributions. Potentially linear and nonlinear transfer operations were conceptually identified in relation to specified mechanisms inherent at each stage. For assessment of linearity, cited mechanisms were assumed to provide shift-invariant image transfer unless otherwise indicated.

1. Exposure/Photoconduction Mechanisms

During exposure, incident radiation is scattered within the photoconductive layer of the film. As the photoconductor medium is isotropic, the radiation scattering can be modeled using a linear spread function. The difference in refractive indices of adjacent photoconductor and conductor layers of the film produces a finite amount of internal reflection at this interface. Depending on the absorption coefficents and thickness of the photoconductor layer, multiple internal reflections may occur. These internal reflections should increase the spread of the exposure impulse function in a linear manner.

Studies of photoconduction mechanisms conducted by Rushing, Hoesterey, and Fritz[19] suggest that linearity of image transfer depends on absorption of radiation in the photoconduction layer. Radiation absorbed in the photoconductor layer releases charge carriers which subsequently migrate along internal field lines. For large area uniform exposure, photogenerated charge carriers migrate in the direction normal to the film surface. On the other hand, sharp gradients in the exposure distribution produce a component of electric field parallel to the film surface. The degree to which charge carrier migrations are deflected from the normal, is determined by the origination distances of charge carrier origins from the photocondutor surface. When the distribution of carrier origins is not linear with distance from the photoconductor surface, the resulting image charge distribution at the surface should be nonlinearly related to the input distribution.

Rushing[20] computed charge carrier trajectories for line and edge exposure distributions, employing a simulation for the influence of parallel field components on the migrating carriers. Radiation was assumed incident at the free surface of the photoconductor layer. Distributions of charge carrier origin vs. photoconductor depth investigated included: (1) all carriers generated at the photoconductor/conductor interface, (2) carriers generated in linear proportion to distance from the photoconductor/air interface, and (3) carriers generated in proportion to exponential absorption of radiation with distance from the photoconductor surface. For each assumed charge carrier distribution, the surface charge distributions were computed for an ideal edge input exposure. The resulting charge distributions are included in Figure 1.

For the purpose of theoretical discussion, Rushing's[21] simulation is employed as a baseline model, emphasizing the case for exponential distribution of charge carriers within the photoconductor. First, the exponential distribution coincides with expected exponential absorption of radiation with depth in the photoconductor. Second, the exponential operator can be used to approximate two of the absorption distributions studied by Rushing. As the absorption coefficient (α) decreases, the exponential function approaches a linear response for a finite photoconductor

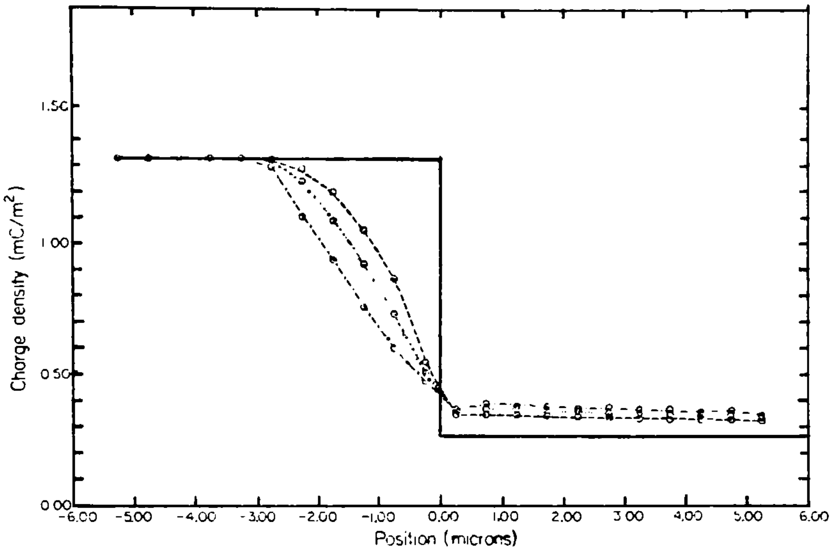

Figure 1. Electrostatic Latent Image Charge Profiles Simulated for a Single Edge Exposure and Varying Film Absorption Distributions. Case 1 (–·–·–·) curve results when all charge carriers are generated at the film's conductor layer; case 2 (············) curve results when carriers are generated uniformly with depth (ℓ) in the film's photoconductor layer; case 3 (------) curve results when carrier generation is attentuated by exp $(-\alpha\ (\ell - z))$ where $\alpha = 2000\ \text{cm}^{-1}$ and z is measured from the conductor layer. The solid curve represents the ideal charge profile that would result if all carriers moved through the photoconductor layer without being laterally deflected. (From Rushing, et al .[6])

thickness. Although the exponential operator is nonlinear, the degree of nonlinearity in the calculated absorption distribution is directly related to the absorption coefficient, assuming a constant photoconductor thickness.

Although Rushing's[22] computations of charge distributions as a function of absorption distribution are complex, the results indicate a relationship between the magnitude of the absorption coefficient and the degree of asymmetry in the charge distribution. Referring to the charge distributions of Figure 1, an absorption coefficient of zero (case 2) produces a charge density distribution that is approximately linear with distance across the edge. On the other hand, a large absorption coefficient (case 3: $\alpha = 2000\ \mathrm{cm}^{-1}$) produces a charge density distribution that is nonlinear, eg. asymmetrical with respect to the resulting edge center.

Establishing mathematical relationships between the charge distribution and the absorption coefficient was beyond the scope of this investigation. Assessing the change in charge distribution as a function of the absorption coefficient was simplified by noting the degree of asymmetry in the distributions for the above cases. Clearly, as the absorption coefficient increases, Rushing's simulated charge distributions indicate increasingly asymmetrical edge responses.

In addition to the increased asymmetry noted with increasing absorption coefficient, the edge center in the resulting charge distribution is displaced from the edge center in the incident exposure distribution. The parallel field component shifts all charge carriers in accordance with a constant vector (direction and intensity). In the frequency domain, this phenomenon may be interpreted as a phase shift as opposed to phase distortion. The asymmetry noted in the edge response is maintained to be the result of a nonlinear exponential operator, and a shift in edge center the result of a linear phase shift.

The photoconductive layers of xerographic films are generally dye sensitized to provide increased absorption coefficients for selected spectral bands of exposing radiation. When the absorption coefficients for the dye sensitized regions are large, the effective nonlinearity for photoconduction may be reduced by restricting exposure radiation to spectral regions of lower absorption. In short, films with sufficient disparity between absorption coefficients for dye sensitized vs. non dye sensitized spectral bands may provide a control mechanism for linearity of image transfer.

2. Calculations for Photoconduction Mechanism

The film employed in this investigation is Transparent Electrophotographic (TEP) XP4-008; an experimental film manufactured by James River Graphics. The construction of this film consists of a polyester substrate (4 mils), a transparent ionic conductive layer (0.01 um), and a photoconductive layer (8±0.5 um). The photoconductive layer consists of a polymeric matrix containing a derivative of phenylene diamine as the organic photoconductor, combined with a dye sensitization system.[23]

Spectrophotometer traces were employed to determine the transmittance vs. wavelength distribution for the TEP XP4-008 film. The transmittance vs. wavelength responses for the entire film structure, and for the film with the photoconductive layer removed, are shown in Figure 2. The absorption coefficients for the photoconductive layer were computed at selected wavelengths using:

$$\alpha(\lambda)=(\log_e \Delta T(\lambda))/d_1$$

where: d_1 = photoconductive (pc) layer thickness, and

$\Delta T(\lambda)$= (transmittance with pc layer) - (transmittance without pc layer)

In order to characterize the change in absorption distribution as a function of wavelength, two wavelengths were selected within the useful spectral sensitivity range of the TEP film. Using a photoconductor thickness of 8 microns, calculated absorption coefficients at 440 and 500 nanometers were: $\alpha(440) = 250\ \text{cm}^{-1}$ and $\alpha(500) = 410\ \text{cm}^{-1}$. The amounts of radiation absorbed at one micron increments of photoconductor thickness are shown in Figure 3. Included in this figure is the absorption distribution for Rushing's[24] (case 3) computation, with $\alpha = 2000\ \text{cm}^{-1}$ and $d_1 = 10$ microns.

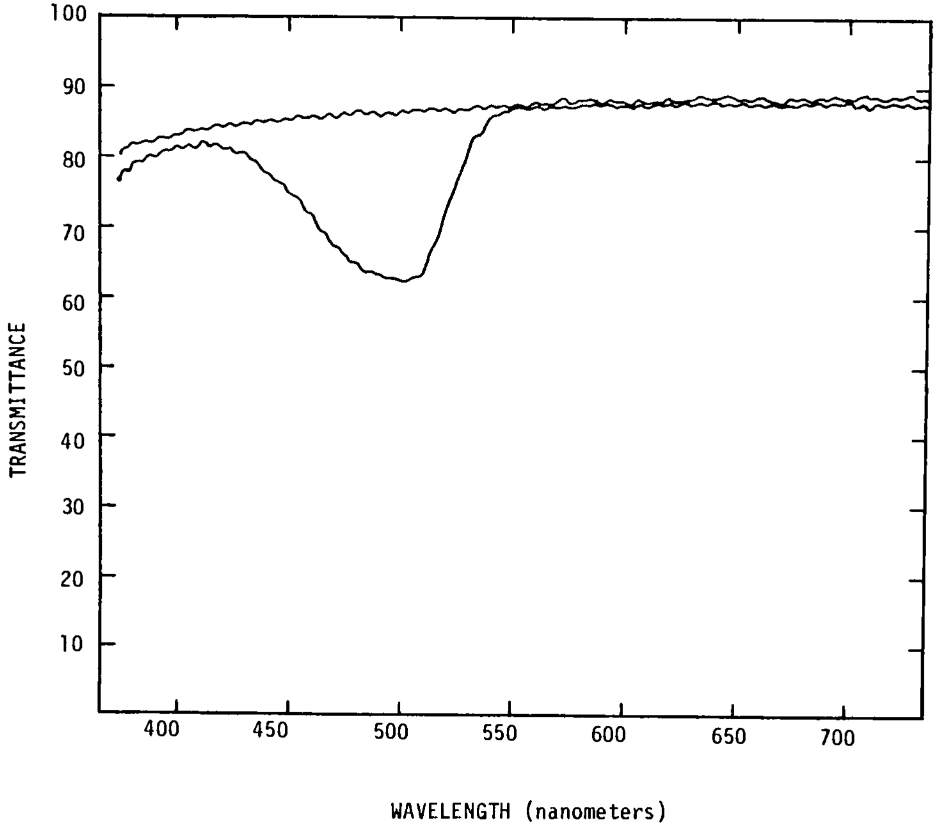

Figure 2. Spectrophotometer Traces for TEP XP4-008 Film. Upper curve represents transmittance spectrum for substrate & conductor layers, lower curve represents entire film.

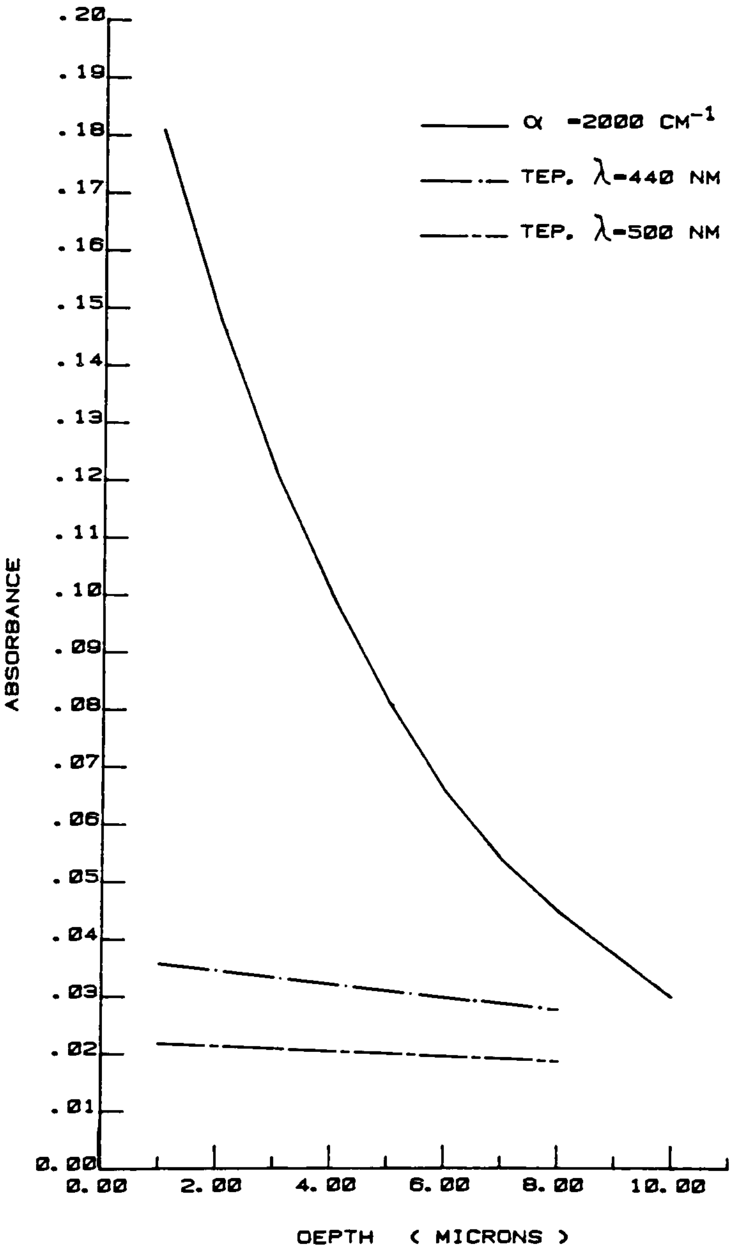

Figure 3. Radiation Absorption with Depth in the Photoconductor. Discrete absorption for one micron depth increments as measured from the free surface of the photoconductor.

By comparison with the film absorption coefficient employed in Rushing's calculations, TEP XP4-008 exhibits little absorption at any wavelength. Furthermore, there is little disparity in absorption coefficients for radiation at different wavelengths having spectral sensitivity in excess of 100 ergs/cm^2. Based on these absorption distributions and Rushing's simulation for charge carrier trajectories in the photoconductor layer, photoconduction induced nonlinearity should be minimal for TEP XP4-008 film.

3. Electrodevelopment Mechanisms

To produce an optically dense image from the latent image surface charge, liquid electrodeveloper (toner) is brought into contact with the film surface. Characteristics of the resulting image are only indirectly related to the surface charge on the film. The output image distribution is governed by complex interactions between the image electric field distribution and charged toner particles in the electrodeveloper. Electrostatic field intensity above the surface is a function of potential gradient in the image charge distribution. The normal component of the electric field distribution has been accepted as the predominant force governing toner deposition to the film surface. A development electrode spaced at a finite distance above the film surface, alters the distribution of these fields and associated toner deposition. A two-dimensional, two-layer model[25] is included in Figure 4 to illustrate the geometry and parameters necessary for electrostatic field calculations.

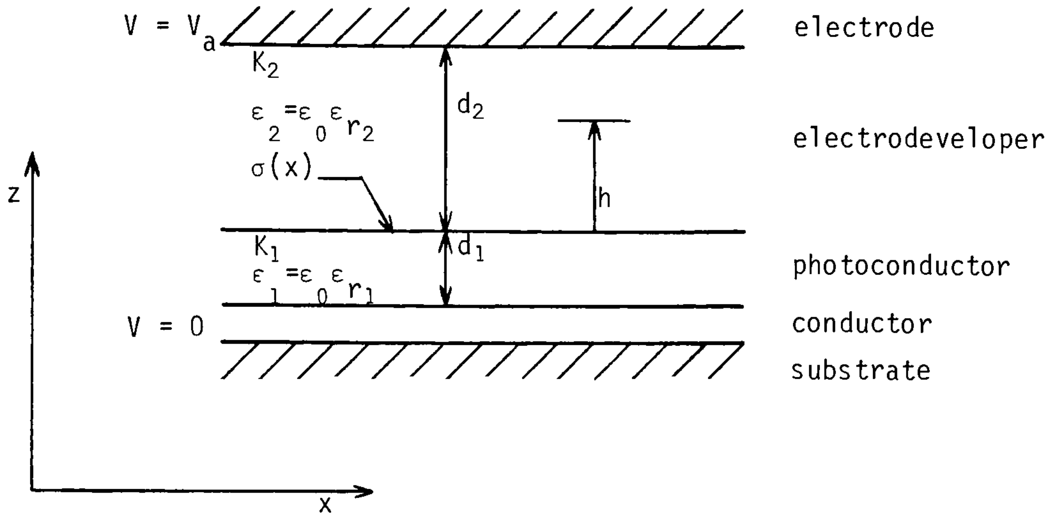

Figure 4. Film and Development Electrode Geometry, Parameters for Electrostatic Field Calculations.

$\sigma(x)$: One dimensional charge distribution at photoconductor surface.

d_1, d_2: Photoconductor thickness, development electrode spacing.

ε_1, ε_2: Relative permittivities of photoconductor, electrodeveloper.

K_1, K_2: Dielectric constants of photoconductor, electrodeveloper.

h: Height above photoconductor at which field distribution is calculated.

V_a: Voltage applied to development electrode.

Kao[26] derived formulas for the normal component of electrostatic field intensity as a function of spatial frequency in the charge density distribution. The electrostatic field spectrum was derived by Fourier transformation of Laplace's equation for electrostatic potential, applying the appropriate boundary conditions at dielectric interfaces. The equivalence between this field spectrum derived using a delta line charge distribution, and Schaffert's[27] derivation based on sinusoidal charge distributions, illustrates the linear relationship between field and surface charge distributions.

Substituting the model parameters of Figure 4 into Kao's expression, the (normal component) electrostatic field spectrum may be written:

$$E_{2\delta}(k,z,h) = \frac{-4\pi^2 (V_a/\varepsilon_2)}{(d_1/\varepsilon_1 + d_2/\varepsilon_2)} + \frac{\exp(2k(d_2-h))\tanh(kd_1)}{(1+\exp(-2kd_2))(\varepsilon_2\tanh(kd_1)+\varepsilon_1\tanh(kd_2))}$$

where: $k=2\pi f$ (cycles/mm).

The second term of the sum characterizes the inherent electrostatic field formation as a function of photoconductor thickness, electrode spacing, and relative permittivities for the photoconductor and electrodeveloper. The first term represents constant field intensity associated with applied electrode voltage. This first term is independent of spatial frequency, effectively adding a constant field intensity to the inherent field intensity spectrum.

For practical electrodevelopment conditions where $d_2 > d_1$, an intensity peak occurs at a certain spatial frequency. This frequency value is a function of photoconductor thickness, and throughout this paper it separates the field spectrum into ranges denoted "lower" and "higher". Following discussions refer to the case where the electrode spacing exceeds the photoconductor thickness ($d_2 > d_1$).

Using the field spectrum as a first order approximation to the electrodevelopment transfer function, the amount of amplitude distortion is cited as a function of the model parameters. An increase in the ratio of electrode spacing to photoconductor thickness (d_2/d_1) produces a sharp drop in lower frequency intensity, as illustrated in Figure 5. The relative enhancement of peak and higher frequency components in the image field distribution, correlates to the edge effect observed in the spatial domain. Although the relative amplitude of the peak response increases with the ratio d_2/d_1, the frequency at which the peak intensity occurs remains constant for a given height above the photoconductor, h.

The relationship between the field intensity spectrum and height at which the distribution is calculated was also explained by Kao's expression. As this distance increases ($h \to d_2$), the decrease in intensity at higher spatial frequencies is much greater than at lower spatial frequencies (see Figure 6). Consequently with increasing height (h), the peak frequency response effectively shifts toward zero spatial frequency. In accordance with this height dependence, Schaffert[28] noted that lower frequency charge components should draw upon particles at further distances above the photoconductor surface than higher frequency components.

The sphere of influence for electrostatic fields associated with varying frequency components of charge was cited in estimating frequency dependent particle deposition rates.[29] Particle deposition to lower frequency components of charge is characterized by field intensities integrated as a function of height above the film surface. On the other hand, particle deposition to higher frequency components is adequately represented by direct field intensity in close proximity to the film surface. Although a greater number of particles in the bulk electrodeveloper region gain mobility toward low frequency components of charge, the greater field intensities near the film surface dictate initially greater particle deposition to the higher frequency components. The contrasting field penetration phenomena and associated difference in deposition rates, introduces time dependence in the toned image frequency response.

Depending on the concentration of toner particles in the electrodeveloper, the differing rates of deposition for low vs. high frequency components may introduce a temporary depletion effect. Rapid deposition of particles to high frequency components of image charge should induce localized depletion of particles in the vicinity of these components. Subsequent deposition to low frequency components of charge would therefore be limited in regions adjacent to high frequency components.

Referring to the spatial domain field distribution, the localized depletion of toner particles above nonuniform charge gradients should temporarily reduce deposition to neighboring image areas. This nonlinear adjacency effect suggests the need for higher order convolution kernals to characterize short time development response. The field frequency spectrum equivalent for varying charge gradients consists of multiple frequency components. In this domain, nonlinear frequency transfer would require terms describing interactions among spectral components of the complex input charge distribution. Emphasis should be placed on the temporary nature of this nonlinear depletion effect, as it is hypothesized in accordance with initial static electric field distributions.

4. Calculations for Electrostatic Fields

The normal component of the electrostatic field distribution was calculated for TEP XP4-008 film with an electrode positioned at various spacings above the film surface. To simulate conditions at development initiation (t=0), Kao's[30] equation was employed. Relative permittivities for the film and T3 electrodeveloper (James River Graphics) were 3.0 and 2.0, respectively.[31] Assuming the manufacturer specified photoconductor thickness (8 um) and zero applied electrode voltage (V_a=0), the Fourier transformed field spectra calculated near the photoconductor surface (h=1 um) are illustrated in Figure 5. Variations in development electrode spacing (d_2) greater than 0.100 mm produced no significant variations in field spectra. Electrode spacings for continuous film electrodevelopment typically exceed 0.100 mm, for which the inherent spectral response effectively remains constant.

Figure 6 shows variations in inherent field spectra as a function of height (h) above the film surface, for a constant electrode spacing: $d_2 = 0.200$ mm. The spatial domain representation of fields for sinusoidal charge distributions are sinusoidal, with amplitudes determined at respective spatial frequencies (Figure 6). The corresponding field intensity for ideal edge (or step) charge distributions are shown as a function of height (h) in Figure 7. These were obtained by integrating the inverse Fourier transformed field spectra at each height. For $d_2/d_1 > 10$, the inherent electrostatic fields dictate no toner deposition for uniform image charge areas ($k \rightarrow 0$).

The proportionality between the normal field component of electrostatic field and developed image density cannot be maintained without an applied electrode voltage.[32] For discussion purposes, further analyses of electrostatic fields are necessarily restricted to the case of negative working sensitometry employed in this study. For this case, the negative field intensity noted in the edge distributions (Figure 7) would repel negatively charged toner particles, without the addition of the constant field associated with negative applied electrode voltage. The constant field contribution places the inherent edge field distribution within the dynamic range of macroscopic density vs. field (or surface charge) response, thereby avoiding nonlinear amplitude distortion. When a d.c. voltage is applied to the electrode, the electrode spacing alters the field spectrum as shown in Figure 8. These spectra were calculated assuming image charge modulation to be centered in the macroscopic charge vs. exposure range.

In the presence of applied electrode voltage, development electrode spacing alters the proportionality of field intensity vs. frequency. Although the inherent field spectrum does not change ($d_2 > 10d_1$), the relative particle depositon rates for low vs. high frequency image areas changes with electrode spacing. The spectral response expected with increasing d_2 is an increase in deposition rates to higher spatial frequencies relative to zero spatial frequency. If particle depletion is significant in the electrodeveloper, the proportionality of rates vs. frequency for absolute spectra suggest greater depletion near high spatial frequencies as d_2 increases. For limited concentration electrodevelopers, the amount of nonlinear spatial interactions associated with this depletion effect should increase with electrode spacing.

5. Dynamic Electrodevelopment

More comprehensive assessment of electrodevelopment transfer characteristics requires an analysis of dynamic fields and electrodevelopment kinetics. During the course of

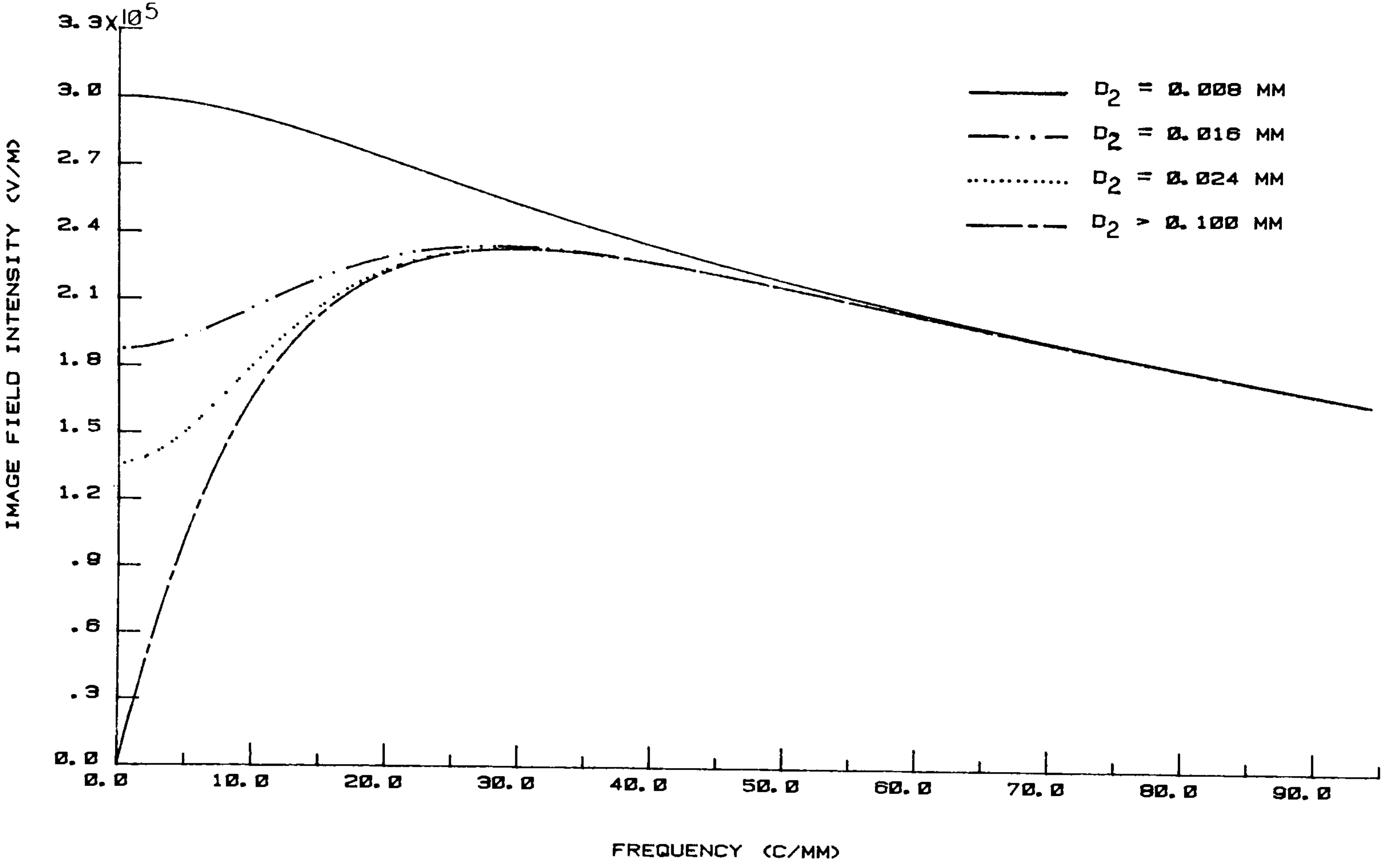

Figure 5. Electrostatic Field Spectra for Various Development Electrode Spacings. Normal component of fields calculated at height, h=1 micron; applied electrode voltage zero.

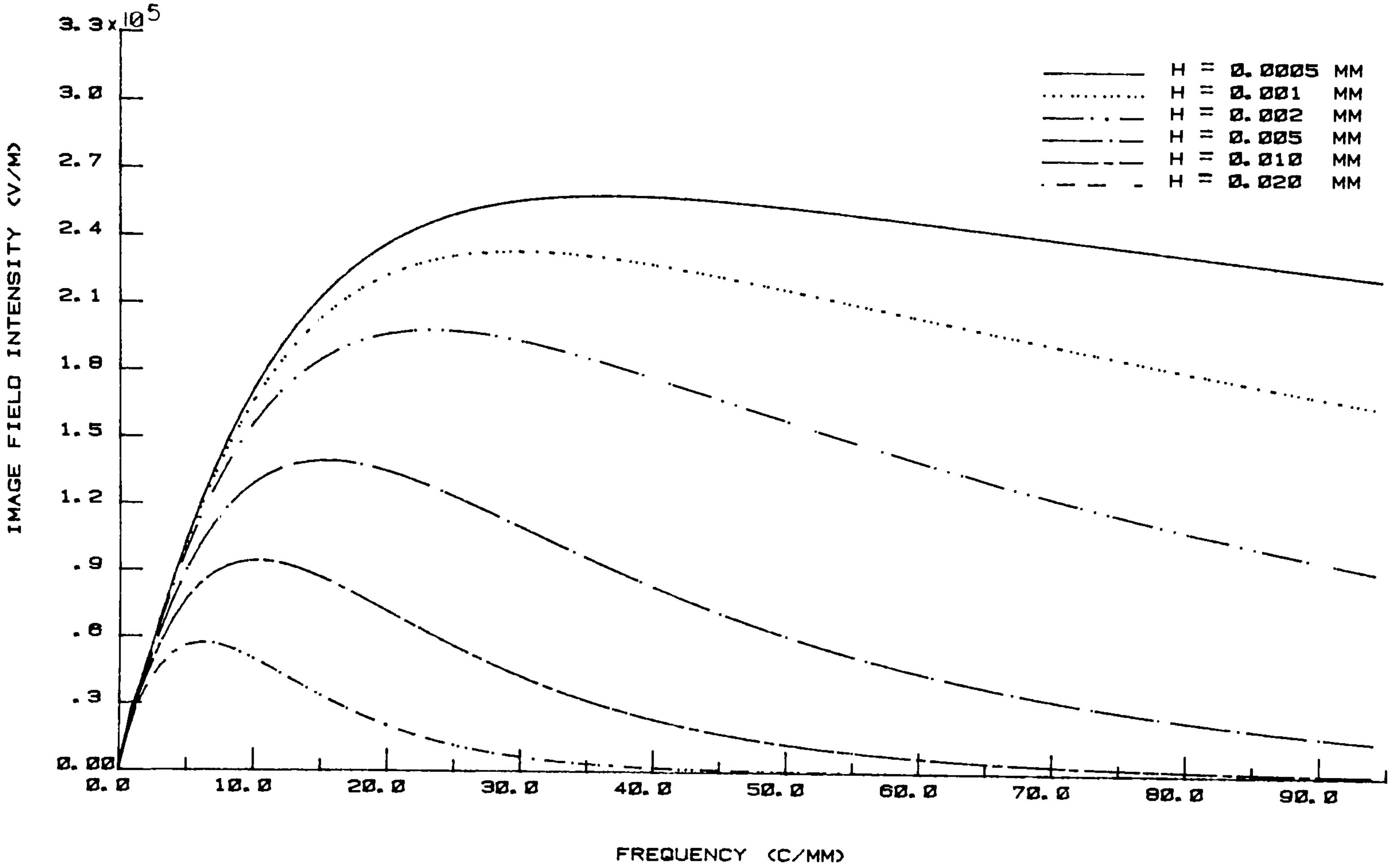

Figure 6. Electrostatic Field Spectra Calculated at Various Heights Above the Photoconductor Surface. Development Electrode Spacing 0.10 mm; applied electrode voltage zero.

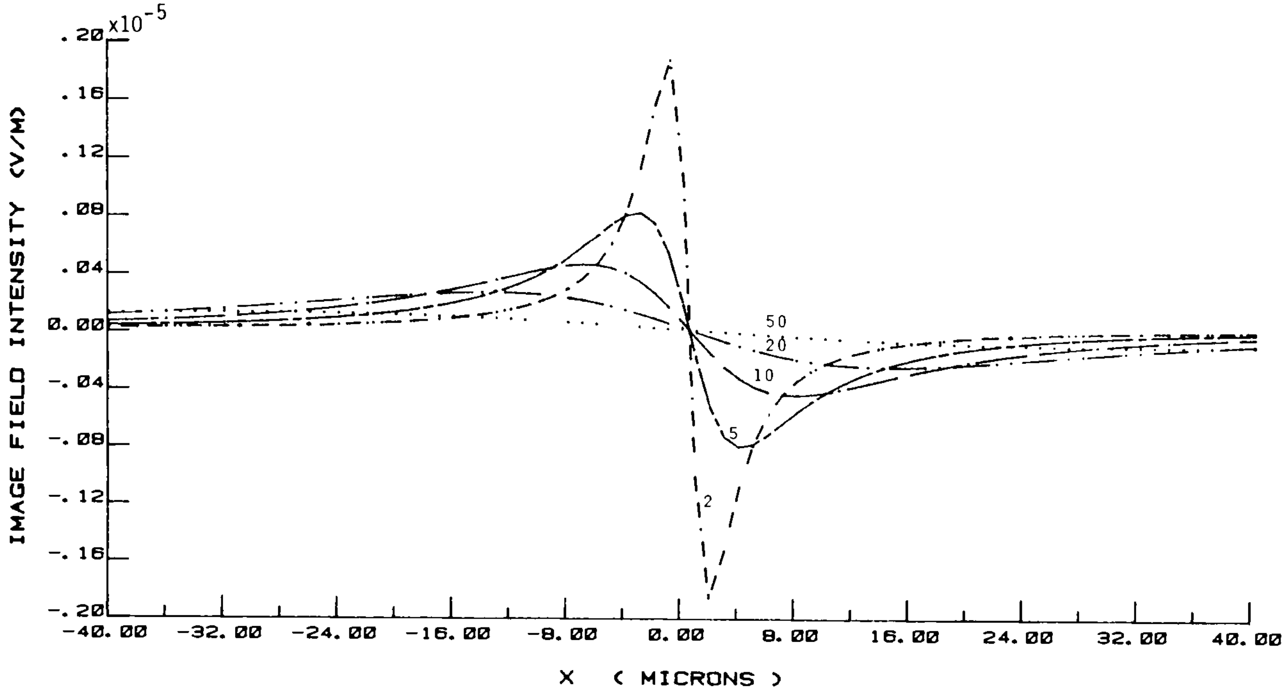

Figure 7. Electrostatic Field Intensity Distribution for Ideal Edge Charge. Height, h, of field calculations above photoconductor surface shown in microns. Development electrode spacing 0.20 mm; applied electrode voltage zero.

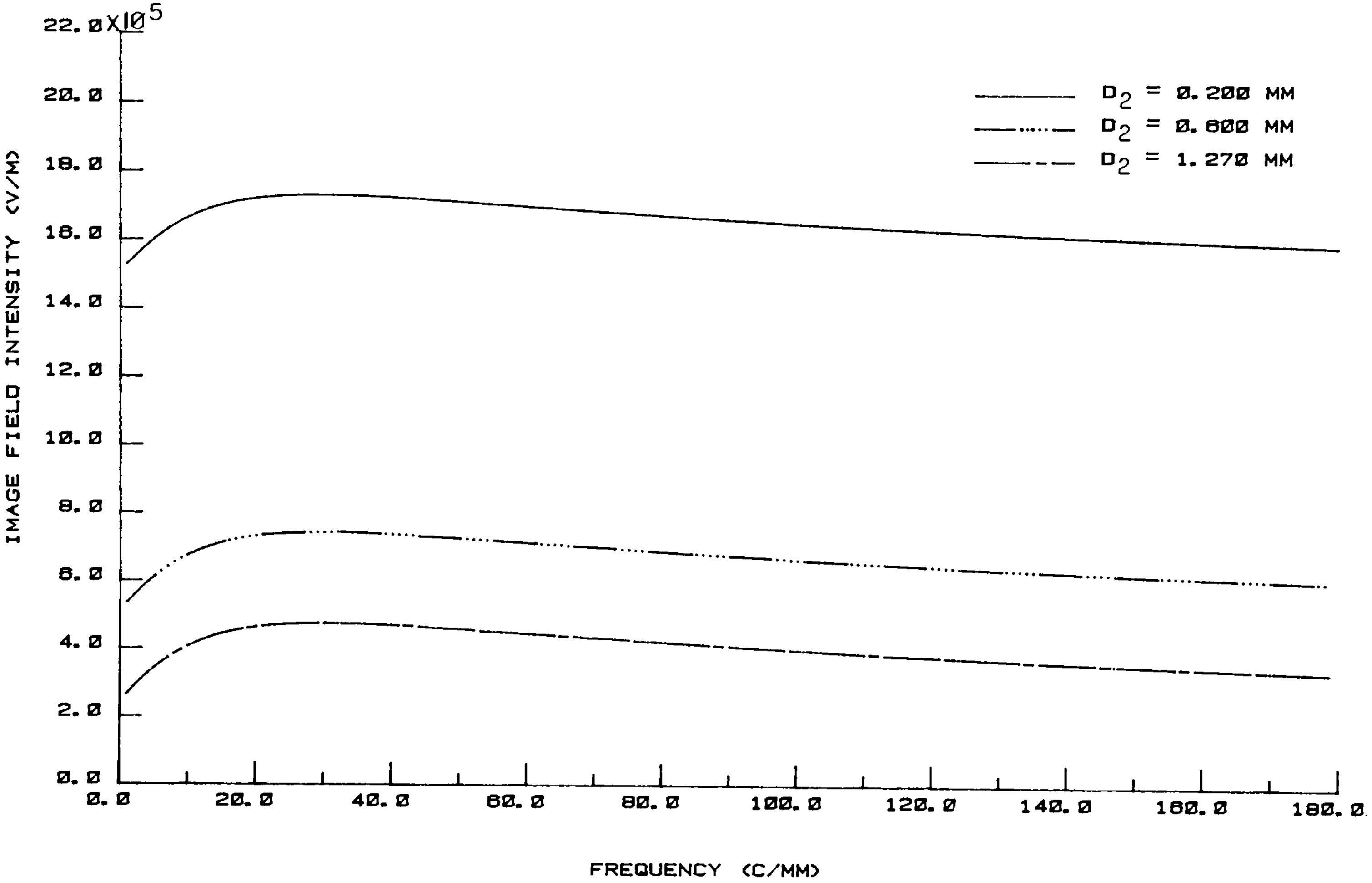

Figure 8. Electrostatic Field Spectra Including Applied Electrode Voltage. Field intensities calculated at height, h of one micron for three electrode spacings.

electrodevelopment the image charge density is neutralized by depositing electrodeveloper species. The corresponding field spectra changes with time, in accordance with the varying rates of deposition to various frequency components. Following temporary depletion effects due to initial differences in deposition rates vs. spatial frequency, permanent depletion effects may occur. Occurance of permanent depletion effects depends on the electrodeveloper species deposited with remaining development time.

Liquid electrodeveloper dispersions contain a number of chemicals as well as charged toner particles. A rather complete list of the chemical components was reviewed by Schaffert,[32] and need not be repeated. The species in the liquid dispersant that are of interest here, are the toner particles with net charge, q, and "free" negative ions. The toner particles are composed of carbon, providing optical density, and resin providing appropriate dielectric constant for ion adsorption to the particle surfaces. At the submicroscopic level, adsorbed ions form a double layer of opposingly charged ions around each particle. The dissociated or "free" negative ions in solution are the same as adsorbed ions which form the inner ionic layer near the particle surface.

The negative charge toner particles and negative "free" ions gain mobility in the direction of positive fields. With application of negative applied electrode voltage, positive fields are established toward the photoconductor for effective particle (and ion) deposition. The concentration and charge of both species, particles and ions, dictates the total conductivity of the dispersion.

The temporal image field distribution is thought to be correlated with the concentration of each species in the dispersion. Model relationships between temporal image fields and the conductivities associated with particle and ionic species, have been postulated for both uniform and complex image charge distributions.[33,34] The models are limited by assumptions of infinite toner particle supply, and initial conductivities associated with each species. Nevertheless, these model relationships provide insight into electrodevelopment rates, time dependent image response, and depletion effects.

For development of large uniformly charged surface areas, Kohler[35] derived an expression relating time dependence of electric fields to electrodeveloper properties. Assuming infinite toner particle supply and applicability of Ohm's law, the temporal field intensity was written:

$$E = E_0 \exp(-t/\tau)$$

where: $\tau = K_2/(K_T+K_I)$

$K_2 = \varepsilon_0(\varepsilon_1 d_1/d_2+\varepsilon_1)$

K_T = initial conductivity of toner particles

K_I = initial conductivity of dissociated ions.

The time constant, τ, was further expressed in terms of individual properties of particles and ions in the dispersion:

$$\tau = K_2/(n_T q_T u_T + n_I q_I u_I)$$

where: n_T, n_I = (number of particles)/cm^3,(number of ions)/cm^3

q_T, q_I = average charge per particle, ion

u_T, u_I = average mobility per particle, ion.

The ratio of toner particles to "free" ions deposited, was postulated as the ratio of initial conductivities according to particles and ions in the dispersion. As these relationships accounted for both species and were applied only to uniform charge areas, they provided reasonably accurate predictions for the number of particles deposited with time[36].

For nonuniform charge distributions, Junginger and Strunk[37] derived an expression for the inherent field distribution as a function of time and electrodeveloper conductivity. These authors imposed dynamic boundary conditions in the solution to Laplace's equation for potential at the interfaces of adjacent dielectric layers. The resulting expression for the temporal electrostatic field normal to the film surface was postulated as:

$$\tilde{E}(x,z,t) = \tilde{E}(0)\exp(-t/\tau(0)) + 1/2\pi\int_{-\infty}^{\infty} \tilde{E}(k,z)\tilde{q}(k,0)\exp(-t/\tau(k)-ikx)dk;$$

where: $\tilde{E}(0)$ is the first term in Kao's expression (p.26)

$\tilde{E}(k,z)$ is the second term in Kao's expression

$\tilde{q}(k,0)$ is the Fourier transformed surface charge distribution

$\tau(k)$ is a frequency dependent time constant

The first term in this expression is essentially Kohler's[38] expression for temporal decay of fields associated with large uniformly charged areas. The second term reduces to a simplified expression relating field spectrum decay to the total electrodeveloper conductivity, K:

$$\tilde{E}(k,z)_{h=0} = 1/K\tau(k)$$

This expression suggests that the image frequency transfer remains linear with increasing electrodevelopment time. Theoretically, modulation increase for each spatial frequency component is uniquely determined by an associated time constant and an invariant conductivity parameter.

The assumption of linear system transfer was maintained in attempt to determine the time constants. Bulk electrodeveloper conductivity was monitored while developing various frequencies of periodic, trapezoidal and rectangular charge distributions. Instantaneous line widths in the periodic image were used to represent modulation of the associated fundamental frequency at various electrodevelopment times. Contrary to theoretical predictions, results[39] indicated that bulk electrodeveloper conductivity decreased with increasing fundamental frequency of the charge distribution.

The explanation offered for this phenomenon was that the effective conductivity near the film surface decreased at a greater rate for higher spatial frequencies, as a result of initially greater deposition of electrodeveloper species. The localized decrease in conductivity was a direct result of particle (and ion) depletion near the film surface, combined with the spectrally dependent deposition rates.

The temporal depletion nonlinearity described for direct field intensities above the film surface, may transition to permanent nonlinearity at extended development times. If the ratio of particle to ion concentration is low in the initially depleted region near the film, ion deposition may dominate in neutralizing the slower developing, low frequency image charge components. At some finite electrodevelopment time, replenishment in accordance with integrated fields should correct for a temporal imbalance between particle and ion concentration. As integrated field intensity remains invariant of electrode spacing, the initial differences in direct field intensity vs. frequency remain the sole source of development nonlinearity. Persistance of initial nonlinearities with continuing development, depends only on the proportion of particles to ions replenished near the film surface. Unfortunately, neither ratios of particles to ions in the depleted region, nor time dependent replenishment by integrated fields, have been adequately studied. To date it remained infeasible to postulate the amount of permanent depletion expected for a given (initial) electrodeveloper composition.

6. Toner Deposition Forces

Toner deposition governed solely by the normal component of electrostatic field, adequately describes electrodevelopment for highly charged toner particles. For particles of weaker charge, a more comprehensive treatment of field and particle interactions is required. Schaffert[42] postulated that both electrophoretic ($\bar{F}_e$) and dielectrophoretic ($\bar{F}_d$) forces influence the mobility of weakly charged particles. The expression for the total force on the charged particles is then:

$$\bar{F}_t = \bar{F}_e + \bar{F}_d = q\bar{E} + 2\pi r^3 \varepsilon_0 \alpha \nabla \bar{E}^2$$

where α is a polarizability constant for the toner particles. Electrophoretic force is a linear function of the electric field vector $\bar{E}$, and is directly proportional to the net particle charge. Dielectrophoretic forces depend on the gradient of the field vector, a quadratic term in field strength, and polarizability of the toner particles.

Pohl[43] defined dielectrophoresis as the mobility of polarized, neutral particles in the presence of highly divergent fields. When dielectric constants for particles (ε_p) and dispersant (ε_d) are different, external diverging fields induce a dipole moment in neutral particles. The dipole moment aligns with these fields, causing the particles to move in the direction of greater flux. Dielectrophoresis of neutral particles[44] requires high intensity fields ($E > 10$ V/mm) and large particle radii ($r > 1$ um), as well as appreciably different dielectric constants ($\varepsilon_p - \varepsilon_d > 1$). Inoue[45] claims that dielectrophoretic force induces mobility of charged particles as well. Requirements for field strength, field divergence, particle radius, and dielectric constants, have not been theorized for charged particles. However, Schaffert[46] claims that dielectrophoresis may be significant relative to electrophoresis for particles of low net charge (quantity unspecified).

In regions where electric fields are both intense and highly divergent, dielectrophoretic force may increase the rate of particle deposition beyond the rate dictated by electrophoretic force alone. When $d_2 > d_1$, the largest field gradient is associated with higher spatial frequency content in an edge charge distribution. Contribution of dielectrophoretic force to the initial deposition rate at high frequency components should increase the depletion effect postulated in accordance with electrophoretic forces. Unfortunately, the parameters required to calculate dielectrophoretic force were not available, hence the significance of this contribution to nonlinear image transfer could not be determined.

7. Electrodeveloper Replenishment

Recognizing the effects of particle depletion on image transfer characteristics, attempts have been made to replenish the electrodeveloper during development. Stark & Menchel[47] and Kohler[48] employed fine mesh screens as development electrodes, in attempts to provide adequate particle supply to the electrodevelopment region while minimizing electrodeveloper agitation. However, a screen electrode limits particle replenishment to diffusion through the screen, offering little replenishment of particles near the film surface. Continuous film processing conditions generally include flow of fresh electrodeveloper into the development region during electrodevelopment. Continuous flow of electrodeveloper, as employed in this investigation, should have provided greater replenishment of particles near the film surface.

As electrodeveloper flows through the electrodevelopment region, concentrations of particles and ions may change as a function of local charge content on the film. It is thought that the rates of deposition for these species will be orders of magnitude greater than the rate of replenishment, for practical rates of electrodeveloper flow into the region. Replenishment rates at various heights above the film surface may vary as a function of electrode spacing. However, complex calculations for stratified regions of particle and ion concentrations were beyond the scope of this study. Assuming an order of magnitude difference in deposition vs. replenishement rates, changes in electrode spacing were not expected to produce significant changes in replenishment rates and permanent depletion phenomena.

Electrodeveloper flow parallel to the film surface may cause changes in component concentrations as particles are deposited to the surface charge. Interactions between flow direction and the image spatial charge distribution have been noted by Lubianez.[49] Electrodeveloper flow predominantly aligned with the charge modulating image dimension were said to produce image distortion. Therefore, attempts were made to align the direction of electrodeveloper along the unvarying image dimension, for the one-dimensional charge distributions employed in this investigation. Phase distortions in the image distribution as a function of flow direction, were initially assumed to be negligable.

Summarizing the electrodvelopment mechanisms affecting linearity of image transfer, it is the direct electrostatic fields that dictate initial differences in particle deposition as a function of spatial frequency. Kao's calculated field spectra indicate that higher spatial frequency components develop at initially greater rates than lower frequency components of the image charge distribution. This rate difference occurs between different levels of practical electrode spacing ($d_2 > 10d_1$) because the proportionality of high frequency to zero frequency field intensities changes in the presence of applied electrode voltage. As a result of the rate difference, depletion of toner particles near high frequency components was expected shortly after development initiation. A temporary nonlinear transfer characteristic was expected as a result of interactions between depleted vs. nondepleted components of the developing image distribution. Increases in electrode spacing beyond $d_2 > 10d_1$, were expected to increase the initial nonlinearity associated with this depletion phenomenon.

Studies relating temporal image response to dynamic fields and electrodeveloper kinetics have indicated that initial depletion of particles near high frequency components altered linearity of image transfer. Persistance of nonlinearities with extended development should depend on the replenishment of particles to initially depleted regions near the film surface. If the proportion of particles to ions in these regions remains low, permanent nonlinearities should be observed in the resulting imagery. Particle replenishment from the bulk electrodeveloper region should occur at rates determined by integrated field intensities. With increasing time, the strong integrated field intensity associated with low frequency components would rectify the initial imbalance between particles and ions near the film surface. As the integrated field intensities are independent of electrode spacing, restoration of linear image transfer should depend only on initial concentration of particles in the electrodeveloper, and electrodevelopment time.

II. EXPERIMENTAL

A. Approach

1. Procedure

Empirical tests for linearity of photoconduction and electrodevelopment mechanisms consisted of reproducing test image distributions for parameters expected to control each meachanism. The wavelength of exposing radiation was varied to test the influence of nonlinear absorption on the image transfer. Development electrode spacing and development time were varied in attempt to alter the amount of localized particle depletion in the the electrodevelopment process. If the latent electrostatic fields above the film surface could be measured, image transfer characteristics could be determined for each subsystem process. Accurate, nondestructive field measurements at the microscopic level could not be performed.[51,52] Therefore, the test parameters were varied according to statistical designs, and image transfer was analyzed using input and output distributions for the complete system.

The levels for exposing wavelength were chosen to maximize the difference in film absorption coefficients within the limits of useful spectral sensitivity. The levels for electrode spacing were chosen to maximize the difference in electric field distributions, within the practical limits for electrodeveloper supply rate to the development region. The levels for electrodevelopment time were chosen in accordance with assumed exponential increase in response with time. Limits for short electrodevelopment times were imposed by the requirement for sufficient density response in sensitometric images to allow translation of test image density into effective exposure. Longer development times were initially chosen to represent development to saturation density.

The test image exposures were formed using sharp edge targets, and a series of sinusoidal transmittance targets at various spatial frequencies. Film targets were reduction imaged to the TEP film plane through a high quality microscope objective. With a reduction imaging system properly aligned relative to the film plane, incident exposures were considered linearly proportional to the target transmittance distributions. To define the input exposure distributions, microdensity measurements were made for each target and the results were converted to transmittance. An initial test was conducted to confirm the alignment of the reduction system optical axis, normal to the film surface.

The resulting experimental test images were measured using a microdensitometer system calibrated to the macroscopic density response of the subject film/electrodeveloper system. Several microdensity traces were obtained at equidistant intervals along the unvarying dimension of each experimental image. Assuming that the film/electrodeveloper system produced spatially invariant and stationary image transfer, independent scans were ensemble averaged to improve the signal to noise ratio for response distributions.

No attempts were made to characterize image noise produced in the system.

Comparison of resulting density distributions with the test (micro) exposure distributions was not performed, as optical density is nonlinearly related to input exposure. Effective exposure distributions were obtained by translation of output density through the macroscopic Hurter and Driffield (H & D) response. Sensitometric images were generated for each set of experimental conditions and experimental treatments, providing appropriate H & D characteristics for corresponding test image translations. Cases were identified for which the dynamic range of the H & D responses were insufficient for translation of image density to effective exposure. Attempts were made to adjust the micro image exposure level so that the input exposure modulation remained within the dynamic range of the H & D response, prior to experimental parameter testing.

Methods for analyzing system transfer characteristics were unique to the (edge or sinusoidal) test distributions. Variability in the edge responses for each experimental design, was subdivided into common components of variance employing "characteristic vector analysis".[52] Using this analysis technique, each of the original edge responses was characterized by a set of coefficients associated with orthogonal basis vectors. The coefficients of each vector were then used to determine statistical correlation between the basis vectors and the experimental parameters. For correlated parameters and vectors, the influence of the parameters on the linearity of edge transfer was assessed with reference to the vector's influence on the symmetry of edge response. Speculations were made regarding the mechanistic cause of nonlinearities, according to the nature and extent of asymmetry observed.

For sinusoidal transfer analysis, the target transmittance and image effective exposure distributions were Fourier transformed to obtain associated frequency spectra. A harmonic distortion measure for each distribution was computed using the ratio of amplitudes at harmonic and fundamental frequencies. The harmonic distortion measures were corrected for modulation losses introduced by the imaging reduction lens and the microdensitometer system.

The response variables for sinusoidal transfer analysis were harmonic distortion factors computed from the ratio of corrected output to input harmonic distortions. Harmonic distortion factors were computed for the first and second harmonics of each fundamental frequency tested. These distortion factors were then analyzed for statistical correlation with the experimental photoconduction and electrodevelopment parameters tested. Distortion factors were compared to the theoretical limit for amplitude distortion based on inherent electrostatic field spectra for the electrophotographic film employed. Distortion values exceeding the theoretical limit for inherent amplitude distortion, indicated nonlinear image transfer for the associated parameter levels.

2. Test Materials

Film: TEP XP4-008 (James River Graphics, lot 8004 MT-06)

Electrodeveloper: T3C-5K-6%T (James River Graphics, lot #s 1042-67B & 101-B)

This liquid electrodeveloper consisted of a concentrate composed of resin, charge director, C-5 solvent, and carbon particles, dispersed in a diluent containing an ionic charge director. The T3C-5K concentrate was mixed with the diluent at a ratio of 34 cm^3/liter, forming a working strength dispersion. In accordance with the manufacturer's specifications, concentration of particles in the dispersion was reported as a relative measure of transmittance (6%T). The carbon/resin "toner" particle sizes ranged in radius from 0.15 to 0.8 um, with a volume mean particle size of 0.2 um. The net particle charge was negative; with a charge of approximately 1.8×10^{-18} coulombs for particles of average radius 0.2 um.[53]

3. Sensitometry

All experiments conducted in this investigation employed negative working sensitometry. The film was initially charged to produce a negative surface potential as measured relative to the conductive layer. For large area deposition of negative particles to the negative surface charge, a negative potential was applied to the development electrode. In areas where the film charge was reduced by exposure to a less negative value, the net field was positive in the direction toward the film surface.

4. Experimental Parameter Levels

(a) Exposing Wavelength

Selection of two test wavelengths was in accordance with spectrophotometer traces (Figure 2), having spectral sensitivity values in the region of dye absorption. The maximum absorbance wavelength, 500 nm, had a spectral sensitivity rating[54] at 100 ergs/cm^2. The wavelength selected to represent a lower absorbance level, 440 nm, had a spectral sensitivity rating at 400 ergs/cm^2.

(b) Development Electrode Spacing

The range of development electrode spacings suitable for testing, were limited by the electrodevelopment apparatus designs and the requirement for uniform sensitometry. Repeatable deposition of toner particles to the image charge, required that a meniscus of electrodeveloper be maintained between the electrode and the film surface. Prior testing indicated practical combinations of electrode spacing and electrodeveloper supply rates required to maintain a liquid menicus for each of the electrodevelopment apparatus employed. For an electrodeveloper supply rate of 3 cm^3/second and film platen velocity of three inches/second, the maximum electrode spacing was 1.27 mm. This electrode spacing was established as the upper extreme for this investigation, within the constraints on supply rate and film platen velocity.

The minimum electrode spacing was determined from the repeatability (tolerance) of the spacing for successive test runs, and the uniformity of sensitometric image responses. The spacing repeatability was estimated to be ± 0.025 mm in accordance with mechanical tolerances for the apparatus employed. Nonuniform sensitometric responses were noted for electrode spacings less than 0.15 mm, when the electrodeveloper supply rate was set to 3 cm^3/second. The minimum electrode spacing was therefore established at 0.20 mm, within the associated constraints on supply rate.

(c) Electrodevelopment Time

As concentrations for particles and ions in the T3 electrodeveloper were not available, theoretical calculations for rate of optical density increase could not be performed. Prior tests for development to completion, were conducted for a continuous electrode apparatus using an electrodeveloper supply rate of 3 cm^3/second. With other parameters set constant for this investigation, development of sensitometric images to saturation density required a film platen velocity of 0.3 inches/second. This velocity approximates an electrodevelopment time of 10 seconds.

B. Experimental Designs

Testing for significance of the experimental parameters relative to image transfer characteristics was reported for four experiments. The experimental designs are crossed factorials with the parameters: exposing wavelength, development electrode spacing, and electrodevelopment time, treated as random factors. Two replicate film samples for each experimental treatment provided estimates for experimental error. Experiment one was a screening experiment which included all experimental test parameters, and was run using edge targets only. The second experiment was an edge transfer experiment, run for an expanded set of electrodevelopment times and a constant exposing wavelength. The third and fourth experiments were edge and sinusoidal transfer experiments, respectively. For these experiments, an alternate electrodeveloper apparatus and a new specification for electrodevelopment time were employed for more accurate analysis of temporal electrodevelopment transfer characteristics.

1. Experiment One

The first experiment was a 2^3 factorial screening experiment for determining the significance of the test parameters at initial levels. The exposing wavelengths tested were 440 and 550 nanometers, dictating minimum and maximum practical absorption factors for TEP XP4-008 film. The electrodevelopment times represented a first attempt to observe the temporal dependence of localized electrodeveloper depletion. The levels included (1) time for complete development: 10 seconds, and (2) half the time required for complete development: 5 seconds.

Exposing wavelength bands were achieved using blocked interference filters centered at 440 and 500 nanometers, with passbands of 12 nanometers, full width at 10% maximum (FW10M). Photoconduction mechanisms other than spectral absorption were held constant by equalizing the exposure times for each spectral band, the incident intensity was adjusted using Inconnel "neutral density" (ND) filters. Table 1 includes the ND filtration required to equalize surface charge decay for exposure times in each spectral band.

As the lens employed for test target reduction exhibited chromatic aberation with respect to focus, the focus setting was adjusted for each spectral band. This procedure insured that maximum image modulation was attained at each exposing wavelength. The settings were determined from resolution tests, as described in the section on Reduction Imaging. (p. 77)

A continuous electrodevelopment apparatus was employed. The electrodevelopment procedure was to apply electrodeveloper to the film sample as the film platen moved at a predetermined velocity under the continuous electrode apparatus. Rinse solution was applied through a slit located 3 inches from the electrodeveloper application slit. The rinse solution was assumed to halt electrodevelopment by displacing the electrodeveloper at the film surface.

Electrodevelopment times were determined in accordance with the film platen velocity under the electrode. The velocities and associated nominal electrodevelopment times were (1) velocity = 0.6 inch/second: 5 seconds, and (2) velocity = 0.3 inch/second: 10 seconds. In the experimental design, platen velocity was reported in place of electrodevelopment time, as actual electrodeposition times could not be accurately determined. Table 1 includes the experimental design and control variables for experiment one.

Six replicate, edge target reduction images were exposed on the film sample, at equal distance intervals in the direction of platen travel. A single sensitometric target image was exposed on each film sample near the test target images. The locations of test target and sensitometric target exposures on the film sample are illustrated in Figure 9. In this figure, the right side of the film sample represents the leading edge with respect to platen motion, and the test target images are numbered in the order of exposure. Microdensitometer scanning was performed for edge image number 2 on each film sample.

2. Experiment Two

This experiment was designed to further test for significance of electrode spacing and electrodevelopment time on edge image

Table 1. Experimental Design and Control Parameters for Experiment One

(a) Experimental Design:

		Development Electrode Spacing (mm)			
		0.20		1.27	
		Velocity (in/sec)		Velocity (in/sec)	
		0.6	0.3	0.6	0.3
Exposing Wavelength (nm)	440	10-8-1 10-8-9	10-8-5 10-8-13	10-8-7 10-8-15	10-8-3 10-8-11
	500	10-8-6 10-8-14	10-8-2 10-8-10	10-8-4 10-8-12	10-8-8 10-8-16

(b) Control Parameters:

Initial Surface Potential: -800 ± 20V

Image Target: NBS edge, 52% modulation

Image Exposure: 440 nm: 0.5 sec, 1.00 ND
500 nm: 0.5 sec, 1.75 ND

Image Focus: 440 nm: 18 psi
500 nm: 21 psi

Sensitometric Exposure: 440 nm: 99 sec.
500 nm: 99 sec, 0.75 ND

Electrodevelopment Apparatus: Continuous electrode

Electrodeveloper supply: 3.0 ± 0.3 cm^3/sec.

Applied Electrode Voltage: -780V

Rinse Supply Rate: 3.0 ± 0.5 cm^3/sec.

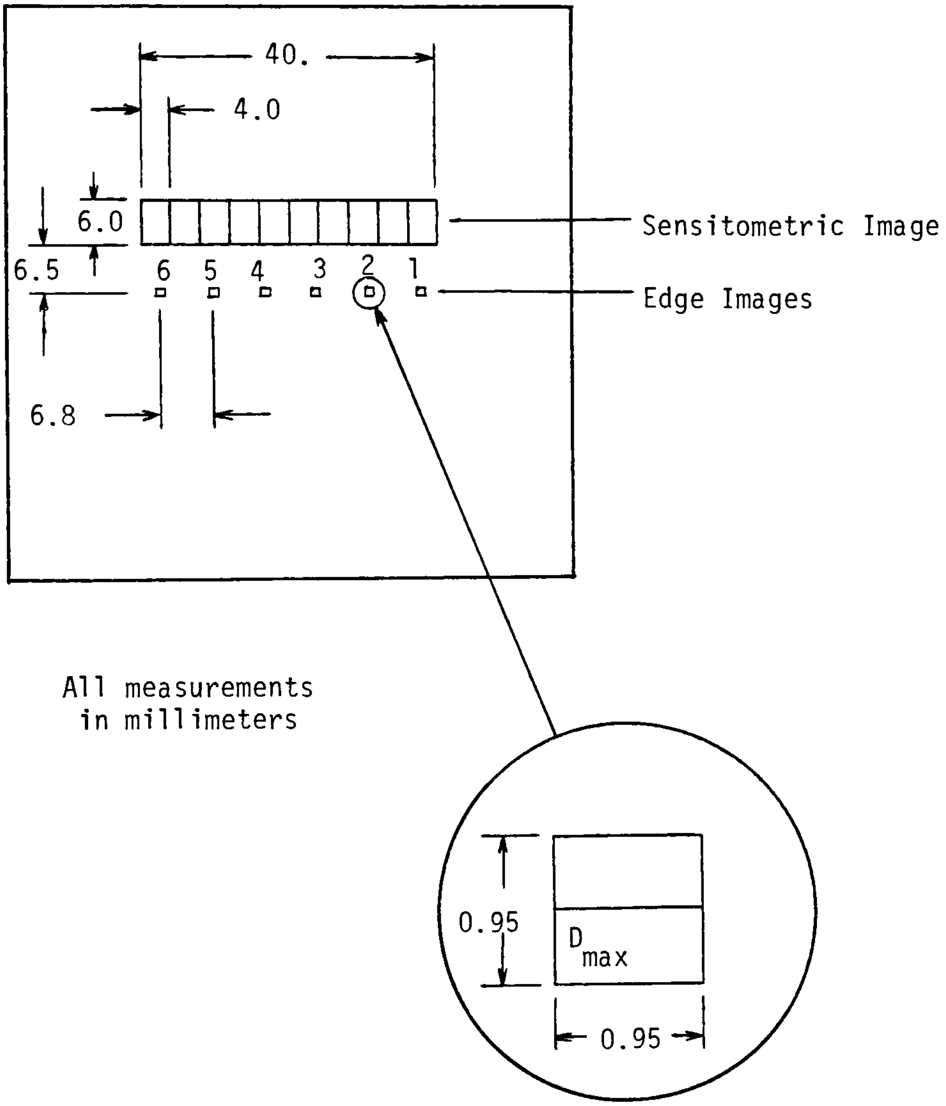

Figure 9. Geometry of Edge and Sensitometric Images on Film Samples for Experiments One and Two.

transfer characteristics. Exposing wavelength was held constant, and additional test levels were selected for the electrodevelopment parameters.

The development electrode spacings were set to 0.20, 0.60, and 1.27 mm; where the intermediate spacing was arbitrarily set to a factor of three times the minimum spacing. The continuous electrode electrodevelopment apparatus was employed (Figure 12), and electrodevelopment control parameters replicated conditions established in experiment one. Two additional levels for film platen velocity were included, at 1.5 and 3.0 inches/second. The series of four velocity levels approximate an exponential increase in electrodevelopment time; as represented by the sequence of 1, 2, 5 & 10 seconds. The exposing wavelength was set to 500 nanometers, employing the blocked interference filter cited in experiment one for both reduction edge exposures and sensitometric exposures. Exposure times for the edge test images were adjusted to produce less than 50% reduction of the initial film charge potential.

The experimental design and control parameters are included in Table 2, where film platen velocity is reported in place of electrodevelopment time. Six replicate, edge images and a single sensitometric image were placed on each sample, as illustrated in Figure 9. Microdensitometer scanning was performed for the second edge image exposed on each film sample.

Table 2. Experimental Design and Control Parameters for Experiment Two

(a) Experimental Design:

		Development Electrode Spacing (mm)		
		0.20	0.60	1.27
Film Platen Velocity (in/sec)	3.0	1-19-14 1-19-16	1-19-10 1-19-12	1-19-2 1-19-4
	1.5	1-19-13 1-19-15	1-19-9 1-19-11	1-19-1 1-19-3
	0.6	1-22-6 1-22-8	1-19-6 1-19-8	1-22-2 1-22-4
	0.3	1-22-5 1-22-7	1-19-5 1-19-7	1-22-1 1-22-3

(b) Control Parameters:

Initial Surface Potential: -800 ± 20V

Image Target: NBS edge, 83% modulation

Image Exposure: 500 nm; 2.0 seconds; opal glass diffuser

Image Focus: 21 psi

Sensitometric Exposure: 500 nm; 30.0 seconds

Electrodevelopment Apparatus: Continuous electrode

Electrodeveloper Supply: 3.0 ± 0.3 cm^3/sec.

Applied Electrode Voltage: -780V

Rinse Supply Rate: 3.0 ± 0.5 cm^3/sec.

3. Experiment Three

This experiment tested the significance of electrodevelopment mechanisms on the linearity of edge image transfer, employing a more accurate method for controlling electrodevelopment time. Electrodevelopment time was defined as the duration of applied electrode voltage while the electrodeveloper remained in contact with the image areas. A fountain toner apparatus was employed (Figure 13), to provide uniform supply of electrodeveloper to all portions of the electrodevelopment region. The gating of applied electrode voltage, and uniformity of electrodeveloper supply, allowed electrodevelopment with a constant film/platen velocity of 0.4 inches/second.

The electrode voltage was gated on before the film sample entered the electrodevelopment region. In this manner, initial particle deposition rates to all image components were determined by the sum of the inherent electrostatic field distribution and the applied d.c. field component. After a predetermined time of platen travel the applied electrode voltage was gated off.

A total of eight edge image exposures were placed on each film sample at equidistant intervals along the direction of platen travel. The time series for applied voltage electrodevelopment was represented by the progression of image exposures on the film sample. For each image the start of electrodevelopment was defined by the initial contact of electrodeveloper with that particular image. The film traveled over the electrode plate while toner was continuously supplied to the development gap. Image number 8 was the first to enter the electrodevelopment gap, and toning for following image numbers started at successive delays of 0.67 seconds. Figure 10 illustrates the effective electrodevelopment times for each image on the film sample. The time durations for applied electrode voltage were 0.0, 1.0, 2.3, and 4.3 seconds for image numbers 1, 3, 5 and 8, respectively.

For each image number, the total time of toner contact was 11 seconds. Electrodeveloper was continuously replaced in the developer region at a rate of 3 cm^3/second. Each test image on the film sample remained in the electrodevelopment region for 8.8 seconds. Therefore, a stagnant layer of toner remained in contact with the image for an additional 2.2 seconds before the image reached the rinse apparatus. Electrodeposition of particles may have occured after the electrode voltage was gated off, in response to remaining inherent fields. However the maximum rate of deposition in accordance with the inherent field distribution, should have occured in the first second of electrodevelopment.[55] The condition for zero seconds applied electrode voltage was included in the time series to establish baseline toning response in accordance with inherent fields alone.

The experimental design is shown in Table 3 where the edge image numbers on each film sample represent the associated time level. Two replicate film samples were run for each electrode spacing.

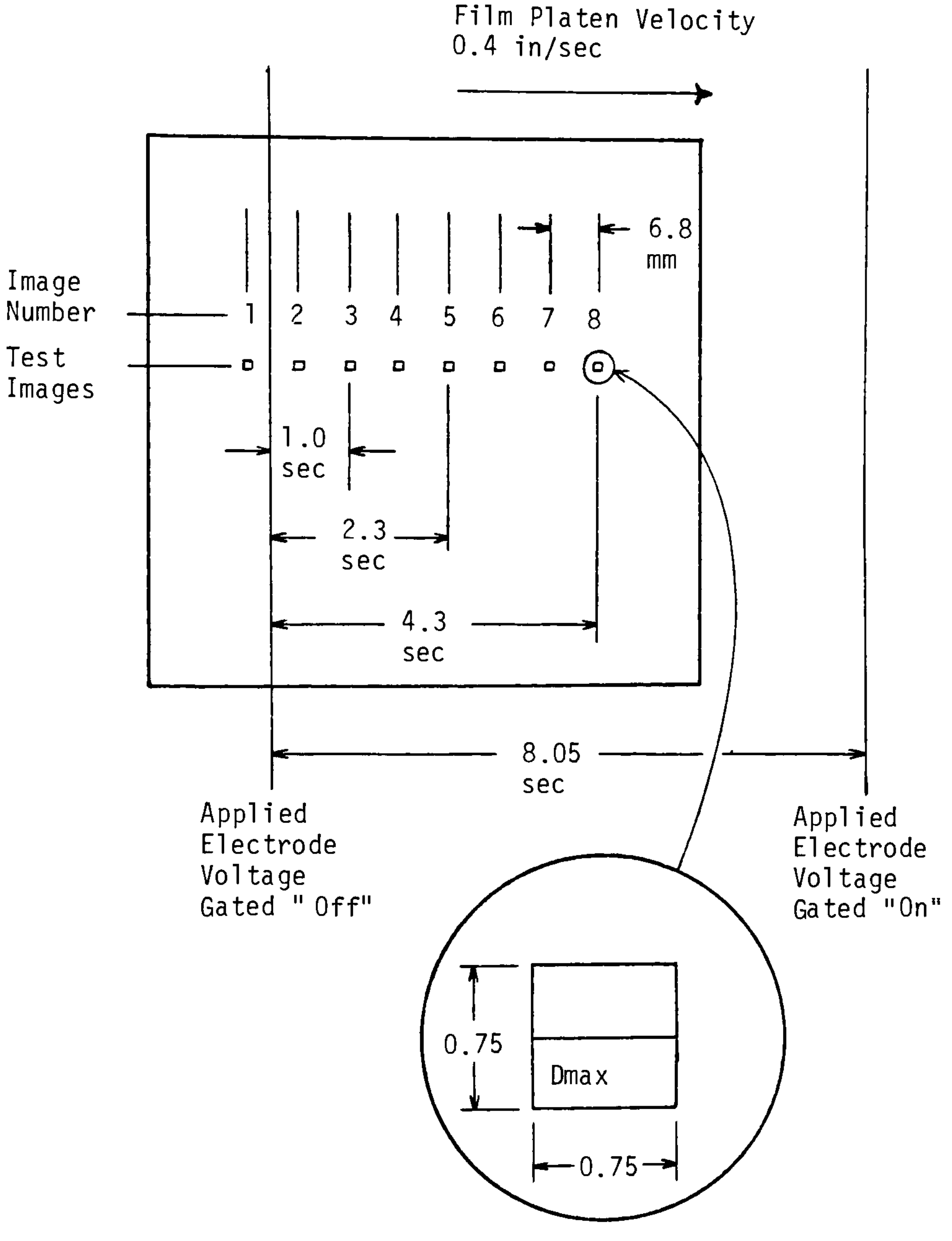

Figure 10. Relation of Test Image Locations to Gated Electrode Voltage Providing Range of Applied Voltage Times.

Table 3. Experimental Design and Control Parameters for Experiment Three

(a) Experimental Design:

		Development Electrode Spacing (mm)					
		0.20		0.60		1.27	
		Film Sample		Film Sample		Film Sample	
		7-16-2	7-16-4	7-16-6	7-16-7	7-15-1	17-15-2
Applied Voltage Time (seconds)	0.0	E-1	E-1	E-1	E-1	E-1	E-1
	1.0	E-3	E-3	E-3	E-3	E-3	E-3
	2.3	E-5	E-5	E-5	E-5	E-5	E-5
	4.3	E-8	E-8	E-8	E-8	E-8	E-8

(b) Control Parameters:

Initial Surface Potential: -800 ± 20V

Image Target: NBS edge, 83% modulation

Image Exposure: 500 nm; 4.5 seconds; opal glass diffuser

Image Focus: 23 psi

Electrodevelopment Apparatus: Fountain electrode

Electrodeveloper Supply: 3.0 ± 0.3 cm^3/sec.

Applied Electrode Voltage: -780 ± 20V

Rinse Supply Rate: 3.0 ± 0.5 cm^3/sec.

4. Experiment Four

In this experiment, the linearity of sinusoidal image transfer was tested as a function of electrode spacing and electrodevelopment time. The fountain toner apparatus and gated electrode voltage procedure were employed, replicating the conditions employed in experiment three. Development electrode spacings were confined to the extreme levels: 0.20 and 1.27 mm. Three sinusoidal targets were employed for each experimental treatment. The experimental design is shown in Table 4. Applied electrode voltage times were the same as those in experiment three. Experimental control parameters were also indentical to those employed in experiment three, with the exception of micro-image exposure time. As the sinusoidal targets had a different average transmittance level than that of the edge target, the exposure time was adjusted to achieve a similar average input exposure level.

5. Sensitometric Response - Experiments Three and Four

Sensitometric responses for corresponding test and control parameters of experiments three and four were generated on separate film samples. Sensitometric target exposures were placed at locations corresponding to the test image exposures 1, 3, 5, and 8. Three replicate samples were generated for each of the three development electrode spacing 0.20, 0.60, and 1.27 mm. The densities were measured with a Macbeth TD-518 densitometer

(1 mm aperture) and plotted as a function of relative log exposure. For each experimental treatment an average H&D curve was estimated by visual examination. The experimental samples are identified in Table 5.

Table 4 - Experimental Design for Experiment Four

		Development Electrode Spacing (mm)			
		0.20		1.27	
Frequency = 25 cycles/mm		Film Sample		Film Sample	
		7-17-2	7-17-8	7-17-13	7-17-18
Applied Voltage Time (seconds)	0.0	S-1	S-1	S-1	S-1
	1.0	S-3	S-3	S-3	S-3
	2.3	S-5	S-5	S-5	S-5
	4.3	S-8	S-8	S-8	S-8
Frequency = 64 cycles/mm		Film Sample		Film Sample	
		7-17-4	7-17-10	7-17-15	7-17-20
Applied Voltage Time (seconds)	0.0	S-1	S-1	S-1	S-1
	1.0	S-3	S-3	S-3	S-3
	2.3	S-5	S-5	S-5	S-5
	4.3	S-8	S-8	S-8	S-8
Frequency = 102 cycles/mm		Film Sample		Film Sample	
		7-17-6	7-17-11	7-17-16	7-17-21
Applied Voltage Time (seconds)	0.0	S-1	S-1	S-1	S-1
	1.0	S-3	S-3	S-3	S-3
	2.3	S-5	S-5	S-5	S-5
	4.3	S-8	S-8	S-8	S-8

Table 5. Sensitometric Images for Experiments Three and Four

		Development Electrode Spacing (mm)								
		0.20			0.60			1.27		
		Film Sample			Film Sample			Film Sample		
		7-28-1	7-28-2	7-28-3	7-28-6	7-28-7	7-28-8	7-28-11	7-28-12	7-28-13
Applied Voltage Time (seconds)	0.0	SEN-1	SEN-1	SEN-1	SEN-1	SEN-1	SEN-1	SEN-1	SEN-1	SEN-1
	1.0	SEN-3	SEN-3	SEN-3	SEN-3	SEN-3	SEN-3	SEN-3	SEN-3	SEN-3
	2.3	SEN-5	SEN-5	SEN-5	SEN-5	SEN-5	SEN-5	SEN-5	SEN-5	SEN-5
	4.3	SEN-8	SEN-8	SEN-8	SEN-8	SEN-8	SEN-8	SEN-8	SEN-8	SEN-8

C. Apparatus and Techniques

1. Image Reproduction System

Functions of image reproduction, with the exception of image fixing, were accomplished using the Mead Electrophotographic Evaluator.[56] This microprocessor controlled apparatus consisted of a mobile film platen and fixed functional stations. The stations performed the functions of a) initial film charging, b) surface potential measurement, c) test image exposure, d) sensitometric exposure, and e) electrodevelopment and rinse. A microprocessor insured repeatable platen velocities, station dwell times, and functional station operations for replicate control settings.

A three-inch square film sample was prepared by clearing a portion of the photoconductor layer with acetone, and adhering conductive tape to the film's conductive layer. The film was held onto the platen with vacuum, and a ground clip was connected to the conductive strip on the film. This procedure insured that the film was uniformly adhered to the platen and the conductive layer remained at ground potential throughout the image reproduction cycle. Specific procedures for the exposure and electrodevelopment stations are identified in the next section. The apparatus and operations for each of the functional stations are explained below.

(a) Initial Charging: A scorotron charging apparatus was used to establish an initial potential across the film's photoconductive layer. During film charging, the corotron and screen wires were maintained at potentials -8000 Volts and -500 Volts respectively, thereby inducing a -780± 20 Volt potential across the photoconductor layer. Uniformity of the surface potential was maintained by moving the platen at 1 inch/second under the scorotron during the charging operation.

(b) Initial Surface Potential Measurement: A Monroe electrometer (model 1009CG) was positioned 5 mm above the film surface. The apparent (measured) surface potential was chart recorded during the charging operation, and examined for uniformity in the direction of platen motion. Acceptable variations in potential were limited to ± 20 Volts.

(c) Test Image Exposure: A reduction printer (Mead Technologies) modified with a pneumatic autofocus mechanism (Aerodyne Research, Model 301), provided precision positioning of the microscope objective used for reduction imaging. Figure 11 illustrates a schematic for the optical components of the Mead Reduction printer. A Zeiss Epiplan, 16x, N.A. 0.32, microscope objective had been previously modified with an air nozzle for use with the pneumatic autofocus control. The air pressure between the nozzle orfice and the film surface was adjusted to control the (focus) distance between the objective and the film surface. Blocked interference filters (Optical Industries, Inc.) were employed, having passbands of 12 ± 2 nanometers, full width at 10% maximum. A Tungsten source 100 Watt, 12 Volt, was attentuated with an opal glass diffuser to insure uniform, diffuse illumination of the test target.

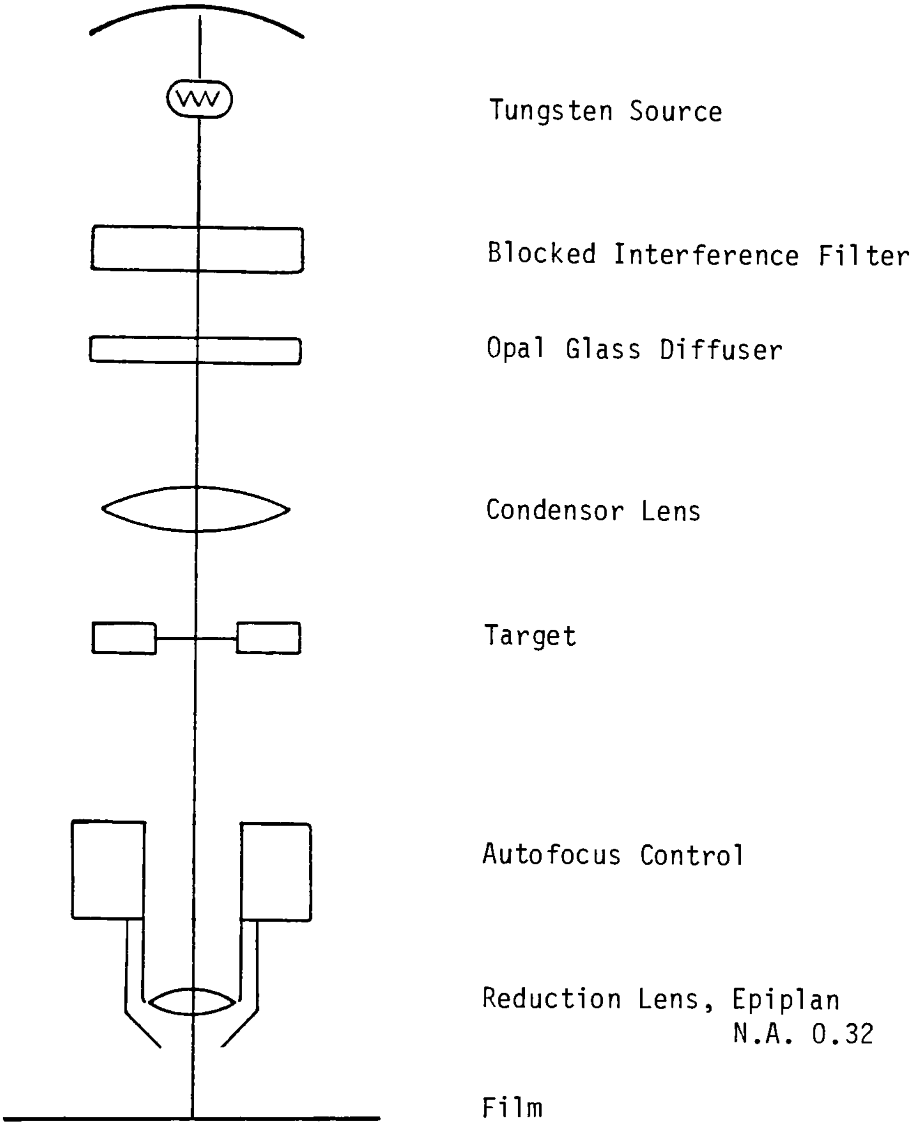

Figure 11. Optical Reduction System Schematic.

At this station, the film platen was stepped in increments of 6.8± 0.1 mm for replicate image exposures along the direction of platen travel. After each platen step, a solenoid controlled hammer secured the platen against a support device to insure (1) an immobile platen and (2) repeatable orientation of the film plane relative to the optical axis. A dwell time of 15 seconds after securing the platen, allowed settling of mechanical vibrations and automatic adjustment of focus prior to image exposure. For eight successive exposures on the film sample this microexposure system produced resolving power measurements at 900± 75 cycles/mm, as determined from 1000:1 contrast USAF 1951 resolution target images on Spectroscopic GS film (Kodak, lot 5063-393).

The orientation of the film plane relative to the optical axis was set by adjusting the platen support relative to the pneumatic autofocus device. With the solenoid controlled hammer activated, both the film surface and a machined surface on the autofocus device were mechanically leveled in orthogonal dimensions. As the optical axis is normal to this machined surface, this procedure provided the best mechanical alignment of the image and film planes.

(d) Sensitometric Exposure: A lamphouse assembly was equipped with a Rodenstock F4.5 enlarging lens for projection imaging the sensitometric target. A 250 Watt, 12 Volt tungsten lamp source was filtered with the same blocked interference filters employed in the micro-exposure lamphouse. The sensitometric target consisted of 10 steps with approximate 0.2 density increments, and was imaged at 2x magnification. When a single sensitometric image was employed (experiments one & two), the increasing density steps were aligned with the platen travel, and the image was placed within 2 cm of the micro image exposures. For experiments three and four, multiple sensitometric exposures were placed on each film sample, with the increasing density steps perpendicular to the direction of platen travel.

(e) Electrodevelopment and Rinse: Two different electrodevelopment and rinse apparatus were employed. The continuous electrode apparatus and the fountain toner apparatus are illustrated in Figure 12 and Figure 13, respectively. For the continuous electrode apparatus, electrodeveloper and rinse solutions were supplied through single slits in a continuous electrode plate. For the fountain toner apparatus, electrodeveloper was supplied through multiple slits in the electrode plate, and rinse was supplied through a separate, single slit. For each of these apparatus, electrodeveloper was drawn from a supply reservoir with a peristaltic pump, and rinse isopar was drawn from another supply reservoir with a gear pump. In both cases, the development electrode spacing was adjusted with micrometer screws that moved the electrodevelopment apparatus relative to the film platen.

The continuous electrode apparatus (Fig. 12) provided uniform electrode spacing during electrodevelopment. The film moved under the electrode at a preset velocity while electrodeveloper was supplied to the developer reservoir at a constant rate. The electrodeveloper entered the development region through a single 0.02 x 2 inch slit oriented with length perpendicular to the direction of platen travel. As the film's leading edge approached the 0.02 x 2 inch rinse slit, an Isopar solution was supplied to the rinse reservoir. Sufficient lead time allowed each reservoir to fill before the leading edge of the platen reached the respective electrode slits. The electrodeveloper and rinse solutions were supplied to respective reservoirs until the film's trailing edge left the electrodevelopment region.

Electrodevelopment time was determined by the length of time for which electrodeveloper was in contact with the image at the film surface. Theoretically, this time was defined as the ratio of the distance between the slits (3 inches) and the associated platen velocity (inches/second). A potential was applied to the electrode for the entire duration of electrodevelopment and rinse application.

The fountain toner apparatus provided a more consistent supply of fresh electrodeveloper simultaneously to all portions of the development region. This apparatus was designed with the electrodeveloper reservoir below the electrode plate, allowing a meniscus of electrodeveloper to be formed above the plate. The film platen moved at constant velocity over the plate while electrodeveloper supply was maintained at a constant rate. According to the electrode design, the electrode spacing was at the

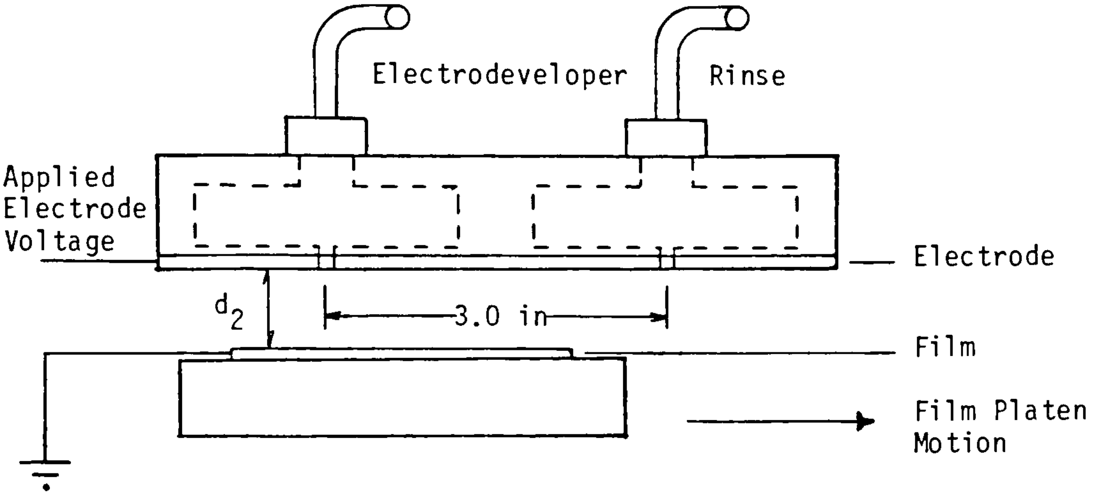

Figure 12. Continuous Electrode Development Apparatus.

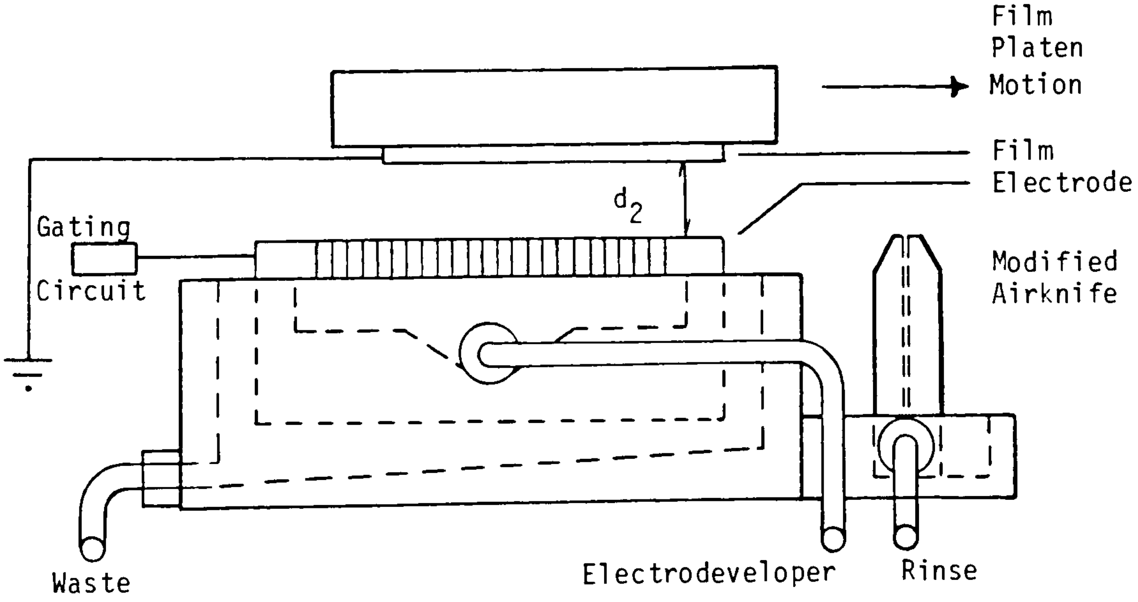

Figure 13. Fountain Toning Development Apparatus.

experimental test level for the first 0.375 inches of film travel into the region. Thereafter, the effective electrode spacing alternated between this level and infinity (no electrode), at 0.10 inch increments along the electrode.

A potential was applied to the electrode using a high voltage power supply (Monroe Electronics, Coronatrol, 152A). An electronic timing circuit was designed to provide preselected gating times for this applied electrode potential. The times of rise and decay in the applied voltage pulse were less than 0.01 seconds, and the pulse duration was monitored using a digital counter (Khronhite #128360). A schematic for the gating circuit is given in Appendix A, Figure A1.

A separate rinse apparatus consisted of an air-knife modified for rinse delivery. In this apparatus, a 0.02 x 2 inch slit was spaced at 0.02 inches from the film surface. Isopar was supplied at a constant rate, forming a "fountain" stream of rinse solution to the film surface.

2. Drying and Fixing

The film sample was aided in drying with the use of a conventional blow dryer before removal from the film platen. Fixing was accomplished off-line with a simple chemical vapor apparatus. This apparatus consisted of a 4 inch diameter metal tray suspended in a water bath at a constant temperature of 100± 5°F. Analytical grade Dichloromethane (MCB Inc., lot 7N31) solvent was placed in the metal tray, and the solvent vaporized at a relatively slow rate. The film sample was attached to a glass plate, which was placed on the rim of the metal tray. In this manner, the film surface received 6 seconds of exposure to the dichloromethane vapors at a distance of 0.30± .10 inches above the surface of the solvent. The vapors fused the carbon/resin electrodeveloper particles to the film's polymeric binder at the film surface. Previous testing for tri-bar resolution (USAF-1951) images indicated that resolution below 500 cycles/mm was not significantly altered by this fixing process.

3. Test Targets

The edge targets employed were National Bureau of Standards (NBS) edge images (generated using X-ray exposures on high resolution spectroscopic film). Two NBS edge targets were employed, with the following nominal density levels and associated modulation factors:

1) Dmin = 0.30, Dmax = 0.80; Modulation 52%
2) Dmin = 0.70, Dmax = 1.65; Modulation 83%

The sinusoidal targets were "Variable Transmittance Sinusoidal Test Objects"[57] (generated using a cylindrical lens to smear a rectangular periodic distribution onto a negative/positive film combination; Eastman Kodak). The test target frequencies employed were nominally 1.50, 3.75, and 6.00 cycles/mm, which translates into 24, 60, and 96 cycles/mm using a 1/16x reduction lens. All targets had nominal modulations at 65%.

4. Reduction Imaging

The test exposure distribution incident at the film surface was determined from the target transmittance distribution and the optical reduction system. The Zeiss microscope objective was assumed to be a linear modulator for the case of incoherent illumination. Other than chromatic aberations, the objective was assumed to be diffraction limited. The incident exposure distribution i(x) was related to the measured target spectrum, F(v), using the expression:

$$i(x) = \mathcal{F}^{-1}\,[F(v)/|OTF(nv)|]$$

In this expression, $\mathcal{F}^{-1}$ denotes the inverse Fourier transform, F(v) is the Fourier spectrum of the target distribution, and OTF(nv) is the Optical Transfer Function for the reduction lens of magnification factor, n. Therefore, higher spatial frequencies associated with image noise in the target spectrum, were effectively reduced by the limiting (OTF) spectrum of the reduction lens.

The OTF for a diffraction limited lens could be calculated[58] as a function of exposing wavelength and defocus. However, if the optical axis is not normal to the target and film planes, the image incident at the film plane could not be characterized using straightforward MTF calculations. The effective focal plane would be located at different distances relative to the photoconductor surface, across the image plane. Along the unvarying image dimension (y) spatially dependent defocus would induce spatially dependent variations in modulation transfer, predominantly for high frequency image components. In the image distribution dimension (x), the effective OTF would introduce phase distortion as a function of spatially dependent defocus. The significance of these optical misalignment effects was assessed for an edge distribution, reduction imaged to the film plane.

A finite amount of dispersion in exposing radiation was expected as a result of image defocus within the photoconductor layer. Assuming that the image and film were coplaner, and the lens was diffraction limited, theoretical geometric defocus indicated the expected OTF modulation loss. An amount of defocus equal to the photoconductor layer thickness (8 um), should produce no less than 50% modulation at image spatial frequencies below 300 cycles/mm. Therefore, exposure spread resulting from uniform defocus within the photoconductor should not have masked nonlinear photoconduction or electrodevelopment transfer characteristics.

To assess the photoconduction mechanism as a function of exposing wavelength, the spectral dependence of the lens OTF was considered. Assuming a diffraction limited lens of numerical aperture 0.32, calculated OTF responses for 440 nm vs. 500 nm indicated the difference in image frequency modulation to be less than 5% at frequencies below 400 cycles/mm. Therefore, image characteristics were not significantly affected by changes in OTF spectra as a function of spectral changes in exposing radiation.

The Zeiss epiplan objective was employed for reduction imaging to maximize uniformity of radial focus in the image plane. However, the lens exhibits second order chromatic aberation[59], which may have produced longitudinal focus shift for the different exposing wavelengths. A through-focus calibration was run for the chosen spectral bands, using the TEP film and a resolution target (USAF 1951, 5:1 CR). The pneumatic autofocus mechanism was adjusted in increments of one pound per square inch (psi), producing approximate distance increments of two microns.[60] The air pressure focus settings that optimized resolution results in each spectral band, were standardized for respective test exposures.

5. Microdensitometer

A Mann-Data Microanalyzer (#4013) was employed for measurement of target and image microdensity distributions. This microdensitometer was equipped with a laser interferometer stage positioning system, providing accuracy of 0.002 microns in reported sampling intervals (Δx). The microdensitometer optics included 10x, N.A. 0.25 influx and efflux objectives (Baush & Lomb). The sampling aperture was physically located between the efflux objective and the photomultiplier, dictating image scanning as opposed to sample scanning. Although this optical assembly was not considered optimal for minimizing partial coherence[61], the linearity of the microdensitometer system was assumed adequate for this study.

The inherent modulation transfer function (MTF) for the microdensitometer system was assumed to remain constant with constant scanning aperature. No corrections were necessary for the edge measurements, as the slit dimensions remained constant for both target and image scans. Scanning slit dimensions differed between sinusoidal target and sinusoidal image scans, requiring corrections for the microdensitometer MTF in each case. The width of the scanning aperture was considered the limiting system parameter for the microdensitometer transfer characteristic. Therefore, an approxmiate microdensitometer MTF was determined in accordance with the slit width, w:

$$\mathrm{MTF}(v) = \sin(wv)/\ wv.$$

The correction function, $1/\mathrm{MTF}(v)$, was employed to remove microdensitometer bias from the measured sinusoidal targets and imagery.

The microdensitometer was calibrated using appropriate uniform density areas provided with the test targets, or a special calibration image produced for the subject TEP/T3 process. The uniform density areas were measured with a MacBeth TD-518 densitometer set to 1 mm circular aperture. Two levels of density were employed for each calibration, near the minimum and maximum levels of microdensity measured on the test targets. Microdensitometer calibration was performed prior to each scanning session, using the appropriate calibration density patches. Maximum error in measured microdensity for the different scanning sessions was estimated to be ± 0.05 density.

All scanning was performed with the Microanalyzer stage velocity set to 2.5 mm/minute. During scanning an electronic filter removed electrical noise above 1000 Hertz, from the photomultiplier signal. At this stage velocity, the electronic filter did not alter the amplitudes of image frequencies below 400 cycles/mm. Noise associated with the measured image microstructure was averaged within the effective scanning aperture. Although random image fluctuations could have been reduced by increasing the slit length, a shorter slit length (70 microns) was employed to reduce modulation loss associated with slit misalignment.[62] Raster scanning allowed detection and correction of slit misalignments. Images were rescanned when the measured response (D vs. x) drifted more than 2 microns over a 150 micron translation distance (y axis).

6. Input Exposure Calibration and Optical Alignment Test

For the purposes of linearity testing, the edge input exposure was checked for (1) symmetry of the distribution with respect to the edge center, and (2) lack of input adjacency effects. The actual input exposure distribution at the film plane was not directly measured. However, the NBS edge target transmittance was measured, and a silver halide film was employed as a photometer for assessing the linearity of an optically reduced edge distribution in the film plane.

(a) Microdensitometer Scans

The NBS (83% modulation) edge target was measured using the microdensitometer in a raster scanning configuration. Each of the density traces were converted to transmittance, and the edge distributions were examined for symmetry and lack of adjacency effects. The silver halide reduction image was scanned in corresponding locations along the edge, i.e. with the translation interval between scans reduced by $\Delta y/16$. Microdensitometer raster scanning configurations for the NBS edge and reduction imaged test edges are illustrated in Figure 14. The scanning parameters for the raster set are listed in Table 6.

The sinusoidal test targets were assumed to be spatially invariant with translation in the unvarying target dimension. The microdensitometer was used to make one scan for each target (y dimension). The calibration densities were 0.29 and 1.65, measured with the Macbeth TD-518 on uniform density patches supplied with the targets. The scanning parameters for each target are listed in Table 6.

Each microdensitometer scan was converted to transmittance, and subsequently processed using a sinewave analysis program.[63]

The program included data interpolation and a Fast Fourier Transform (FFT) routine, providing the following outputs:

(1) Fundamental frequency (first harmonic) in cycles/mm

(2) Modulation of the fundamental frequency

(3) Harmonic percent distortions for second through fifth harmonics, normalized to the fundamental

(4) Signal to Noise ratio, with noise represented by the square root of the sum of squares for all frequency amplitudes computed above the fundamental frequency.

7. Output Effective Exposure

(a) Microdensitometer Scans

Both edge and sinusoidal images produced on the electrophotographic film samples were raster scanned using the microdensitometer system. Figure 14 illustrates the locations of scans on edge images produced in the first two experiments. Figure 15 illustrates the locations of scans for edge images produced in the third experiment. Sinusoidal image scanning was performed in the same configuration employed for experiment three edges, except for the scan lengths. Scanning parameters for all images are listed in Table 7. Calibration densities for all scans were 0.29 and 1.67. Translations between scans (Δy) were 40.0 microns, so that alternate scan numbers represented independent microdensity traces relative to the scanning aperture.

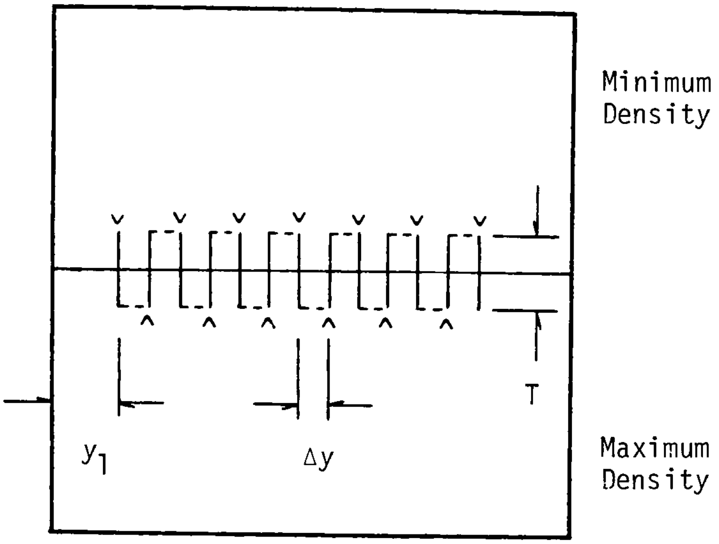

Figure 14. Microdensitometer Scanning Configuration for Target Edge, Optical Alignment Test Image, and Electrophotographic Images of Experiments Three and Four.

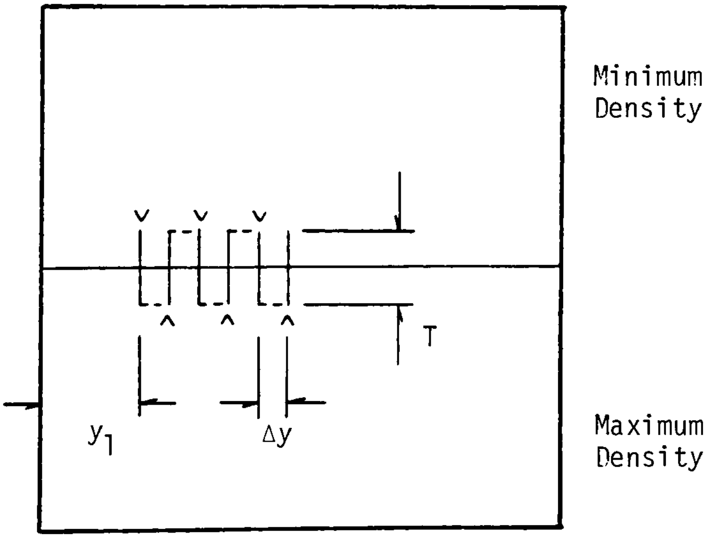

Figure 15. Microdensitometer Scanning Configuration for Electrophotographic Images of Experiments One and Two.

Table 6. Microdensitometer Scanning Parameters for (a) NBS Edge Target and Optical Alignment Test Image, (b) Sinusoidal Targets.

(a)

Specimen	Calibration Densities	Number of Scans	Scan Aperture (microns)	Sampling Interval Δx (microns)	Scan Length T (microns)	Starting Location y1 (microns)	Translation Distance Δy (microns)
NBS Edge 83% Mod.	0.65 1.70	13	2. x 70	1.00	64.0	880	640
SO-192 Edge Image #10-30	0.36 1.30	13	2. x 70	1.00	64.0	55	40

(b)

Sinusoidal Targets Frequency: (cycles/mm)	Calibration Densities	Number of Scans	Scan Aperture (microns)	Sampling Interval Δx (microns)	Scan Length T (microns)	Starting Location y1 (microns)	Number of Cycles Total
1.50	0.34 1.27	1	15.3 x 184	4.00	4000	2640	6
3.75	0.34 1.27	1	15.3 x 184	4.00	4000	2840	14
6.00	0.34 1.27	1	15.3 x 184	4.00	4000	2800	24

Table 7. Microdensitometer Scanning Parameters for Electrophotographic Images

Specimens	No. of Scans	Scan Aperture (microns)	Sampling Interval Δx (microns)	Scan Length T (microns)	Starting Location y_1 (microns)
Experiment 1 10-8 Edges.....	6	2 X 70	0.32	162.3	95
Experiment 2 1-19 & 1-22 Edges..........	6	2 X 70	0.32	162.3	95
Experiment 3 7-15 & 7-16 Edges..........	13	2 X 70	1.00	64.0	55
Experiment 4 7-17 Sinusoidal					
25 cycles/mm	13	2 X 70	1.00	300.0	55
64 cycles/mm	13	2 X 70	1.00	200.0	55
102 cycles/mm	13	2 X 70	1.00	200.0	55

(b) Ensemble Averaging

Random signal fluctuations and microstructure noise in the microdensity distributions were reduced by ensemble averaging three independent scan records for each image. The independent scans were considered to be unbiased estimators for the characteristic image response. Assuming the image noise to be wide-sense stationary, ergodic, and Gaussian distributed, the signal to noise ratio (S/N) should be improved by emsemble averaging. In accordance with the Central Limit Theorem, three unbiased estimators for the mean microdensity response with zero mean and variance σ^2, should have provided a factor of $\sqrt{3}$ increase in S/N.[64]

(c) Edge Data Reduction

A computer program was written to perform the following operations for edge microdensity scans:

(1) Translate independent scans (D vs x) from microdensity to effective exposure, using sensitometric density vs. log exposure data and linear interpolation.

(2) Ensemble average a number of effective exposure distributions (E vs x) corresponding to scan locations denoted 1, 3, & 5 in the raster set for experiments one and two; 7, 9, 11 for experiments three and four. This procedure was accomplished by adding effective exposure values at corresponding point numbers and dividing by three. The resulting ensemble average effective exposure distribution represented the edge response function for a given experimental image.

(3) Convolve the ensemble average effective exposure distribution with a rectangle of width equal to an odd integer number (n) of Δx. Save only the resulting average values at the center of each interval $n\Delta x$. This routine was applied to the microdensitometer scans of experiments one and two, in order to provide approximate equivalence to sampling intervals used in experiments three and four. With the integer set to three, sampling intervals: Δx=0.96 microns were obtained for effective exposure edge responses of experiments one and two.

(4) Determine the center of each edge response distribution based on the sum of minimum and maximum effective exposure levels divided by two. The maximum and minimum values were computed as the average of the first 21 and last 21 effective exposure values in the 64 point scan.

(5) Locate the computed edge center at the center point in a 41 point array. The centered and truncated effective exposure distribution defined the edge response vector, to be employed in subsequent characteristic vector analysis.

(d) Sinusoidal Data Reduction

Independent microdensitometer traces selected from the raster set were entered into a sinusoidal analysis program. This program accomplished the following:

(1) Translation of microdensity response to effective exposure using the appropriate sensitometric H&D table and linear interpolation.

(2) Ensemble averaging for the three effective exposure distributions.

(3) Fourier transformation of the ensemble average distribution, using a portion of the distribution representing an integer number of cycles. The number of cycles analyzed was constant for all responses of the same sinusoidal test frequency.

(4) Computations for modulation, S/N, and harmonic distortions as defined previously (pp. 14 and 83).

8. Response Variables

The method for characterizing edge response independent of adjacency effects, consisted of representing edge distributions as a series of orthogonal vector components. For a given set of edge response vectors, a unique set of vector components was derived using the method known as characteristic vector analysis, or principle component analysis. This multivariate statistical analysis technique, exemplified by Simonds[65], provided a set of vector components (basis vectors) and associated coefficients which explained variations among each experimental set of edge vectors. The vector components (eigenvectors) were extracted from a calculated covariance matrix, with an indication of percent variability (covariance) explained by each component. For each edge transfer experiment, the calculated coefficients of component vectors served as response variables. Components which explained greater than 2.5% variability in the original vector set, were analyzed for correlation with the experimental parameters. The influence of correlated vectors on the mean vector response, were determined by adding and subtracting that particular component to the mean vector.

The response variables for sinusoidal image transfer analysis were harmonic distortion factors computed from the ratio of output to input harmonic percent distortions. The computation for input harmonic percent distortion included correction factors for both the exposure reduction lens and the microdensitometer system. The computation for output harmonic percent distortion included a correction factor for the microdensitometer. Harmonic distortion factors were computed for second and third harmonics of each fundamental frequency as measured in the image plane. The equations for computing these harmonic distortion factors were:

Input Harmonic Percent Distortion:

$$IH\%D_k = \left[\frac{C_{kf}^{*}C_{kf}}{C_f^{*}C_f}\right]^{1/2} \left[\frac{|OTF(nkf)|}{MTF_i(kf)}\right] \times 100$$

Output Harmonic Percent Distortion:

$$OH\%D_k = \left[\frac{C_{kf}^{*}C_{kf}}{C_f^{*}C_f}\right]^{1/2} \left[\frac{1}{MTF_o(kf)}\right] \times 100$$

Harmonic Distortion Factor:

$$HDF_k = \left[\frac{OH\%D_k}{IH\%D_k}\right] \times 100$$

where: $k = 2,3$ (second and third harmonics)
n = magnification factor for the imaging lens.

As explained in the theoretical basis, C_f denotes the coefficient of the fundamental frequency and C_{kf} denotes the coefficient of the harmonic at k times the fundamental frequency. The OTF for the reduction lens and the MTF for the microdensitometer were theoretically obtained, as described in the apparatus and techniques section.

The OTF modulus spectrum for the reduction lens was computed for 500 nm wavelength and 0.32 numerical aperture. The magnification factor (n) was determined from the average ratio of measured output to input fundamental frequencies. The MTF spectrum for the microdensitometer system employed to scan the targets, was computed using the 15.3 micron width scanning aperture. The MTF spectrum for the microdensitometer system employed to scan the electrophotographic images, was computed using the 2.0 micron scanning aperture. The modulus values associated with the measured harmonic frequencies were employed in the above computations for input and output harmonic percent distortions.

D. Experimental Statistics

For each of the experiments, significance of experimental parameters was analyzed relative to experimental error. All experiments contained two replicate image responses for each experimental treatment. Coefficients of each basis vector corresponding to the original edge vectors, were employed for analysis of variance (ANOVA) in experiments one, two, and three. The mean square and F statistics were calculated for all experimental factors and their first order interactions. The computed F statistics were compared with table F statistics[66] to determine the confidence for significance. There were no missing data points (response variables) for the edge experiment ANOVAs.

For experiment four, the harmonic distortion factors for second and third harmonics of each input sinusoidal frequency were employed for statistical calculations. For input fundamentals at 25 and 64 cycles/mm, there were no missing data points (response variables). Analyses of variance were conducted according to standard procedures for the cited response variables. For the input fundamental at 102 cycles/mm, two of the 16 response variables were not obtained as a result of severe anomalies in the resulting images. "Dummy" values were computed using the mean of the remaining response variables in the associated Applied Voltage Time column.[67] Analysis of variance for this case was conducted with a loss of two degrees of freedom associated with the error sum of squares.

III. RESULTS

A. Input Exposure Distributions

1. Targets

The transmittance distribution at y axis increments along the NBS 83% modulation edge target are shown in Figure 16. These edge traces indicated that the input edge distribution was uniform in modulation over the region of interest. The transmittance distributions confirmed the symmetry of the input edge with respect to the edge center, and the lack of input adjacency effects. The single transmittance traces for each sinusoidal target are illustrated along with their respective FFT spectra in Figures 17 through 19. The modulation, S/N, and harmonic percent distortions for second and third harmonics were tabulated for each target frequency in Table 8. The harmonic percent distortions for second and third harmonics of for all sinusoidal targets were less than 5 percent.

Table 8. Sinusoidal Target Measures Derived from Fourier Transformed Target Transmittance Distributions

Fundamental Frequency (cycles/mm)	Fundamental Modulation	S/N	Second Harmonic	Third Harmonic
1.5D	63.1	16.6	0.87%	2.58%
3.75	64.0	14.7	2.10%	4.51%
6.00	63.7	13.3	4.53%	2.80%

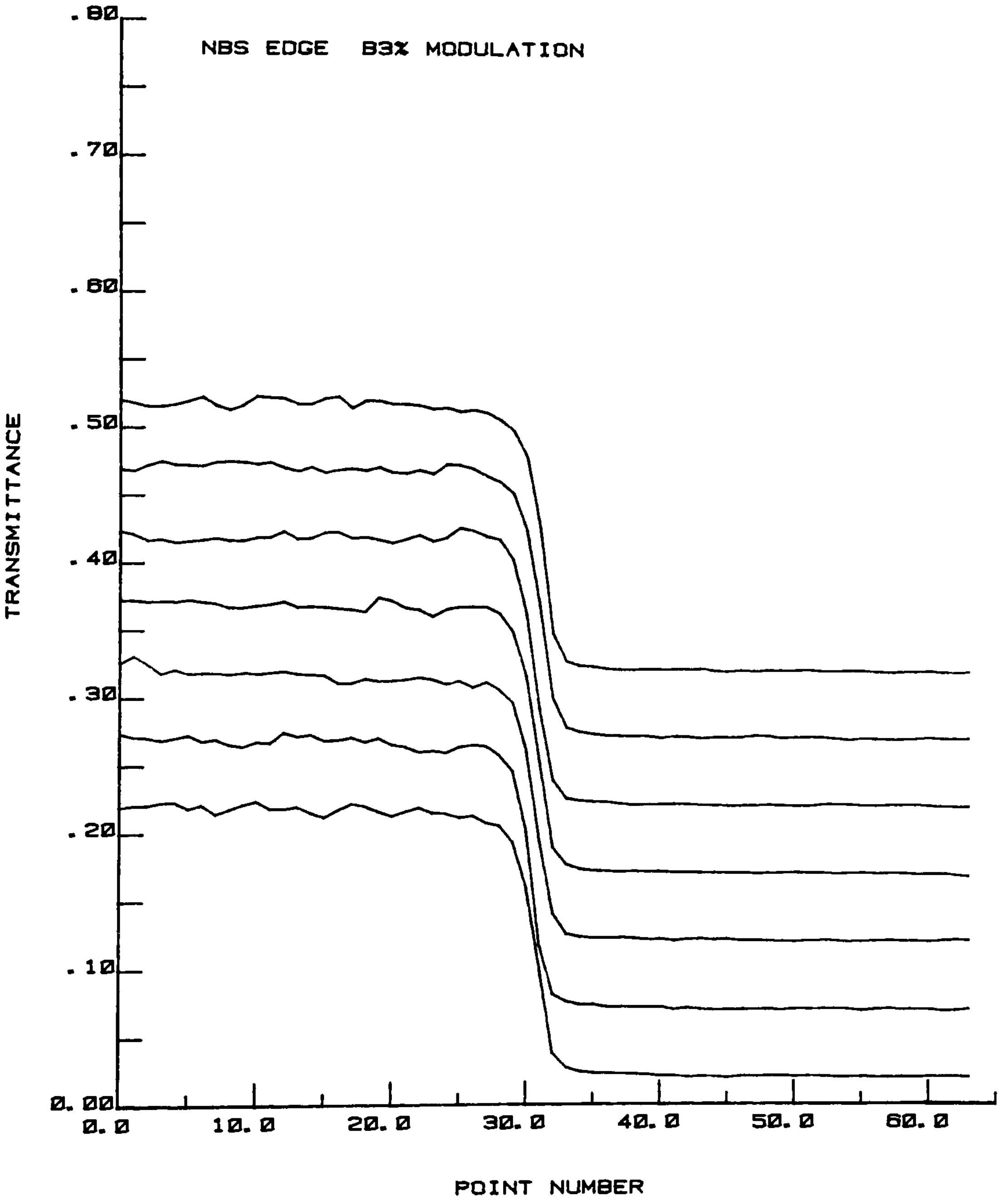

Figure 16. Edge Target Transmittance Distributions for Y Axis Translations. NBS edge, 83% modulation. Individual scan traces cascaded with Δ transmittance = 0.05.

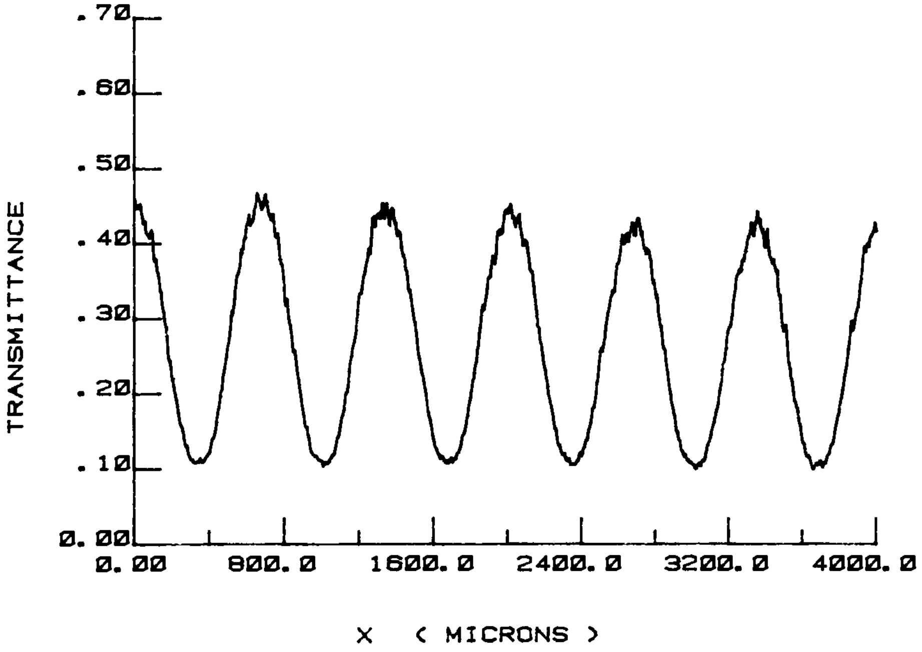

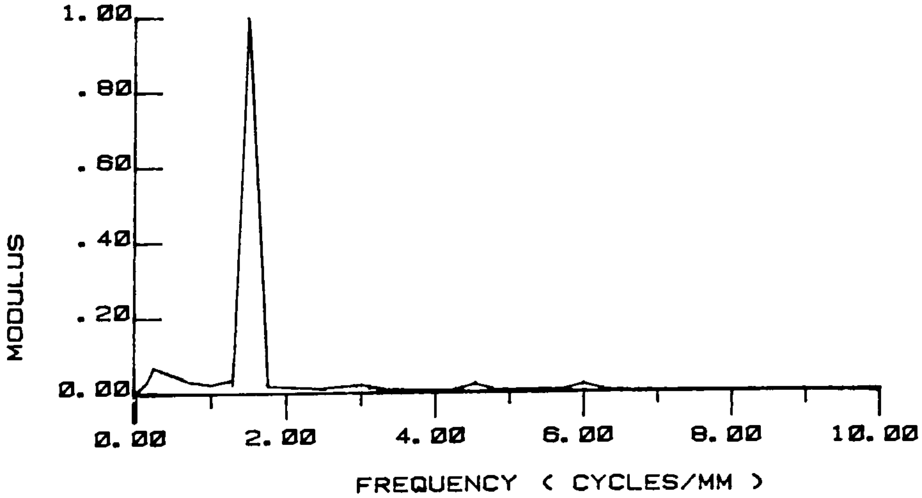

Figure 17. Sinusoidal Target Transmittance Distribution and Fourier Spectrum Frequency 1.50 cycles/mm. Modulus in Fourier Spectrum Normalized to 1.0 at the Fundamental.

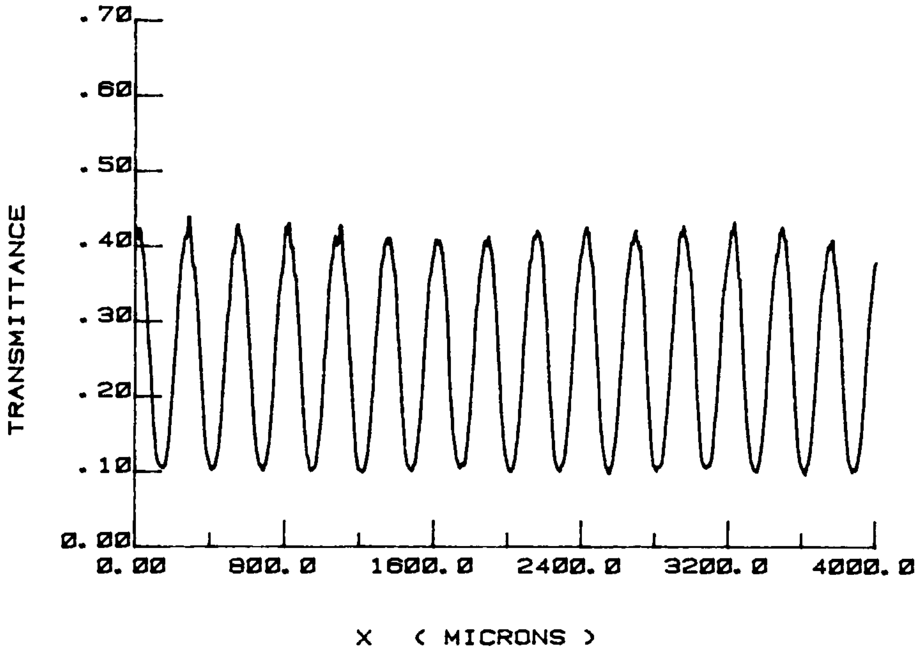

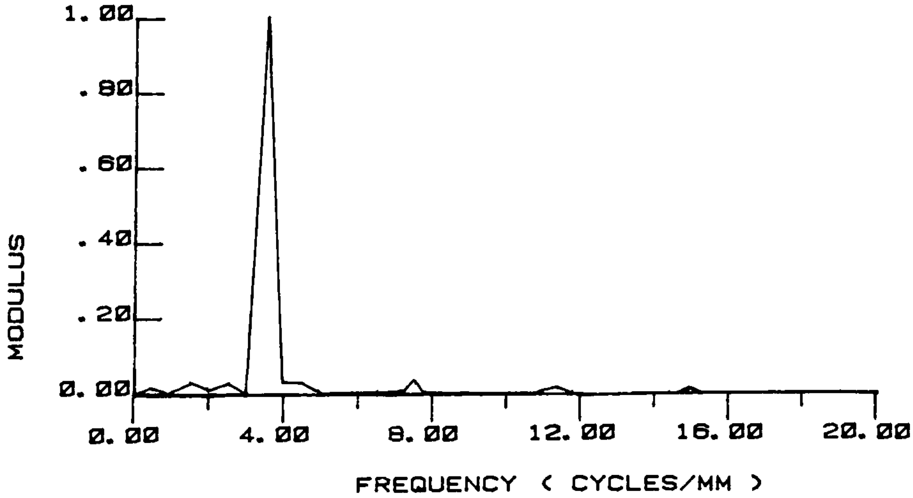

Figure 18. Sinusoidal Target Transmittance Distribution and Fourier Spectrum, Frequency 3.75 cycles/mm. Modulus in Fourier Spectrum Normalized to 1.0 at the Fundamental.

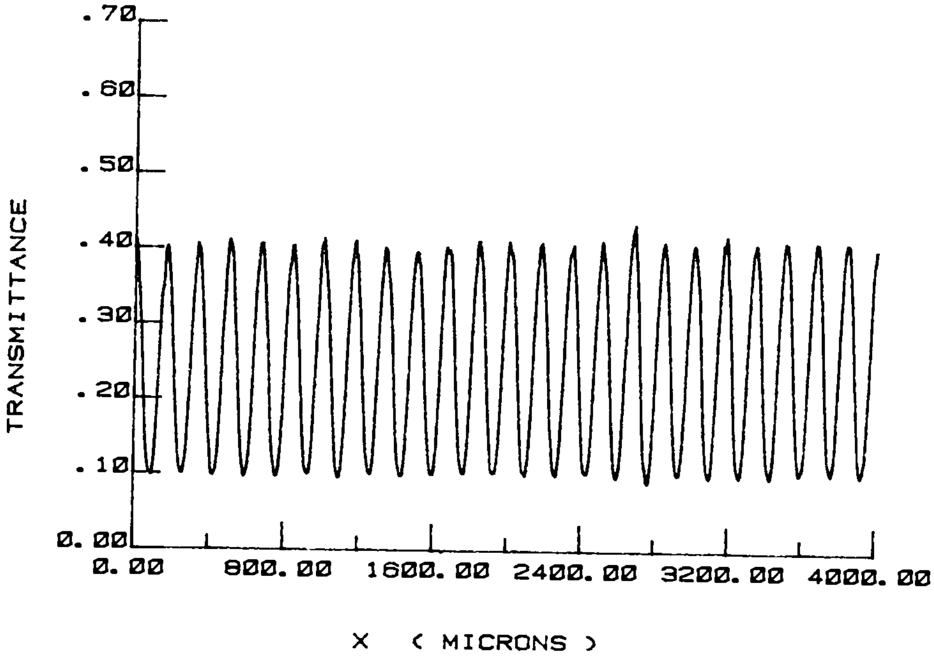

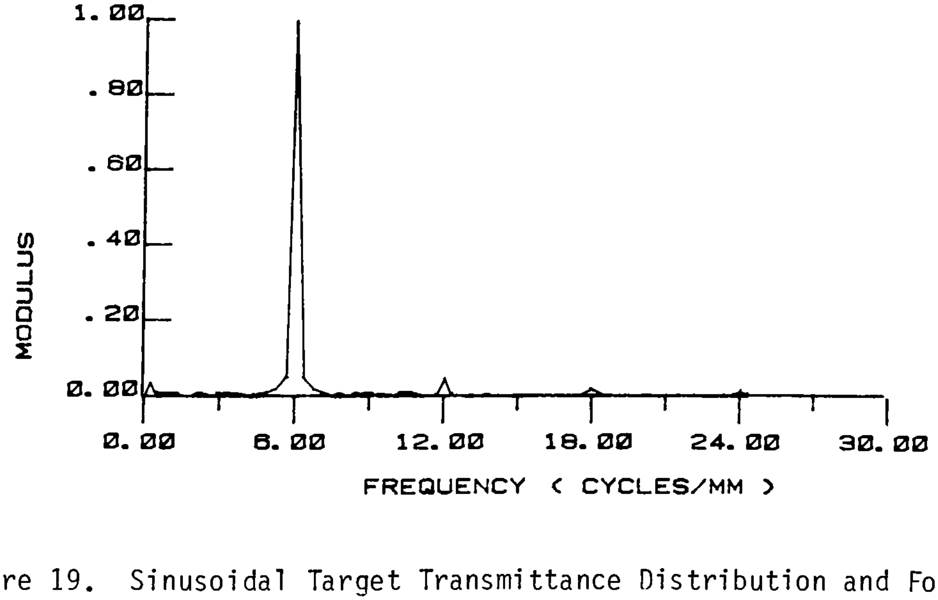

Figure 19. Sinusoidal Target Transmittance Distribution and Fourier Spectrum, Frequency 6.00 cycles/mm. Modulus in the Fourier Spectrum Normalized to 1.0 at the Fundamental.

2. Reduction Lens Optical Alignment

Effective exposure distributions for the reduction edge image on SO-192 film are shown in Figure 20. These distributions were obtained by conversion of microdensity traces, at 40 micron translations along the y axis, through the appropriate SO-192 sensitometric curve. The individual distributions were artificially cascaded along the effective exposure axis of the graph, with the increment: ΔExposure = 150. For analysis of effective defocus with y translations across the image plane, a measure for the variations in edge response was employed. Edge widths served as an estimate for edge gradients, and were computed based on the central 70% of the effective exposure edge modulation. Figure 21 illustrates the edge width variation as a function of distance along the image y axis, as well as a linear regression for edge width points. The linear regression of edge width on distance indicated less than 10% edge width change along the y image axis.

For analysis of optical misalignment along the x axis, evidence of effective defocus represented by phase distortion was sought in the effective exposure edge distributions. Visual examination of the edge distributions in Figure 20 revealed no significant asymmetrical responses with respect to the edge centers. A lack of asymmetrical responses in the x dimension and negligable variations in edge width along the y dimensions, indicated that the optical axis was sufficiently aligned with the normal axis of the film plane. All input target distributions were therefore

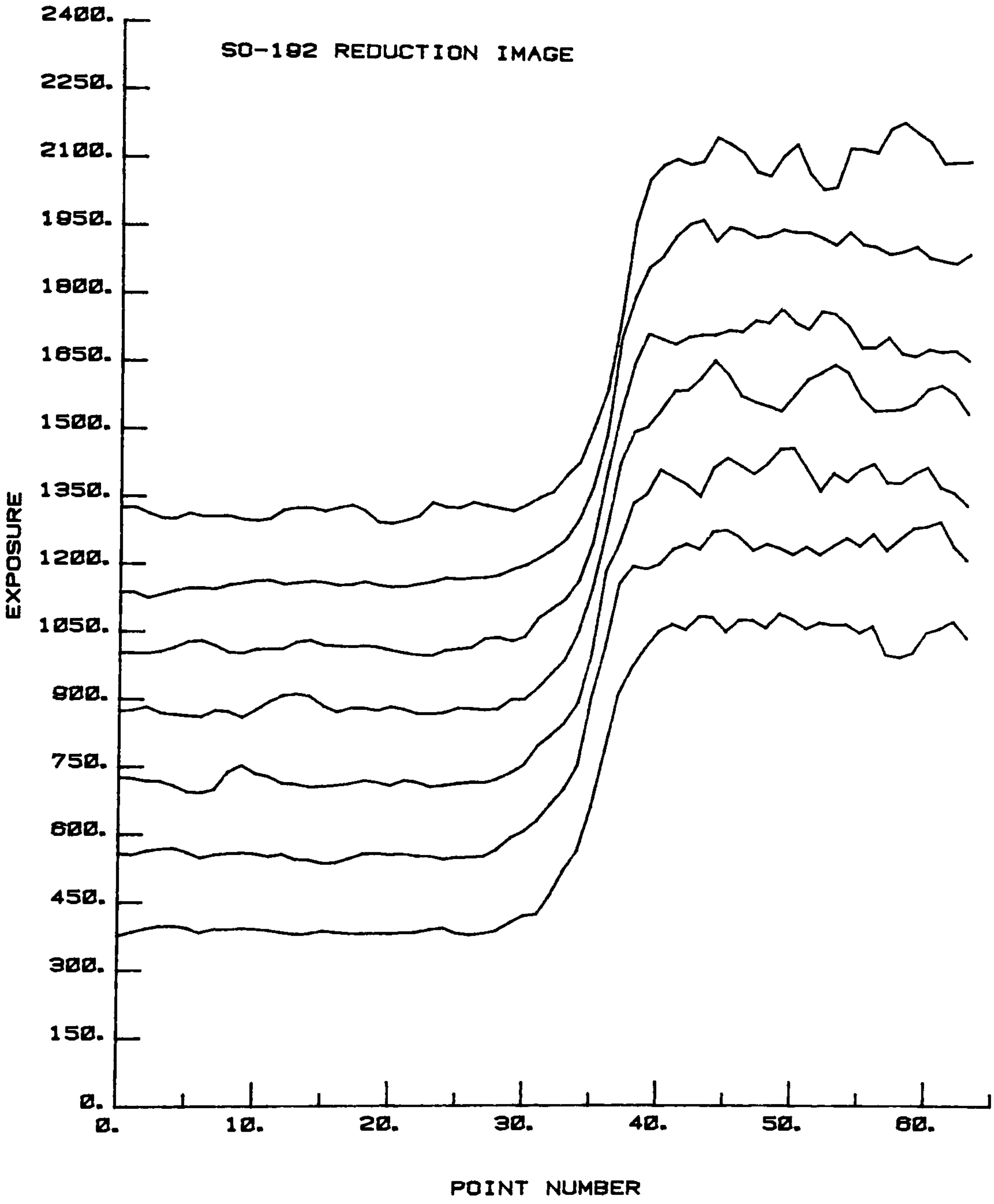

Figure 20. Edge Effective Exposure Distributions for Y Axis Translations, SO-192 Reduction Image.

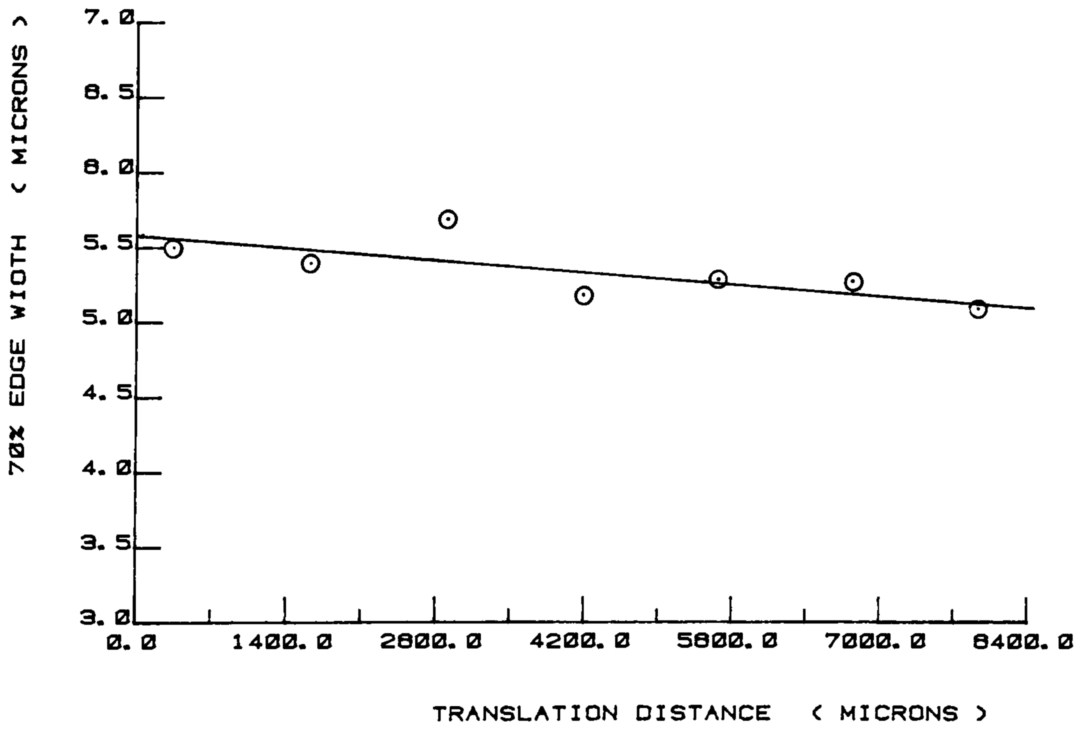

Figure 21. Edge Width Variations with Y Axis Translations for Optical Alignment Test Image.

considered to be linearly and uniformly reduced by the micro-exposure reduction lens.

B. Results for Experiment One

Sensitometric responses for the 2^3 screening experiment were grouped according to exposing wavelength, as shown in Figures B1 and B2 in Appendix B. The test image densities for all edge responses were within the range: 0.30-0.90. No significant variability was noted in the corresponding sensitometric responses in this density range, for the tested factor variations. Effective exposure edge response vectors are included in Appendix B, Figures B3-B6, with responses grouped according to levels of film velocity and exposing wavelength tested.

Characteristic vector analysis applied to the 16 edge response functions produced the mean and basis vector components shown in Figure 22. Percentages of total variability explained by each of the basis vectors were: $V(1)=91.5\%$, $V(2)=4.2\%$, and $V(3)=2.2\%$. Coefficients of basis vectors that correspond to original edge response vectors, were tabulated in the experimental design matrix. In this manner, separate matrices of coefficients for basis vectors $V(1)$ and $V(2)$ are shown in Table 9. As vector $V(3)$ explained less than 2.5% of the total variability, it was considered to represent experimental error and was not analyzed for statistical correlation with experimental factors.

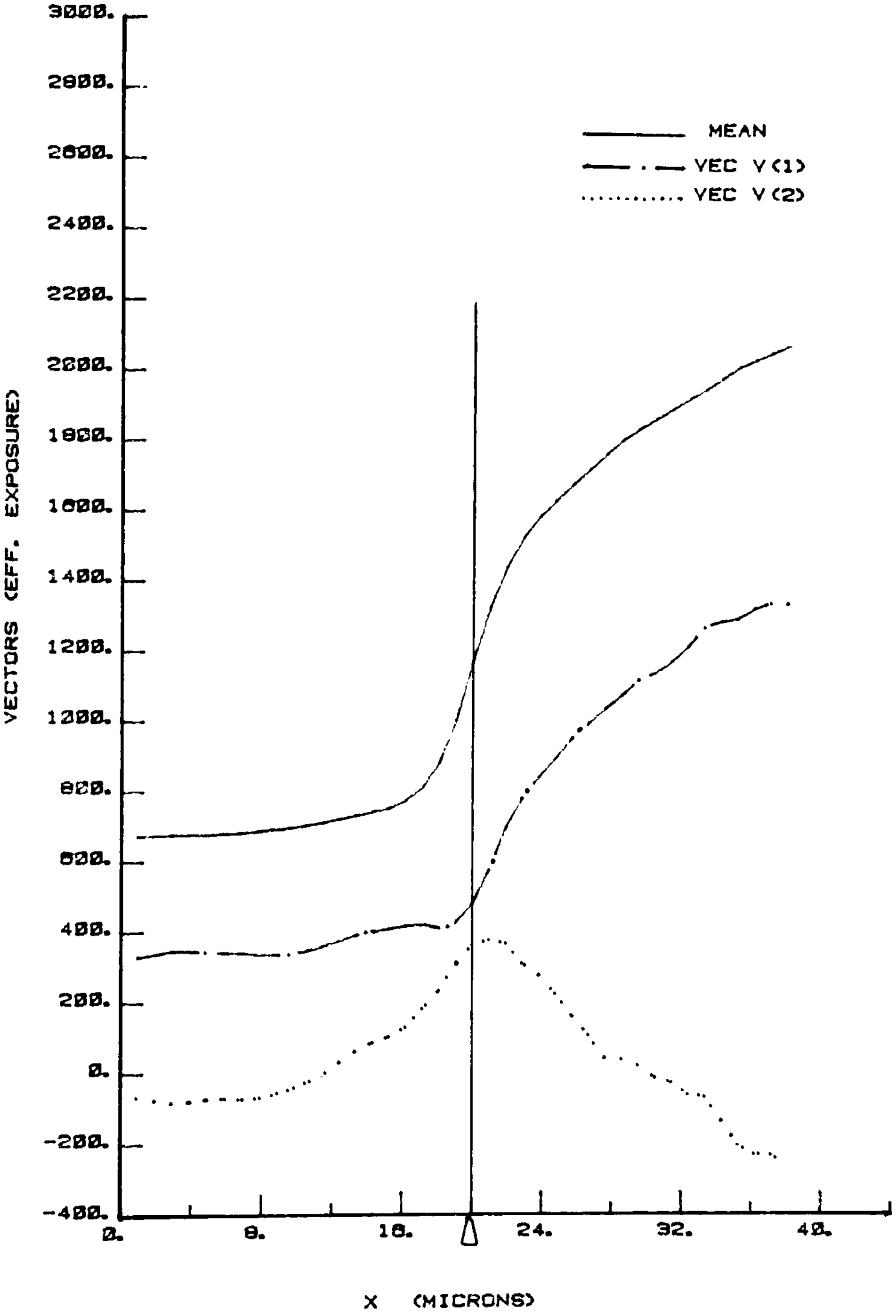

Figure 22. Mean and Basis Vectors for Experiment One Edge Responses.

Table 9. Basis Vector Coefficients for Experiment One Edge Responses. Averages of vector coefficients according to each parameter level are included below individual coefficient value matrices.

(a) Vector V(1) coefficients: a_1

		Development Electrode Spacing (mm)			
		0.20		1.27	
		Film Platen Velocity (in/sec)		Film Platen Velocity (in/sec)	
		0.6	0.3	0.6	0.3
Exposing Wavelength (nanometers)	440	-0.73	0.20	0.09	-0.04
		0.10	0.09	0.27	0.08
	500	-0.18	-0.32	0.21	0.06
		-0.04	-0.19	0.28	0.13

Exposing Wavelength	440 nm: 0.06 , 500 nm: -0.05
Development Electrode Spacing	0.20 mm: -0.13 , 1.27 mm: 0.14
Film Platen Velocity	0.6 in/sec: 0.0 , 0.3 in/sec: 0.0

(b) Vector V(2) coefficients: a_2

		Development Electrode Spacing (mm)			
		0.20		1.27	
		Film Platen Velocity (in/sec)		Film Platen Velocity (in/sec)	
		0.6	0.3	0.6	0.3
Exposing Wavelength (nanometers)	440	-0.26	0.43	0.25	0.30
		-0.09	0.28	0.01	0.06
	500	-0.15	-0.20	-0.46	-0.12
		0.03	-0.09	-0.46	-0.11

Exposing Wavelength	440 nm: 0.12 , 500 nm: -0.12
Development Electrode Spacing	0.20 mm: 0.07 , 1.27 mm: -0.07
Film Platen Velocity	0.6 in/sec: -0.14 , 0.3 in/sec: 0.14

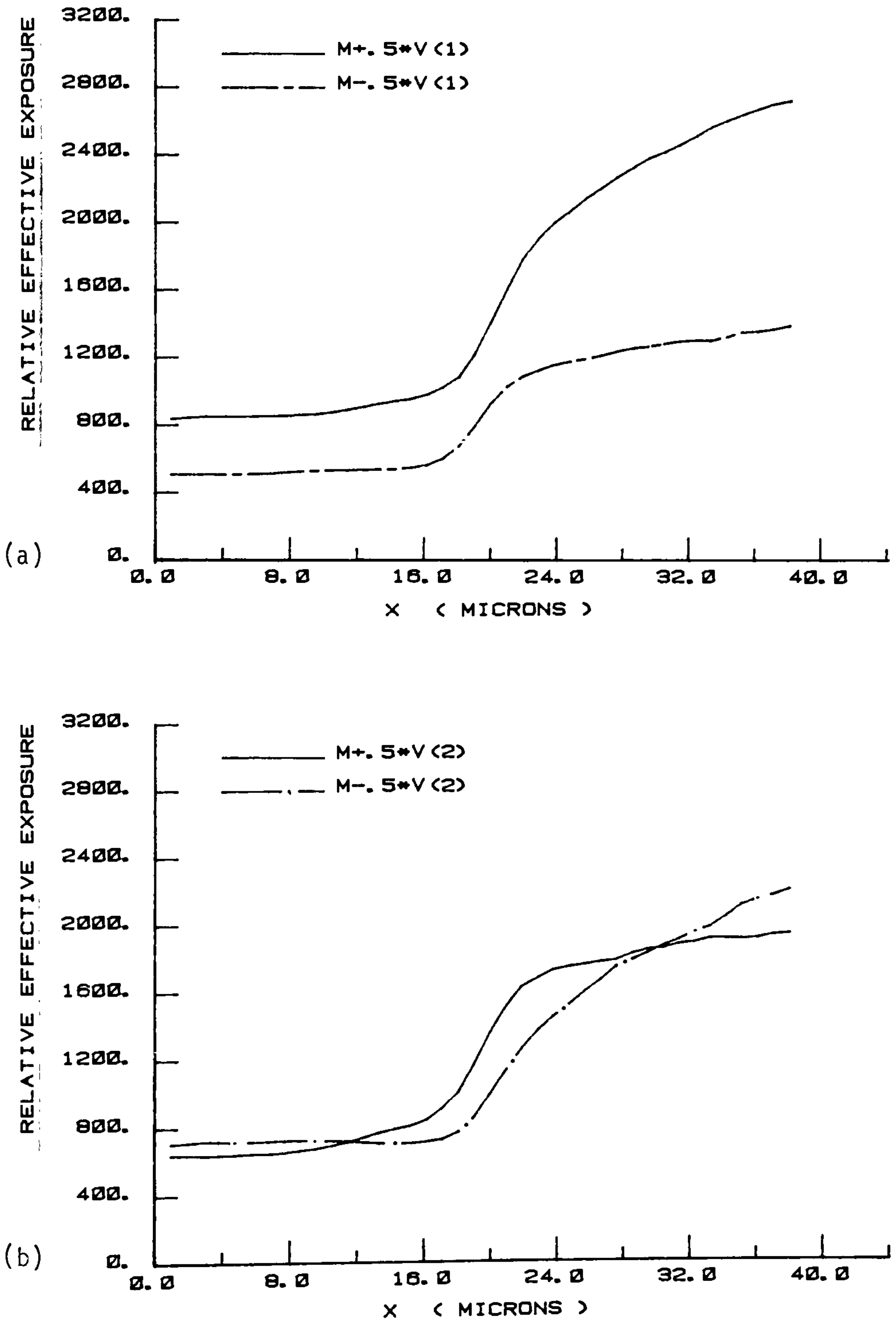

Figure 23. Variation in Edge Response Associated with Coefficient Shifts, Experiment One Vectors: (a) Vector V(1); (b) Vector V(2).

The contributions of each basis vector to the experimental edge response were determined by adding the basis vectors to the mean vector, in proportion to coefficient values of ± 0.5. Although these coefficient values exceeded the range of average experimental coefficients, they were chosen to emphasize the influence of basis vectors on the mean response vector. This approach allowed an assessment for the trends in edge response symmetry as a function of experimental parameter variation. For experiment one, Figure 23 illustrates the resulting edge responses for additions of ± 0.5V(1) and ± 0.5V(2) to the mean edge vector.

Analysis of variance for vector V(1) coefficients indicated significance of this vector with respect to electrode spacing (α=0.05). The average values for coefficients grouped according to electrode spacing (DES) were: a_1=-0.13 at DES=0.20 mm and a_1=+0.14 at DES=1.27 mm. Referring to Figure 23(a), positive coefficients at the higher electrode spacing increased the degree of asymmetry, average effective exposure level, and modulation in the edge response function. At the lower electrode spacing, negative coefficients were noted to decrease asymmetry of the edge response, as well as lower the average exposure level and modulation.

The asymmetry observed for the higher electrode spacing could be described as a reduction in effective particle deposition vs. image charge density at the high spatial frequency components. This form of asymmetry was contrary to the expected form exhibiting reduction in deposition vs. charge at lower spatial frequency components in the distribution. Proportionately lower deposition to the lower spatial frequency components would characterize the adjacency effects expected for localized nonlinear depletion upon image transfer. Both the observed and expected forms of asymmetry could be characterized as microsensitometry variation, i.e. frequency dependent, nonlinear deposition vs. image charge density. However, the term adjacency effects was chosen to describe only nonlinear reductions at lower frequency components.

Analysis of variance for vector V(2) coefficients indicated significance of this vector with respect to wavelength (α=0.01), and film platen velocity (α=0.01). The effects of vector V(2) on the mean response vector were noted as a change in edge response symmetry, and an apparent shift in edge response along the x axis (Figure 23(b)). Averaging coefficients according to the levels of each factor indicated that (1) increasing the absorption coefficient and (2) increasing the film platen velocity, produced equivalent amounts of asymmetry in the edge response. The average value for coefficients a_2 summed at each wavelength, shifted from +0.12 at exposing wavelength: 440 nm, to -0.12 at exposing wavelength: 500 nm. The average value for coefficients summed at each velocity, shifted from -0.14 for velocity 0.6 inches/second to +0.14 for velocity 0.3 inches/second.

The apparent shift in edge response along the modulating image dimension (x axis), was caused by errors in aligning the edge distributions prior to characteristic vector analysis. Averaging the first one-third and last one-third of each edge distribution for the minimum and maximum response levels, produced an artificial shift in edge centers among the experimental edge vectors. The apparent shift did not represent phase shifts or phase distortions upon image transfer for this experiment.

C. Results for Experiment Two

Sensitometric H & D curves revealed limited dependence of large area deposition on the electrode spacing and velocity parameters. For electrode spacings 0.20 and 0.60 mm, H & D responses for all film velocities were essentially equivalent below 0.6 density. For electrode spacing 1.27 mm, density response increased at all exposure levels with decreasing test velocity. Slower macroscopic deposition rates to the sensitometric exposure steps were noted for the 1.27 mm electrode spacing, within the tested levels for film platen velocity. Figure C1 through C3 in Appendix C illustrate the sensitometric curves, grouped according to test levels for electrode spacing.

Effective exposure edge responses exhibited edge effects for certain samples, but no consistent trends were noted by observation alone. Edge response vectors were grouped according to tested velocity levels, in Figures C4 through C6 of Appendix C.

Characteristic vector analysis applied to the 24 edge response vectors, produced mean and basis vectors illustrated in Figure 24.

Percent of total variability explained by basis vectors were for vector V(1): 94.5%, vector V(2): 2.6%, and vector V(3): 1.3%. As vector V(3) explained less than 2.5% of the total variability, it was considered to represent experimental error and was not analyzed for statistical correlation with experimental factors. Coefficients for the first two vectors were tabulated in the experimental design matrix, as shown in Table 10. Influence of individual basis vectors on the mean response vector were determined by adding and subtracting each basis vector to the mean vector. Figure 25 illustrates the effects of ±0.5 V(1) and ±0.5 V(2) on the mean vector. The arbitrary coefficients ±0.50 were chosen to illustrate the total range of alterations produced by each basis vector on the mean response vector.

Analysis of variance applied to coefficients a_1 indicated that variations associated with vector V(1) were correlated with velocity ($\alpha = 0.01$) and an electrode spacing/velocity interaction term ($\alpha = 0.01$). Vector V(1) explained alterations from the mean response indicative of adjacency effects for positive a_1 values. In proportion to negative a_1 values, vector V(1) altered the mean response to an approximately symmetrical response indicative of linear image transfer. The trends in coefficients as a function of significant parameters were analyzed with the aid of Figure 26. In this figure the replicate coefficient values and their averages (for each experimental treatment) were plotted as a function of tested velocity levels. Nominal electrodevelopment times

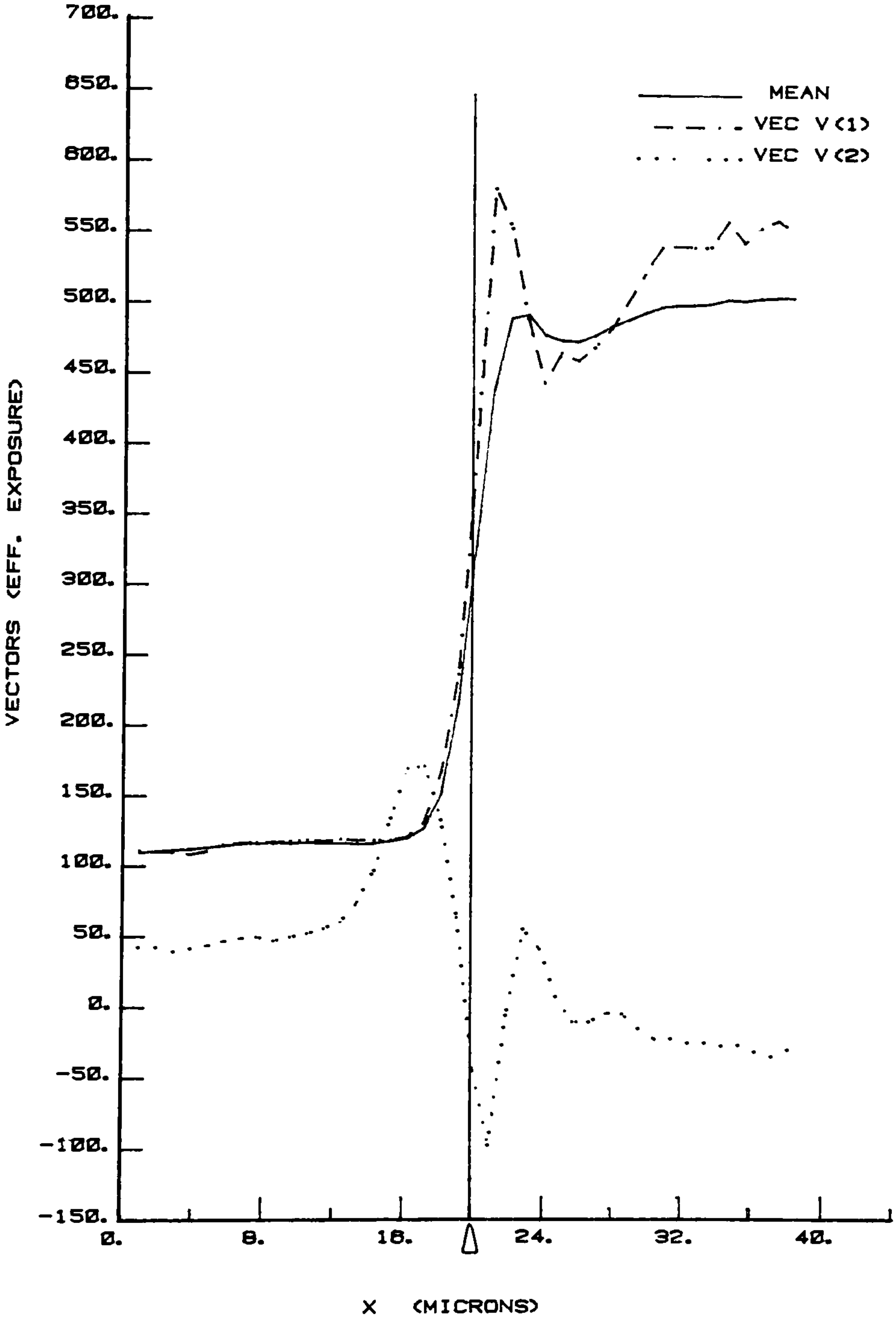

Figure 24. Mean and Basis Vectors for Experiment Two Edge Responses.

Table 10. Basis Vector Coefficients for Experiment Two Edge Responses

(a) Vector V(1) coefficients: a_1

		Development Electrode Spacing (mm)		
		0.20	0.60	1.27
Film Platen Velocity (in/sec)	3.0	0.30 -0.10	0.07 0.16	0.51 0.46
	1.5	0.00 -0.70	0.02 -0.02	0.07 0.18
	0.6	-0.38 -0.17	-0.07 0.03	-0.21 -0.12
	0.3	0.16 -0.19	0.03 0.04	-0.37 -0.06

(b) Vector V(2) coefficients: a_2

		Development Electrode Spacing (mm)		
		0.20	0.60	1.27
Film Platen Velocity (in/sec)	3.0	-0.08 -0.24	0.22 -0.05	-0.13 -0.32
	1.5	-0.07 -0.10	0.45 -0.01	-0.04 0.10
	0.6	-0.18 -0.07	0.11 0.32	-0.14 -0.24
	0.3	-0.19 -0.04	0.14 0.49	-0.11 0.02

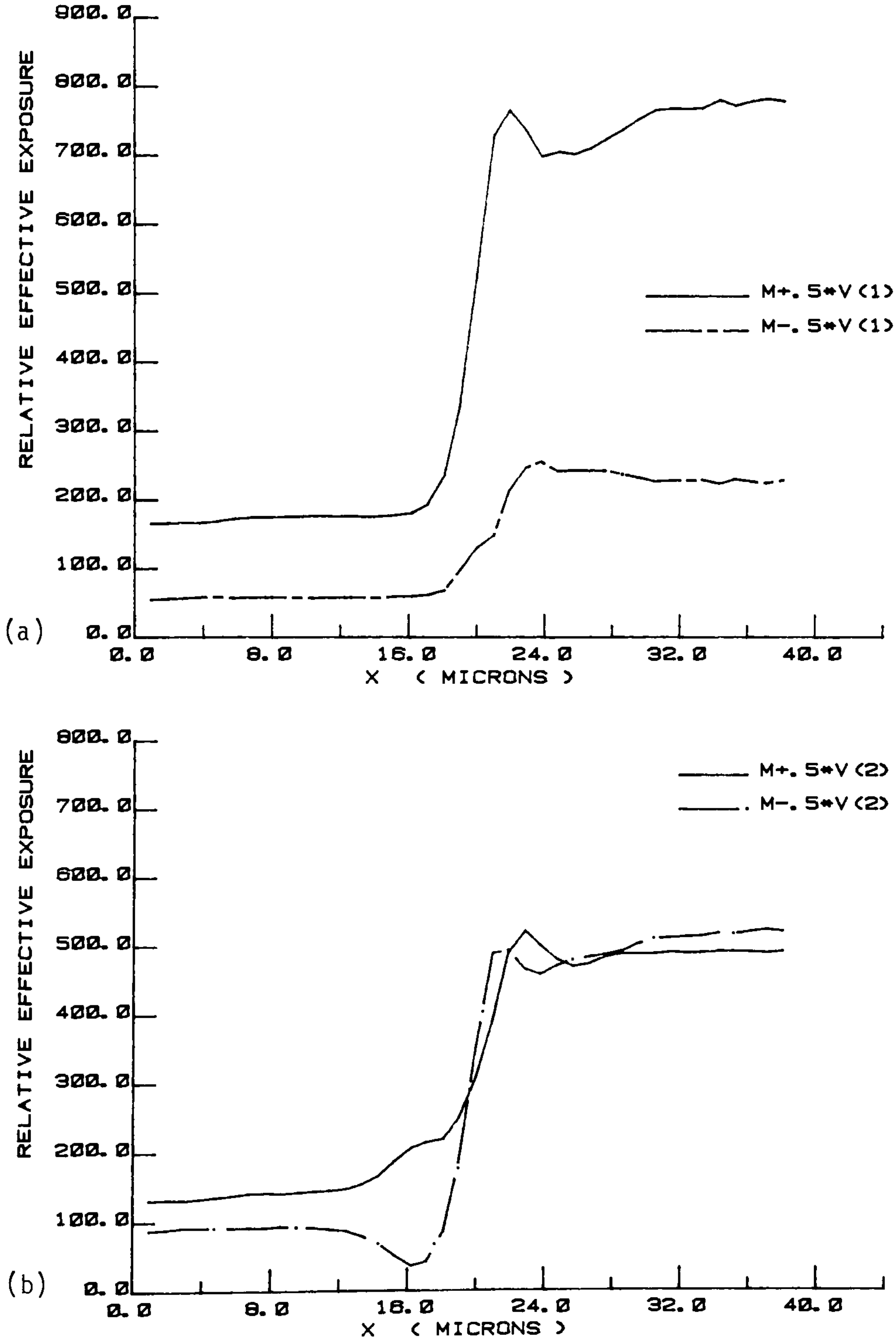

Figure 25. Variation in Edge Response Vectors Associated with Coefficient Shifts, Experiment Two Vectors: (a) Vector V(1), (b) Vector V(2).

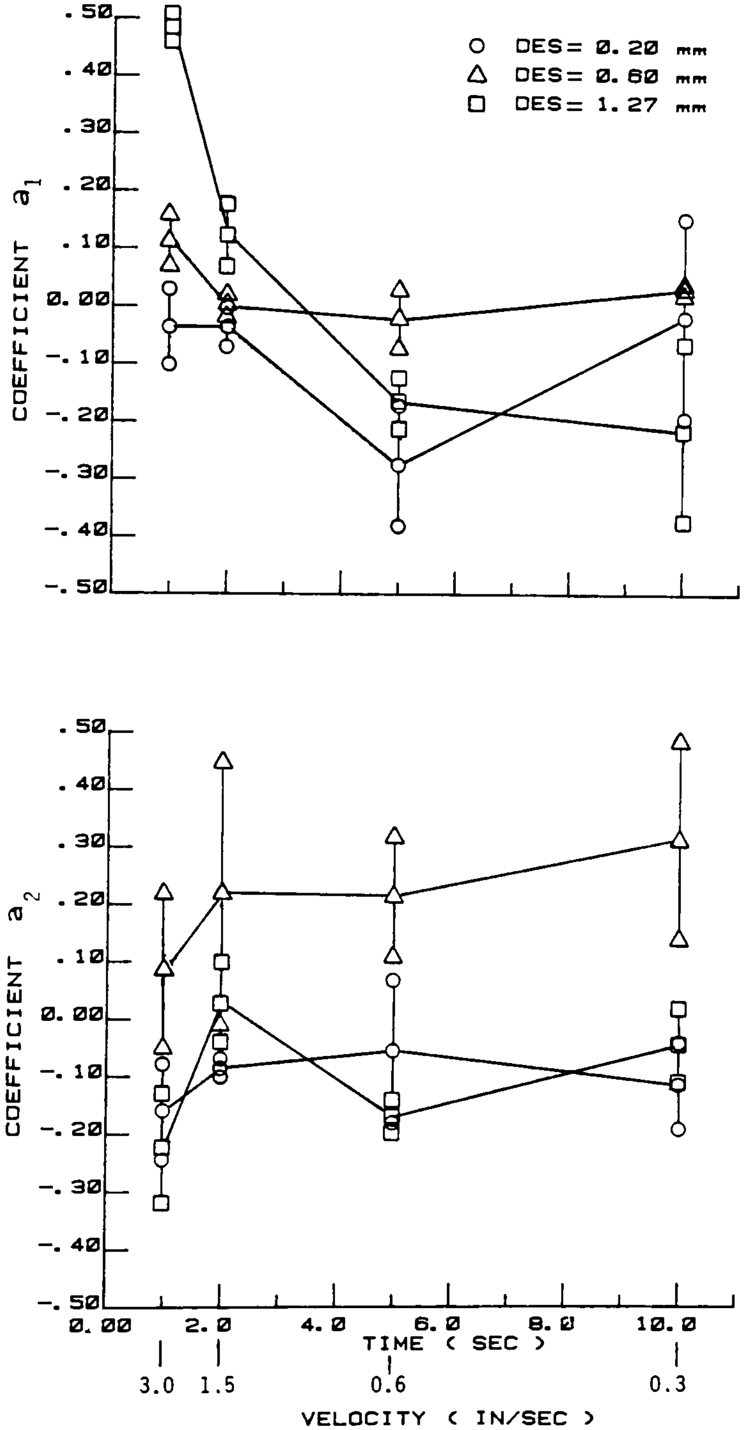

Figure 26. Influence of Film Platen Velocity on Basis Vector Coefficients, Experiment Two.

corresponding to these film platen velocity levels were included in this figure for analysis of temporal transfer characteristics.

At the 1.27 mm electrode spacing, experimental responses varied from: Mean + 0.50 V(1) at the highest velocity, to Mean -0.40V(1) at the lowest velocity. Referring to Figures 25(a) and 26, the trend indicated initial adjacency effects that diminished rapidly with electrodevelopment time. For the 0.60 mm electrode spacing, edge responses ranged from: Mean + 0.10 V(1) at the highest velocity to: Mean + 0.0V (1) at 1.5 inches/second and lower velocities. This trend indicated only a slight decrease in adjacency effects with increasing development time. For the 0.20 mm electrode spacing, V(1) coefficients remained near zero except for a negative value, a_1=0.25, at 0.6 inches/second film platen velocity. Hence, the responses at this electrode spacing exhibited small amounts of adjacency effect except at the velocity of 0.6 inches/second, which exhibited less adjacency effect and significantly lower modulation.

Analysis of variance applied to coefficients a_2 revealed significance of vector V(2) with respect to electrode spacing (α = 0.01) and velocity (α= 0.10). This vector introduced two differing forms of edge responses when added to the mean vector in proportion to negative or positive coefficient values. Referring to Figure 25(b), addition of -0.50 V(2) to the mean edge vector produced a symmetrical response indicative of linear edge effects. Addition of + 0.50 V(2) to the mean edge vector produced asymmetry in the form of positive deviations on both sides of the edge center. The combination of a positive deviation at the lower effective exposure level and a shifted peak response at the higher level, appeared characteristic of phase distortion.

To assess the relation between vector V(2) and the electrodevelopment parameters, experimental a_2 values were plotted as a function of time in Figure 26. Nominal electrodevelopment times were included in this figure for association with the test film platen velocities. At electrode spacings of 0.20 and 1.27 mm, average coefficient values for replicate edge responses fluctuated between zero and -0.22. These flucuations indicated changes in the amount of linear edge effects produced with velocity variations. However, no consistent trends were noted as a function of velocity. Sample responses for the 0.60 mm electrode spacing were characterized by positive a_2 values, suggesting the presence of phase distortions in image transfer. Apparent phase distortion increased with the velocity increment from 3.0 to 1.5 inches/second, and remained consistently high for slower test velocities.

D. Results for Experiment Three

Sensitometric H & D curves for the fountain toner and gated electrode voltage experiments are included in Figures D1 through D3 in Appendix D. The response curve for zero seconds applied electrode voltage produced less than 0.11 density, at all exposure levels and all development electrode spacings (DES). This was the expected result for zero frequency image response with no applied electrode voltage. The sensitometric curves were independent of electrode spacing at 4.3 seconds, indicating equivalent rates of toner depositon to low frequency components (f→0) as electrodevelopment approached completion.

Edge density distributions included edge enhancement for the 0.0 and 1.0 seconds applied voltage times, at all electrode spacings. Edge density for the electrode spacing 0.60 mm combined with applied voltage times of 1.0 and 2.3 seconds, exceeded the dynamic range of the associated H & D response. These experimental treatments produced nonlinear amplitude distortion in the transfer from charge to effective exposure distributions. Statistical analysis of effective exposure distributions was therefore limited to the samples produced at electrode spacings 0.20 and 1.27 mm, combined with applied voltage times of 1.0, 2.3, and 4.3 seconds. The edge response vectors for these samples were plotted according to experimental treatments in Figures D4 through D15 of Appendix D.

Characteristic vector analysis was run using the 12 effective exposure edge response vectors, producing mean and basis vectors shown in Figure 27. Percentages of total variability explained by each of the basis vectors were: V(1)=75.5%, V(2)=18.4%, V(3)=4.9%, and V(4)=0.7%. As vector V(4) explained less than 2.5% of the total variability, it was considered to represent experimental error and was not analyzed for statistical correlation with experimental parameters.

Coefficients for the first three vectors were tabulated in a reduced experimental design matrix. The matrices matrix for a_1, a_2, and a_3, associated with basis vectors V(1), V(2) and V(3), are included in Table 11. Influence of individual basis vectors on the mean response vector were determined by adding each basis vector to the mean vector in proportion to arbitrary coefficient values of ± 0.50. Figure 28 illustrates the responses for: (a) Mean ± 0.5V(1), and (b) Mean ± 0.5V(2). Figure 29 illustrates the responses for: Mean ± 0.5V(3).

Analysis of variance for vector V(1) coefficients indicated V(1) to be significant only with respect to applied voltage time (α=0.05). As illustrated in Figure 28(a), increasing negative values of coefficient a_1 altered the mean response toward an asymmetrical edge distribution indicative of adjacency effects. With increasingly positive a_1 values, vector V(1) altered the mean response toward a different form of asymmetry. This latter asymmetry suggested losses to high frequency image components as a function of effective exposure level, i.e. microsensitometry variation. Comparing the mean response vector in Figure 27 to the arbitrary edge response vectors for ± 0.50 V(1) + Mean in Figure 28(a), it was noted that approximate symmetrical edge responses corresponded to a_1 values between -0.50 and 0.00.

Coefficient values a_1 corresponding to experimental edge responses were plotted as a function of applied electrode voltage time, in Figure 30(a). The average coefficient values were used to denote trends as a function of voltage time, with bounds indicated by the experimental replicate values. As average a_1 values increased with applied voltage time, edge responses changed from an asymmetry characteristic of adjacency effects to an asymmetry characteristic of microsensitometry variation. The coefficient trends were similar for both electrode spacings, indicating a transition through approximate symmetrical edge responses between 1.0 and 2.3 seconds applied voltage time. Although the transition appeared to be more rapid for the lower electrode spacing, statistical analysis did not indicate significance for electrode spacing.

Analysis of variance applied to coefficients a_2 indicated vector V(2) to be marginally correlated with applied voltage time ($\alpha = 0.10$, sum of squares for electrode spacing/time interaction pooled with the error sum of squares). The influence of vector V(2) on the mean edge response is shown in proportion to arbitrary coefficients ± 0.50, in Figure 28(b). For positive a_2 values the resulting edge vectors included asymmetry indicative of adjacency effects. For negative a_2 values, the resulting edge responses were essentially symmetrical about the edge centers.

Experimental a_2 values and their averages (according to replicate edge responses) were plotted as a function of applied

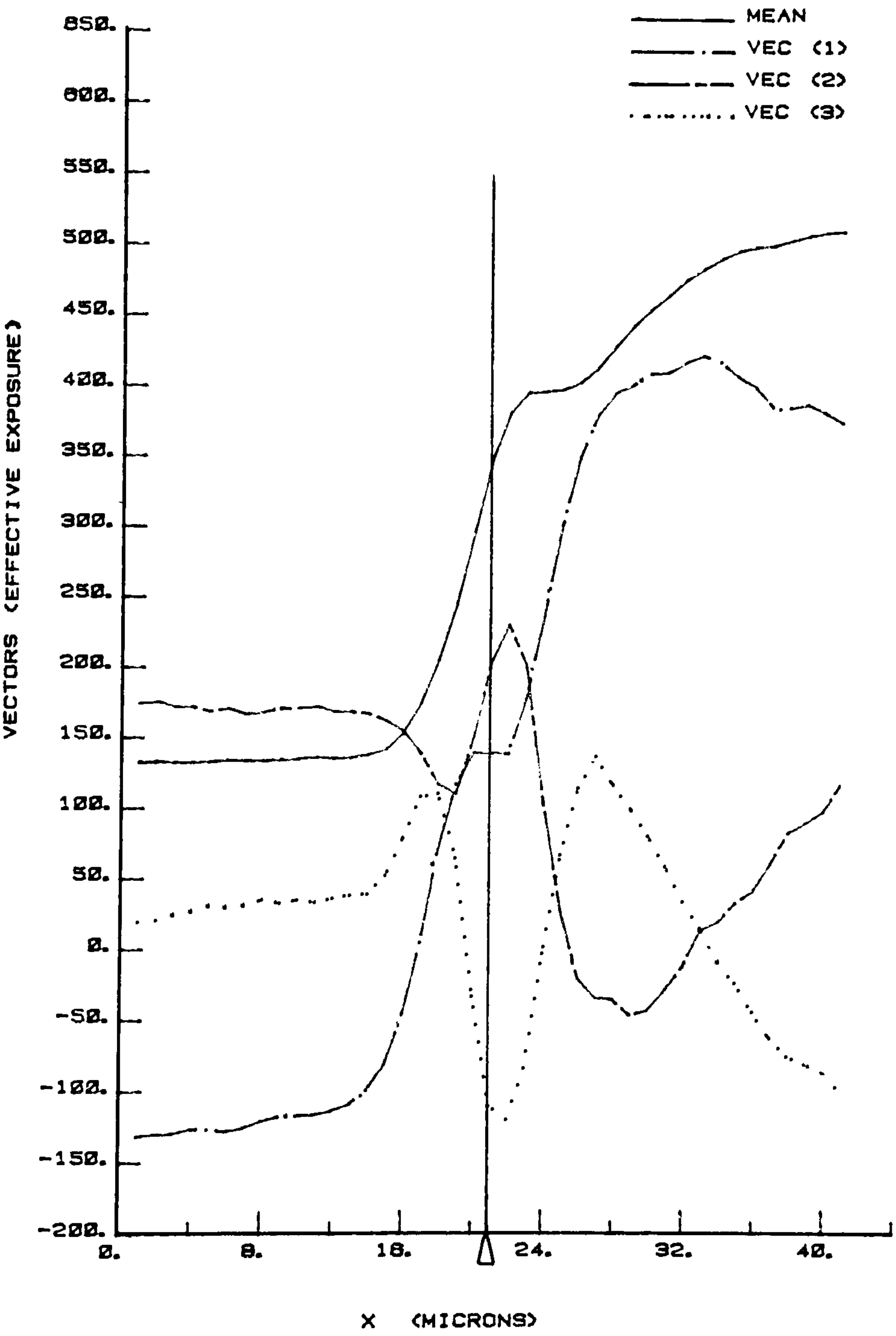

Figure 27. Mean and Basis Vectors for Experiment Three Edge Responses.

Table 11. Basis Vector Coefficients for Experiment Three Edge Responses

(a) Vector V(1) coefficients: a_1

		Development Electrode Spacing (mm)					
		0.20		0.60		1.27	
		Film Sample		Film Sample		Film Sample	
		7-16-2	7-16-4	7-16-6	7-16-7	7-15-1	17-15-2
Applied Voltage Time (seconds)	1.0	-0.37	-0.03	--	--	-0.47	-0.35
	2.3	0.25	0.04	--	--	-0.11	0.19
	4.3	0.16	0.53	--	--	-0.10	0.27

(b) Vector V(2) coefficients: a_2

		Development Electrode Spacing (mm)					
		0.20		0.60		1.27	
		Film Sample		Film Sample		Film Sample	
		7-16-2	7-16-4	7-16-6	7-16-7	7-15-1	17-15-2
Applied Voltage Time (seconds)	1.0	0.09	0.42	--	--	-0.09	0.20
	2.3	0.46	-0.18	--	--	-0.07	0.30
	4.3	-0.33	-0.08	--	--	-0.52	-0.19

(c) Vector V(3) coefficients: a_3

		Development Electrode Spacing (mm)					
		0.20		0.60		1.27	
		Film Sample		Film Sample		Film Sample	
		7-16-2	7-16-4	7-16-6	7-16-7	7-15-1	17-15-2
Applied Voltage Time (seconds)	1.0	-0.32	-0.50	--	--	0.12	0.27
	2.3	-0.11	-0.27	--	--	0.30	0.60
	4.3	-0.06	-0.09	--	--	-0.06	0.10

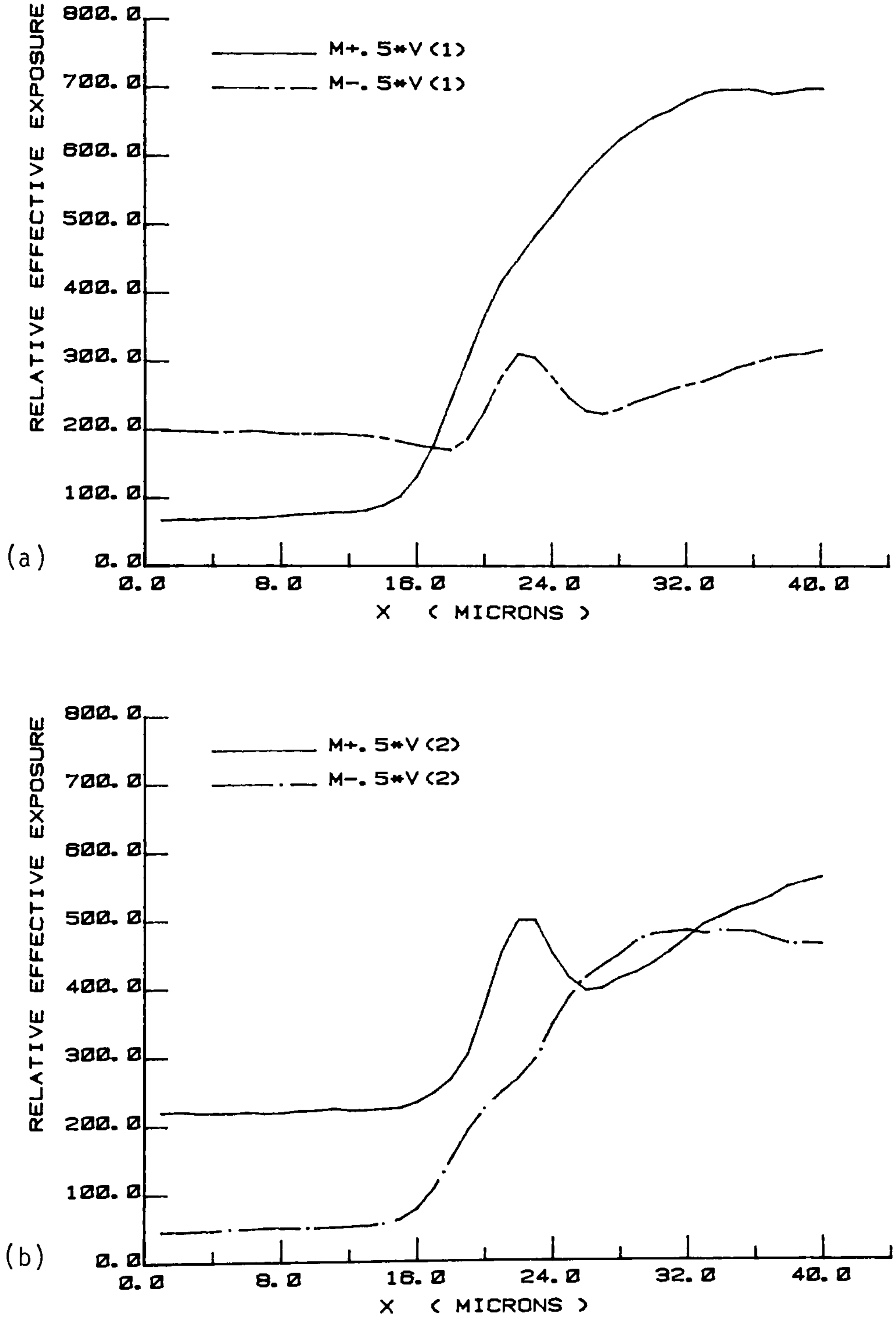

Figure 28. Variation in Edge Response Associated with Coefficient Shifts for (a) Vector V(1), and (b) Vector V(2), of Experiment Three.

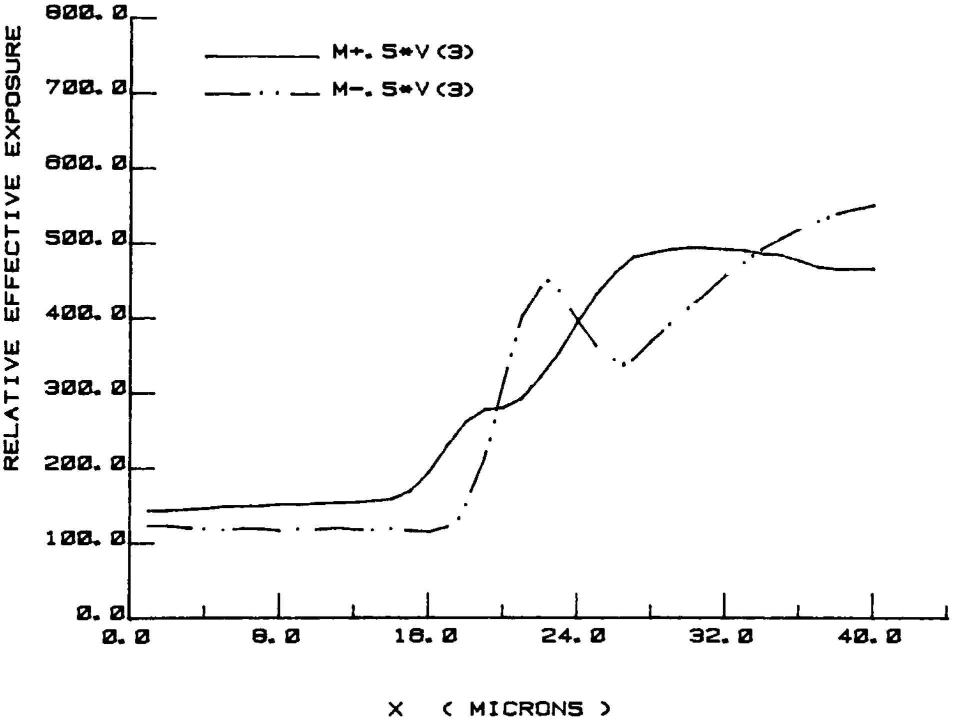

Figure 29. Variation in Edge Response Associated with Coefficient Shifts for Vector V(3) of Experiment Three.

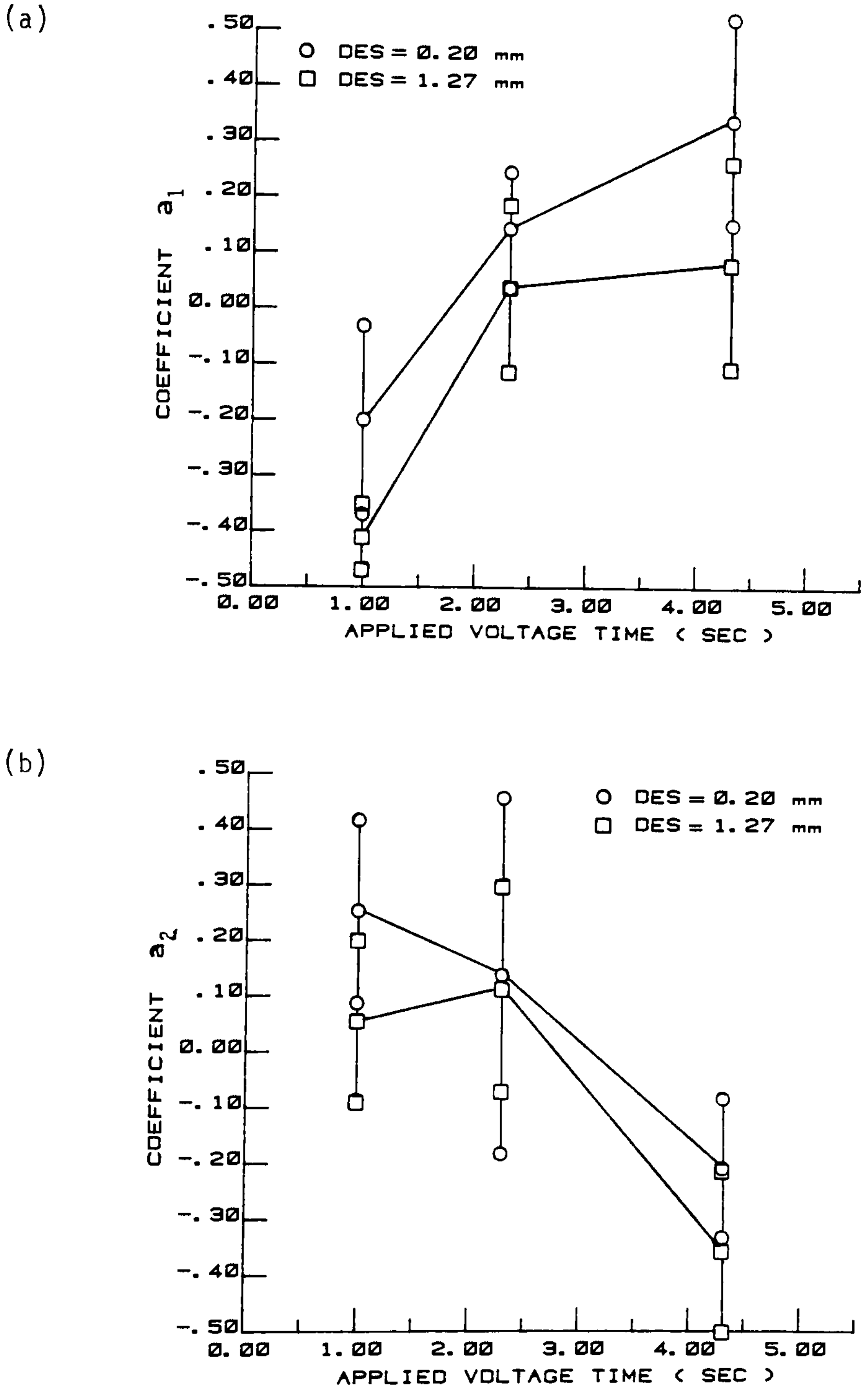

Figure 30. Influence of Applied Voltage Time on Coefficients of (a) Vector V(1), and (b) Vector V(2), of Experiment Three.

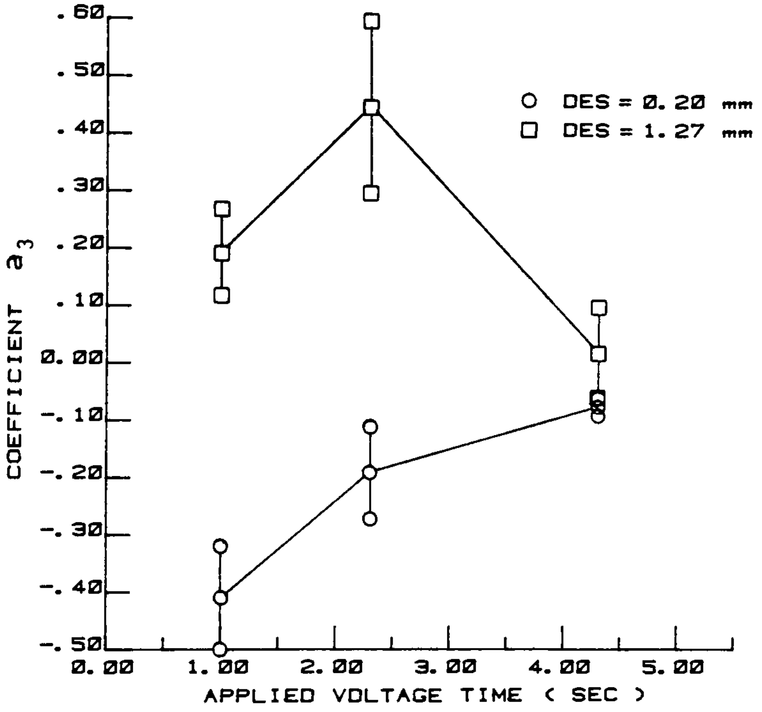

Figure 31. Influence of Applied Voltage Time on Coefficients of Vector V(3) of Experiment Three.

voltage time in Figure 30(b). At 1.0 seconds time, both electrode spacings produced responses indicative of localized depletion near high frequency components. In particular, intermediate image frequencies (20 c/mm $< f <$ 40 c/mm) exhibited disproportionate deposition vs. charge density. The trends noted with average a_2 values indicated decreasing degree of asymmetry in the edge responses with increasing applied voltage time.

Increased edge modulation and apparent decrease in average effective exposure level were also noted for the symmetrical responses at longer times. The decrease in average effective exposure level was caused by translation of edge image density through H & D curves exhibiting greater density response at lower macroscopic exposure levels. Vector V(2) therefore explained effective differences between microscopic and macroscopic image sensitometry as a function of applied voltage time. With the microsensitometry vs. spatial frequency equalized, near symmetrical edge responses were noted for the longer applied voltage times.

Analysis of variance for vector V(3) coefficients indicated the influence of this vector to be significant with electrode spacing ($\alpha = 0.01$), time ($\alpha = 0.10$), and electrode spacing/time interaction ($\alpha = 0.05$). In proportion to arbitrary coefficient values (a_3) at ± 0.50, vector V(3) explained changes in the form of asymmetry, and an apparent shift in the edge center. Associated with positive coefficients, vector V(3) produced edge responses with positive effective exposure deviations on both sides of the edge center. Combined with an apparent shift in edge center, these deviations suggested phase distortion in the effective image transfer function. Associated with negative a_3 values, edge responses exhibited adjacency effects characteristic of disproportionate response vs. charge at intermediate frequency components.

For each treatment, experimental coefficient values and replicate averages were plotted vs. applied voltage time (Figure 31). Average coefficient levels were employed in analyzing edge response trends as a function of test parameters and their interactions. In accordance with small coefficient values ($0.00 < a_3 < 0.30$) the 1.27 mm electrode spacing produced approximate symmetrical responses near development initiation (1.0 second). Large positive values of a_3 for 1.27 mm spacing and 2.3 seconds applied voltage time indicated diversion to phase effects at intermediate development. Associated with negative a_3 values, the 0.20 mm electrode spacing produced adjacency effects at 1.0 second. Increased time of development using this electrode spacing, increased proportionality in response vs. charge level for the intermediate frequency components. Both electrode spacings produced small amounts of adjacency effect in edge responses for 4.3 seconds applied voltage time.

E. Results for Experiment Four

Sinusoidal density distributions measured for electrode spacings 0.20 and 1.27 mm combined with applied voltage times 1.0, 2.3, and 4.3 seconds, were all within the dynamic ranges of associated H & D response curves. These sensitometric (H & D) response curves are shown in Figures D1-D3 of Appendix D. The resulting effective exposure distributions and their Fourier transformed frequency spectra are included in Figures E1 through E18 of Appendix E. Less than the total number of cycles in the sinusoidal distributions were employed in the Fast Fourier Transform calculations. This procedure was necessary to avoid inclusion of an adjacency effect near the sinusoidal image borders. The number of cycles and the resulting frequency sampling resolution were held constant for each test sinusoidal frequency.

The sinusoidal analysis program results for modulation, signal to noise ratio, and harmonic percent distortions are listed for each sample in Tables 12 through 14. Input harmonic percent distortions (IH%D(i)) were computed using the target distortions in Table 8, and the associated modulus values of the reduction lens and microdensitometer MTFs. Output harmonic percent distortions (OH%D(i)) were computed using the sample harmonic distortions in Tables 12 through 14, and the associated modulus values for the microdensitometer MTF. The ratios of these (corrected) output to input harmonic percent distortions determined the harmonic distortion factors used in the Analysis of Variance. Harmonic distortion factors for the second and third harmonics of each test frequency: 25, 64, and 102 cycles/mm, were plotted as a function of applied voltage time in Figures 32 through 34.

For the 25 cycles/mm test frequency, analyses of variance run for second and third harmonics revealed lack of significance with respect to electrode spacing or applied voltage time (Table 18 and Figure 32). The combined parameter levels: 0.20 mm spacing and 1.0 second time, produced measured harmonic distortions that were confounded with the frequency response of image noise. At 4.3 seconds applied voltage time, this electrode spacing produced large disparity in harmonic distortions among the replicate samples. This disparity appeared to be related to the inconsistent modulation at the fundamental frequency.

At 1.27 mm electrode spacing, the second and third harmonic responses indicated different trends with increasing applied voltage times. The modulation of the fundamental frequency: 25 cycles/mm, increased monotonically with time for this electrode spacing. The amount of third harmonic distortion decreased with increasing time, i.e. inversely proportional to modulation change at the fundamental. However, the second harmonic remained constant with applied voltage time.

Analysis of variance for the higher test frequencies 64 and 102 cycles/mm, revealed significance of harmonic distortions with respect to both electrode spacing and applied voltage time. In

Table 12. Results of Sinusoidal Analysis for Measured Fundamental Frequency at 25. ± 1.0 cycles/mm

(a) Results for images processed with Development Electrode Spacing at 0.20 mm

Applied Voltage Time (sec.)	Film Sample	Fundamental Modulation	S/N	Second Harmonic	Third Harmonic
1.0	7/17-2	17.5	2.2	3.6%	16.0%
	7/17-8	10.6	2.5	16.8%	4.6%
2.3	7/17-2	24.3	5.5	8.2%	1.6%
	7/17-8	16.1	5.7	8.9%	9.1%
4.3	7/17-2	44.6	10.2	6.6%	2.5%
	7/17-8	18.6	3.6	22.5%	11.2%

(b) Results for images processed with Development Electrode Spacing at 1.27 mm

Applied Voltage Time (sec.)	Film Sample	Fundamental Modulation	S/N	Second Harmonic	Third Harmonic
1.0	7/17-13	19.3	6.2	11.5%	6.7%
	7/17-18	10.9	3.7	17.0%	13.7%
2.3	7/17-13	32.7	6.0	15.2%	1.0%
	7/17-18	27.4	7.5	10.3%	2.6%
4.3	7/17-13	30.3	6.7	13.7%	1.2%
	7/17-18	40.0	5.7	15.6%	1.1%

Table 13. Results of Sinusoidal Analysis for Measured Fundamental Frequency at 64 ± 1.4 cycles/mm

(a) Results for images processed with Development Electrode Spacing at 0.20 mm

Applied Voltage Time (sec.)	Film Sample	Fundamental Modulation	S/N	Second Harmonic	Third Harmonic
1.0	7/17-4	8.7	1.4	59.1%	28.8%
	7/17-10	7.3	1.0	92.4%	34.4%
2.3	7/17-4	15.0	2.4	36.6%	11.6%
	7/17-10	14.8	2.2	41.7%	10.0%
4.3	7/17-4	33.4	5.8	15.7%	1.0%
	7/17-10	39.6	5.0	18.3%	0.7%

(b) Results for images processed with Development Electrode Spacing at 1.27 mm

Applied Voltage Time (sec.)	Film Sample	Fundamental Modulation	S/N	Second Harmonic	Third Harmonic
1.0	7/17-15	7.8	2.3	38.6%	12.6%
	7/17-20	41.9	2.3	42.3%	7.1%
2.3	7/17-15	16.1	4.3	21.2%	2.8%
	7/17-20	19.3	5.4	16.0%	1.4%
4.3	7/17-15	28.2	4.6	20.4%	2.1%
	7/17-20	26.0	6.0	15.8%	2.4%

Table 14. Results of Sinusoidal Analysis for Measured Fundamental Frequency at 102. ± 2.1 cycles/mm

(a) Results for images processed with Development Electrode Spacing at 0.20 mm

Applied Voltage Time (sec.)	Film Sample	Fundamental Modulation	S/N	Second Harmonic	Third Harmonic
1.0	7/17-6	4.7	1.2	39.0%	8.1%
	7/17-11	--	--	--	--
2.3	7/17-6	5.4	2.9	30.5%	4.2%
	7/17-11	5.8	3.6	23.9%	2.0%
4.3	7/17-6	5.0	3.9	15.4%	2.5%
	7/17-11	16.0	5.5	16.2%	1.3%

(b) Results for images processed with Development Electrode Spacing at 1.27 mm

Applied Voltage Time (sec.)	Film Sample	Fundamental Modulation	S/N	Second Harmonic	Third Harmonic
1.0	7/17-16	4.6	2.1	37.2%	5.8%
	7/17-21	3.9	2.6	31.3%	4.3%
2.3	7/17-16	11.4	4.9	18.2%	1.3%
	7/17-21	11.1	5.9	14.3%	1.4%
4.3	7/17-16	--	--	--	--
	7/17-21	13.4	11.3	7.5%	1.0%

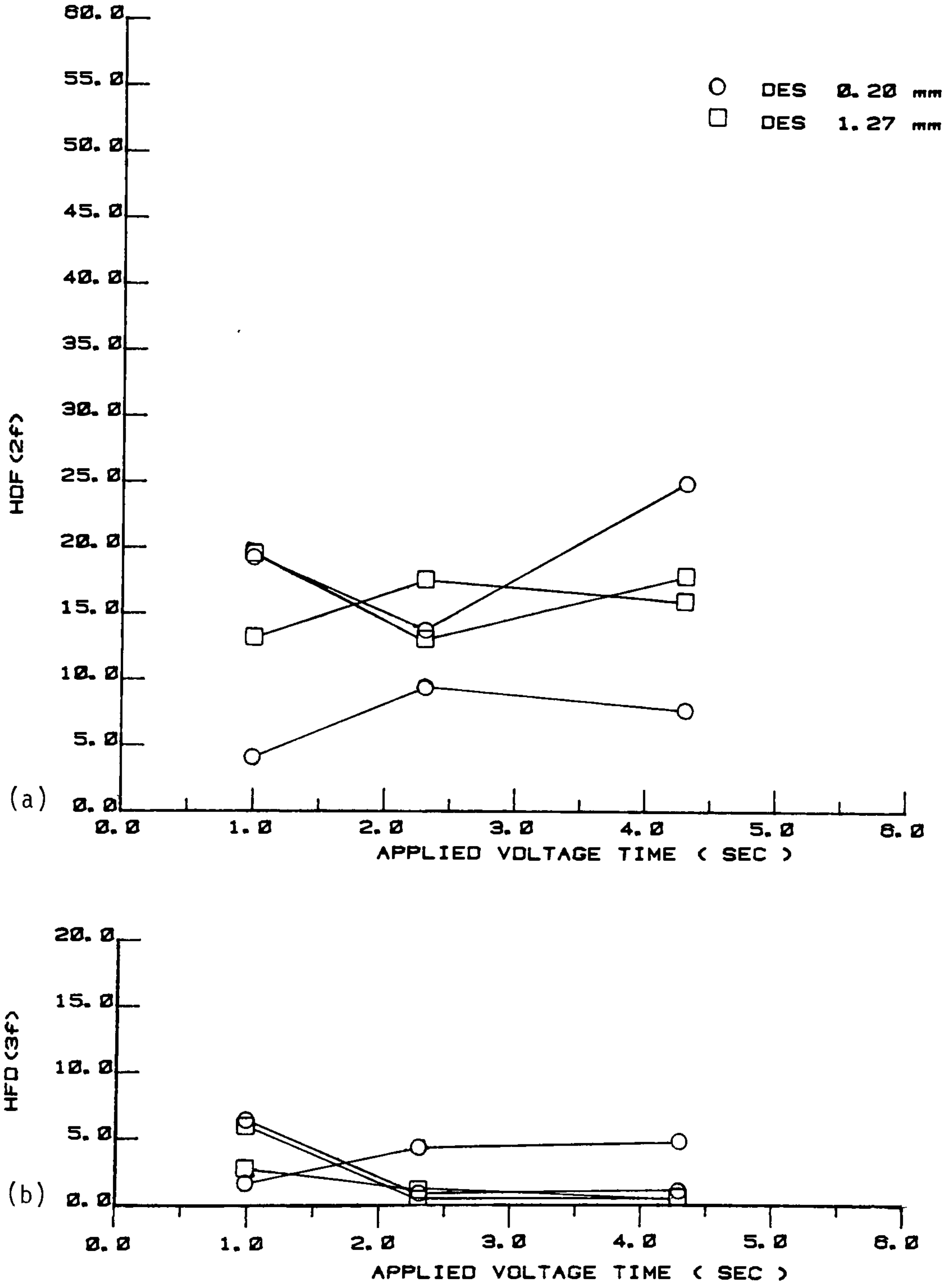

Figure 32. Influence of Applied Voltage Time on Harmonic Distortion Factors for (a) Second Harmonic, and (b) Third Harmonic. Sinusoidal Transfer with Fundamental: 25 cycles/mm.

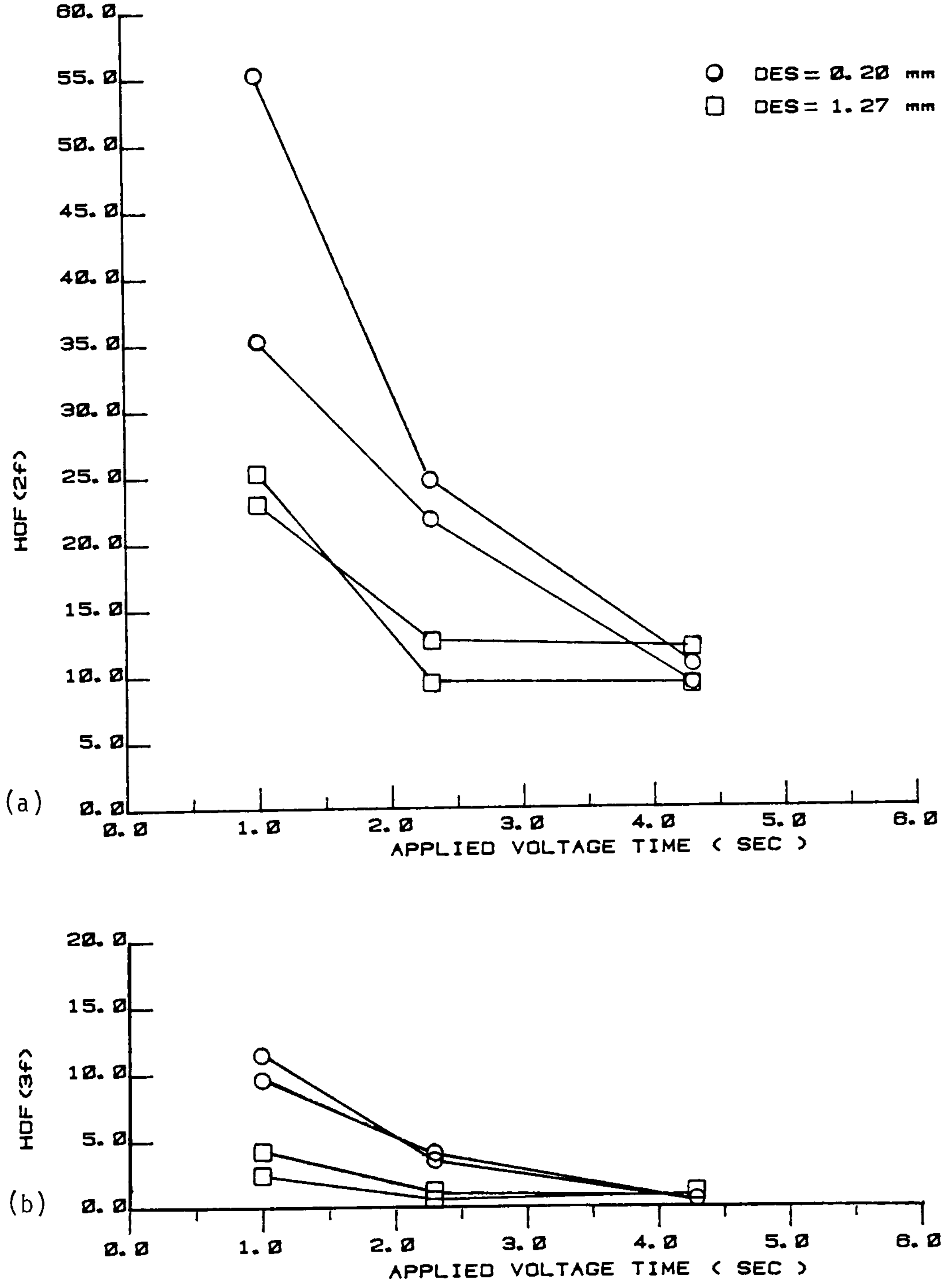

Figure 33. Influence of Applied Voltage Time on Harmonic Distortion Factors for (a) Second Harmonic, and (b) Third Harmonic. Sinusoidal Transfer with Fundamental: 64 cycles/mm.

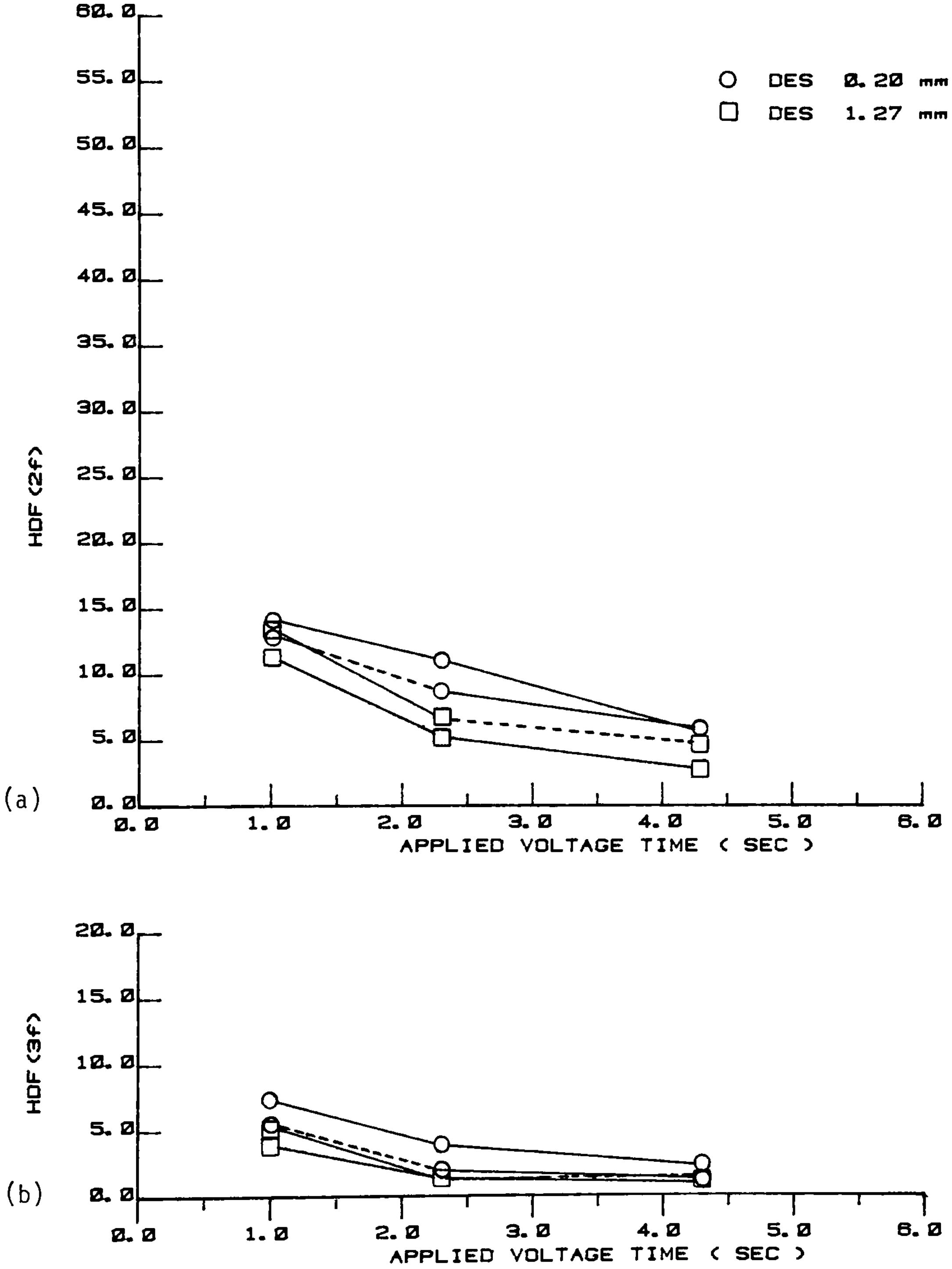

Figure 34. Influence of Applied Voltage Time on Harmonic Distortion Factors for (a) Second Harmonic, and (b) Third Harmonic. Sinusoidal Transfer with Fundamental: 102 cycles/mm.

addition, harmonic distortions for 64 cycles/mm were correlated with an electrode spacing/time interaction. The confidence levels (alpha risk) for statistical significance of second and third harmonic distortions are included in Table 15. Trends in distortion content vs. electrodevelopment time were determined using the plots for each distortion factor of each test frequency (Figures 33 and 34).

For both 64 and 102 cycles/mm, second and third harmonic distortion factors were largest for 1.0 second applied voltage time. The distortion factors decreased with increasing times of applied electrode voltage, at both test frequencies. Relating the output harmonic percent distortions to fundamental modulations in Tables 13 and 14, a monotonic decrease in distortion factors accompanied an increase in modulation with increasing applied volatge time.

At 64 cycles/mm the change in electrode spacing altered the initial levels of harmonic distortion, and their rate of decrease with increased applied voltage time. With increased time ($t \rightarrow 4.3$ seconds), distortion factors for both electrode spacings decreased to the same level. At 102 cycles/mm, the electrode spacing altered the levels of harmonic distortions, but did not alter the rate of decrease in distortion with time. Again the lower electrode spacing produced greater distortion factors at both second and third harmonics. Within experimental error, distortion levels for the 0.20 mm electrode spacing decreased at the same rate as those for the 1.27 mm spacing.

Table 15. Significance Levels (alpha risk) for Correlation Between Experimental Parameters and Harmonic Distortion Factors.
N.S. denotes: not significant

Fundamental, f (cycles/mm)	Harmonic, (nf)	Electrode Spacing	Applied Voltage Time	Electrode Spacing/ Applied Voltage Time
25	Second, (2f)	N.S	N.S	N.S
	Third, (3f)	N.S	N.S	N.S
64	Second, (2f)	$\alpha=0.01$	$\alpha=0.01$	$\alpha=0.10$
	Third, (3f)	$\alpha=0.01$	$\alpha=0.01$	$\alpha=0.01$
102	Second, (2f)	$\alpha=0.05$	$\alpha=0.01$	N.S
	Third, (3f)	$\alpha=0.10$	$\alpha=0.01$	N.S

IV. DISCUSSION

Influence of exposing wavelength on linearity of edge image transfer was tested in the first (screening) experiment. A shift in exposing wavelength was employed to test influence of exponential absorption on the transfer from input exposure to image charge distributions. Characteristic vector analysis applied to the resulting effective exposure distributions, revealed a correlation between linearity and exposing wavelength. A shift in exposing wavelengths from spectral bands of lower absorption to maximum absorption within the photoconductor, produced a shift from symmetrical to asymmetrical edge responses.

The form of asymmetrical responses observed at the peak absorption wavelength did not concur with postualted effects of exponential absorption in the photoconductor. Rushing's[68] simulation suggested an edge response with less abrupt changes in slope from the minimum level to the edge center than from the edge center to the maximum level of effective exposure. Theoretically, an increase in absorption coefficient should have increased the degree of asymmetry in accordance with Rushing's simulated edge response (Figure 1, case 3). The experimental results did indicate an increase in asymmetry for the wavelength of greater absorption. However, the asymmetrical edge responses exhibited transitional slopes opposite to the predicted response for increased absorption coefficient. This discrepancy between theoretical and empirical asymmetry suggested that the change in edge response was probably caused by a latent variable correlated with the wavelength factor.

The degree of nonlinearity introduced by exposing the film at the wavelength of maximum absorption was not large. The coefficients of the extracted basis vector, averaged according to the wavelength factor, indicated only a small deviation from symmetrical edge responses at the wavelength of maximum absorption in the photoconductor. Relative to total experimental edge response variations, the basis vector correlated to the exposing wavelength shift explained only 4.2% of this variation. The small amount of asymmetry observed and the small percentage of edge variations explained, indicated that the exposing wavelength shift produced little change in linearity of overall system transfer.

Employing a continuous electrode development apparatus, the influence of electrode spacing and film platen velocity on linearity of image transfer were tested in the first two experiments. The first experiment revealed a component of edge variability uniquely correlated to development electrode spacing, explaining 91.5% of experimental edge variations. A second component was correlated with film platen velocity, explaining 4.2% of experimental edge variations. These components, or basis vectors, illustrated transitions from symmetrical to asymmetrical edge responses with shifts in tested parameter levels. In each case, the form of asymmetry observed was characteristic of microsensitometry variation, i.e. frequency dependent reductions in response vs. input exposure level.

Reductions in response at higher exposure (or charge) levels for higher frequency components of the image were observed for both increased electrode spacing and increased film platen velocity. For the shift from 0.20 mm to 1.27 mm electrode spacings, an increase in edge asymmetry was probably caused by the increased difference in relative particle deposition rates to high vs. low frequency components. Relatively greater electrostatic field intensity above the sharp edge charge gradient were expected to provide initially greater deposition to image components near the edge center. Subsequently, particle depletion near these image components was expected to reduce deposition to neighboring image areas. The observed reductions to high frequency components ($f>40$ cycles/mm) associated with the sharp charge gradient did not support this expected adjacency effect. However, the disproportionate reductions at these frequency components did indicate frequency dependent, nonlinear depletion effects.

For the extended electrodevelopment times represented by the slower film platen velocities, ion deposition may explain the observed reduction at higher frequencies components. Although proportionately lower in electric field intensity, fields above lower frequency ($f<40$ cycles/mm) components penetrated further into the electrodevelopment region. These fields probably caused more consistent particle deposition rates with electrodevelopment time.

Fields associated with the higher frequnecy components were stronger, but limited to short distances above the photoconductor surface. Following initial fast rates of deposition to the higher frequency components, a greater proportion of ions may have been deposited to these components in the absence of adequate toner particle concentrations near the film surface.

Time dependence of nonlinear depletion effects was expected in accordance with experimental variation in film platen velocity. Within the experimental velocity range for experiment one, no adjacency effects were observed. Transition from edge responses characteristic of microsensitometry variation to symmetrical responses were observed with the decrease in film platen velocity. Restored particle deposition to higher frequency components was apparent in this transition. Changes in edge response with decreased velocity did not concur with postulations for frequency dependent depletion effects. The results indicated either a complex transition in deposition vs. frequency with electrodevelopment time, or an influence of film platen velocity on replenishment rates near the film surface.

In the second experiment additional levels of electrode spacing and film platen velocity were employed to clarify trends in edge response and associated linearity of transfer. Two components of edge variability were required to explain 97.1% of the experimental response variations. The first component (94% variance explained) illustrated changes in edge response correlated with velocity and an interaction between velocity and electrode spacing. This basis vector indicated that a spacing/velocity interaction altered edge responses from those characteristic of adjacency effects, to responses characteristic of linear image transfer.

Changes in edge response for electrode spacing and film platen velocity variations indicated limited concurrance with deposition rates, as postulated using Kao's[69] electrostatic field spectra (Figure 8). At the largest electrode spacing, 1.27 mm, the difference between high and low spatial frequency deposition rates prduced a pronounced change in edge response with decreased film platen velocity. Initially higher rates of deposition to higher frequency components produced localized depletion above lower frequency components. With increasing time, particle depositon effectively restored proportional response to the lower frequency image components, as observed in accordance with the predominant basis vector V(1). The largest electrode spacing 1.27 mm produced significant temporal nonlinear depletion effects.

Results for the intermediate electrode spacing, 0.60 mm, suggested less dependence of relative deposition rates on spatial frequency. Minimal adjacency effects, associated with depletion to lower frequency, were observered near development initiation (3.0 inches/second). As initial differences in deposition vs. spatial frequency were lower, this adjacency effect was not as pronounced as for 1.27 mm spacing. Results for the lowest electrode spacing, 0.20 mm, indicated the least dependence of initial depositon rates on spatial frequency. Edge responses for this electrode spacing exhibited small amounts of adjacency effect that remained fairly consistent within tested levels of platen velocity. For both 0.60 mm and 0.20 mm electrode spacings, little relative difference in electrostatic field intensities between higher and lower spatial frequency components would explain less significance of temporal nonlinear depletion effects than observed for 1.27 mm electrode spacing.

The effects of vector V(2) did not support the postulated influence of electrode spacing on spectrally dependent deposition and depletion rates. The amounts of edge effect observed were approximately equivalent for the extreme electrode spacings. In addition, these edge effects were small and relatively insensitive to film platen velocity variations.

The predominant effect explained by this component of edge variation was a deviation from linear edge effects at the extreme electrode spacings, to apparent phase distortion at the intermediate electrode spacing. Assuming responses at the electrode spacing were characteristic of phase distortion, edge response variations in accordance with vector V(2) could be described by changes in the form of characteristic linear transfer operators. No transitions from nonlinear adjacency effects or microsensitometry variation to linear edge responses were observed in accordance with this vector.

Sensitometric responses for experiments one and two produced sufficient density for translation of all edge density distributions into effective exposure. Based on electrostatic field spectra, rates of deposition to zero spatial frequency components were initially slower than high frequency components. In accordance with integrated field intensities, total deposition to zero frequency component should have been equivalent to that of high frequency components only at extended development times. Macroscopic density responses in the range of (micro) edge densities were equivalent for all velocity settings, except in conjunction with 1.27 mm electrode spacing. These results indicated that the velocity parameter in general provided actual electrodevelopment times in excess of the nominally represented times.

Comparisons of edge response trends between experiments one and two indicated similarities and differences in the effects of development parameters on edge image transfer. The 1.27 mm electrode spacing provided nonlinear reduction vs. charge level to high frequency components in experiment one. At the same film platen velocities in experiment two, this electrode spacing produced no significant depletion effects in edge responses. The 0.20 mm electrode spacing produced near symmetrical edge responses in both experiments. The nonlinear depletion effect observed for 1.27 mm spacing in experiment one probably resulted from greater average charge density for the latent image edge distribution. For a limited supply of toner particles in the electrodevelopers, depletion to higher frequency components was more severe for the latent images requiring greater toner deposition.

The difference in average charge (and resulting effective exposure) levels between experiments one and two also explained differences in the influence of film platen velocity. In the screening experiment, an increase in nonlinear reductions to high frequency components occurred with increased film platen velocity. Within the same velocity range, experiment two indicated changes in amounts of adjacency effects and/or phase distortions. Although the physical mechanisms could not be ascertained for each case, the observed differences were thought to result from different temporal depletion mechanisms as a function of film platen velocity.

Because of the difference in average input exposure levels for edge images in the first two experiments, linearity as a function of test parameters was addressed independently for each experiment. In the screening experiment unique correlations were determined between linearity and both electrode spacing and film platen velocity. A decrease in electrode spacing from 1.27 mm to 0.20 mm produced a decrease in degree of nonlinearity of image transfer, as determined from vector V(1). However, the magnitudes of coefficients for V(1) were not sufficient to alter the asymmetrical mean vector to a symmetrical adge response at the lower electrode spacing. A decrease in film platen velocity from 0.6 to 0.3 inches/second produced a decrease in nonlinearity of image transfer, as noted in accordance with vector V(2). However, the amount of reduction in nonlinearity was not large, as determined from the coefficient a_2 values. Therefore neither electrode spacing nor film platen velocity were said to alter the effective transfer function from nonlinear to linear forms in experiment one.

Results for experiment two indicated changes in linearity as a function of both film platen velocity and an electrode spacing/velocity interaction term. In accordance with vector V(1), changes in nonlinearity were highly correlated to the interaction term. Large changes in coefficient values a_2 observed for edge responses at 1.27 mm electrode spacing indicated a large decrease in nonlinearity with decreasing film platen velocity. By comparison, changes in coefficient values with decreasing velocity observed for the 0.60 and 0.20 mm electrode spacings, indicated minimal changes in the degree of nonlinearity.

Specific cases for which electrodevelopment parameters provided linear image transfer were sought for each experiment. In the screening experiment, no combination of electrode spacing and film platen velocity was found to preserve linearity of edge image transfer. This observation was made with regards to a strict correlation between linearity and symmetrical edge responses. The best approximations to linear image transfer were noted for the 0.20 mm electrode spacing, with insignificant dependence on film platen velocity. These observations were confirmed by analysis of individual edge response vectors in Appendix B.

For experiment two, specific test conditions preserving linearity of edge image transfer were indicated by the vector sum: Mean + a_1 V(1) + a_2 V(2). Experimental parameter combinations characterized by coefficient values: $a_1 < 0$ and $a_2 < 0$, provided approximately symmetrical edge responses. These parameter combinations included all velocities for the 0.20 mm electrode spacing, and velocities less than 1.5 inches/second for the 1.27 mm electrode spacing.

In light of the objective to find conditions providing both linear transfer and edge enhancement, it was noted that the conditions preserving linearity included slight edge enhancement as well. In combination with $a_1 < 0$, large negative values for a_2 would indicate significant amounts of linear edge effect in the associated edge response. However, no parameter combinations were found to provide these levels of coefficient values. Therefore, no combinations of film platen velocity and electrode spacing produced significant amounts of linear edge enhancement. These observations, as derived from vector component analysis, were confirmed by examination of individual edge response vectors in Appendix C.

In experiment three gating of applied electrode voltage, used in conjunction with a fountain toning apparatus, provided more accurate representation of actual development times. As a result, edge densities for 1.0 to 2.3 seconds applied voltage times and 0.60 mm electrode spacing exceeded the associated macroscopic density responses. All edge densities exceeded the macroscopic density response for zero applied voltage times. These results indicated nonlinear amplitude distortion, and therefore the parameter combinations were not analyzed for additional nonlinear transfer effects.

With increasing times of applied electrode voltage, rates of sensitometric density increase were proportional to electrode spacing. As rates predicted in accordance with electrostatic field intensities varied in _inverse_ proportion to electrode spacing, an explananation was sought. One possible explanation was that the total volume of available toner paticles mobilized in the bulk electrodevelopment region was greater at any instant for the larger electrode spacing. Another possible explanation was that the electrode configuration itself, having an alternate bar and slit configuration, provided more uniform fields between the electrode and film for the larger electrode spacing. The cause of the discrepancy between theoretical field intensities and density response for the zero frequency component could not be pinpointed. However, the results suggested that disparity in deposition rates between low and high frequency components should not depend on electrode spacing to the extent predicted in accordance with calculated electrostatic field spectra.

Edge variations in accordance with vector V(1) suggested that initial high rates of particle deposition to high frequency image components produced temporary adjacency effects. The initial reduction of particle concentration near high frequency components (f>40 cycles/mm) of charge appeared to cause reduction in deposition vs. charge level to intermediate frequency components (20 cycles/mm<f<40 cycles/mm). The response for low frequencies (f<20 cycles/mm) remained unaffected by the initial localized depletion. At extended development times it appeared that both high and intermediate frequency components were affected by the initial depletion mechanism. The results suggested that ion deposition to both intermediate and high frequency image components was significant beyond 1.0 seconds applied voltage time. Initial localized depletion and subsequent ion deposition would explain the transition from nonlinear adjaceny effects to nonlinear microsensitometry variation with increasing time.

Edge variation in accordance with vector V(2) indicated similar nonlinear adjacency effects to those noted for vector V(1) near development initiation. Hence, this component of edge variation indicated the same influence of temporal localized depletion effects on image responses at 1.0 and 2.3 seconds applied voltage time. However, at 4.3 seconds applied voltage time the edge responses exhibited symmetry characteristic of linear image transfer. This trend with increasing electrodevelopment time suggested that proportionality of particle deposition vs. charge was restored for the initially depleted frequency components. No permanent depletion effects were noted in accordance with vector V(2).

Edge response variations in accordance with vector V(3) indicated effects of complex interactions among the electrodevelopment parameters electrode spacing and applied voltage time. The trends in responses as a function of parameter levels suggested little concurrance with postulated depletion mechanisms. At 1.27 mm electrode spacing, a trend from near symmetrical responses, to responses characteristics of phase distortion, to responses exhibiting small amounts of adjacency effects occurred with increasing applied voltage time. Lack of significant amounts of adjacency effect for this electrode spacing was contrary to a postulated frequency dependent depletion mechanism induced by disparity in deposition rates vs. frequency. The lower electrode actually produced greater adjacency effects, as noted near development initiation (1.0 second applied voltage time). No interpretation of frequency dependent deposition rates (in accordance with electrostatic field spectra) would explain the occurrance of adjacency effects with increased time for the 0.20 mm electrode spacing.

The influence of applied voltage time on linearity of edge image transfer was significant for all three of the extracted basis vectors. Because of the inherent dissociation between experimental parameters and the characteristic vectors, no unique correlation was observed between linearity and applied voltage time. However, trends observed in accordance with the two vectors explaining the majority of edge variance, supported the same trends in temporal nonlinear depletion.

Both vectors V(1) and V(2) described pronounced adjacency effects at the 1.0 second time, and a sharp decrease in adjacency effects between 1.0 and 2.3 seconds. This response trend concurred with predictions for initial enhanced deposition to higher intensity fields near the edge center, producing nonlinear depletion to neighboring image components. At the 4.3 seconds applied voltage time, restored particle deposition to initially depleted image components confirmed that significant adjacency effects were limited to shorter electrodevelopment times.

Statistical determination for specific parameter levels preserving linearity of image transfer could not be readily attained from the resulting characteristic vectors. Three basis vectors were required to explain 98.8% of experimental edge variations. Each of these vectors indicated changes in nonlinearity as a function of applied voltage time. In addition, the third basis vector indicated changes in nonlinearity as a function of electrode spacing and an electrode spacing/time interaction.

Without attempting multivariate statistical analysis for vector coefficient interactions, approximate determination of transfer characteristics were noted in accordance with the first two basis vectors. Vectors V(1) and V(2) in combination explained

93.3% of experimental edge variations, allowing limited assessment of linearity vs. applied voltage time. Using the vector sum: Mean + a_1 V(1) + a_2 V(2), the best approximations to linear edge transfer were conceptually determined as occuring between 2.3 and 4.3 seconds. Reasonable approximations for linear edge transfer were obtained at 4.3 seconds applied voltage time. Examination of experimental edge responses in Appendix D supported these conclusions.

Experiment four tested the influence of electrode spacing and applied voltage time on linearity of sinusoidal image transfer, specifically for the fountain toner apparatus. The intermediate electrode spacing, 0.60 mm, was not tested in this experiment. Image transfer characteristics were determined for individual sinusoidal exposure distributions with fundamental frequencies: 25, 64, and 102 cycles/mm. As the sinusoidal density responses exceeded the dynamic range of sensitometric density for zero seconds applied voltage time, this test condition produced nonlinear amplitude distortion. Analyses for harmonic distortions were therefore limited to samples produced at 1.0, 2.3, and 4.3 seconds applied voltage time, for both 0.20 mm and 1.27 mm electrode spacings.

Before analyzing the responses to individual sinusoidal test frequencies, it was noted that the observed distortions could not be theoretically explained in accordance with linear amplitude distortion. Referring to Figure 6, calculated normal electrostatic field spectra indicated only one test frequency at which the second or third harmonic amplitude exceeded the fundamental amplitude. For the fundamental frequency at 25 cycles/mm, the field intensity at 50 cycles/mm exceeded that of the fundamental by 6%. The third harmonic for 25 cycles/mm, and all harmonics for the 64 and 102 cycles/mm test frequencies, did not exceed the amplitude of the fundamental. As particle deposition neutralizes the source of enhanced frequency components first, the expected shift in dynamic frequency response was toward the lower frequencies (< 40 cycles/mm). Integrated field intensities theoretically dictated more constant deposition rates for frequencies less than 40 cycles/mm. Therefore, neither electrostatic nor dynamic field forces should have produced amplitude distortion upon transfer of the sinusoidal test frequencies.

Harmonic distortion factors computed for the lowest fundamental (25 cycles/mm) were determined not significant with respect to either electrode spacing or applied voltage time. For this fundamental, lack of significance was thought to result from erratic particle depositon as well as errors in effective electrodevelopment time. Erratic particle deposition at short applied voltage times would explain the low signal to noise ratios observed for the 0.20 mm electrode spacing. Large disparities among harmonic distortions coincided with disparities among fundamental modulations for replicate samples produced at 0.20 mm spacing.

These disparities suggested experimental error in effective electrodevelopment times.

At the 1.27 mm electrode spacing, 25 cycle/mm sample replicates produced sufficient repeatability in both fundamental modulation and harmonic distortion levels to provide monotonic trends with increased applied voltage time. These trends indicated a constant level of second harmonic distortion for 1.0 to 4.3 seconds time, producing a transfer harmonic distortion factor of 17 ± 3%. The third harmonic distortion factor was observed to decrease from 4.5 ± 1.5% at 1.0 second, to 1.0 ± 0.5% for 2.3 and 4.3 seconds applied voltage time. Although these trends appeared significant in explaining temporal nonlinear depletion effects, further analysis was not appropriate in light of the errors obtained for the lower electrode spacing. A greater number of experimental samples would be required to insure adequate repeatability in electrodevelopment time, before addressing significant trends as a function of electrode spacing or development time.

Harmonic distortion factors computed for fundamentals: 64 and 102 cycles/mm, were correlated with electrode spacing and applied voltage time. Both second and third harmonics for these fundamentals were greater than 5% at 1.0 seconds development. Both harmonics decreased with increasing applied voltage time, in inverse proportion to modulation increase at the fundamental. Shortly after development initiation, the fields associated with the test sinusoidal distributions would have reduced the concentration of toner particles near the film surface. As a result of this depletion, microsensitometry at these spatial frequencies appeared to deviate from large area macrosensitometry (H & D) response. Nonlinear particle depositon vs. image charge density would explain both second and third order interaction terms in the characteristic frequency transfer function.

A second order (square) term in an equation characterizing microsensitometric transfer would account for the majority of observed nonlinear depletion. The microsensitometric transfer curve would illustrate decreasing optical density vs. charge density, as a result of inadequate particle supply for proportional deposition to higher image charge levels. A third order (cubic) term in this transfer curve possibly indicated an unstable deposition/depletion phenomenon near development initiation.

With increasing time of applied electrode voltage, the driving force of uniform fields in the electrodeveloper region would replenish particles near the film surface. This replenishment would explain the observed increase in proportional deposition vs. image charge level with increased time of applied electrode voltage. A sharp drop in third order distortion factors (to less than 5%) was noted for the time increase 1.0 to 2.3 seconds at both electrode spacings. The actual amount of decrease was dependent on the particular electrode spacing and frequency tested. The rates of decrease with time for second order distortion factors indicated pronounced dependence on both the electrode spacing and the fundamental frequency.

In attempts to determine a conductivity parameter explaining temporal frequency response, Junginger, Schmidt, and Strunk[70] found that depletion near the film surface was frequency dependent. In their study for development of periodic image distributions, depletion was found to be more pronounced at spatial frequencies exhibiting greater electrostatic field intensities. Frequency dependent deposition and depletion would explain the differences in distortion factors obtained for 64 and 102 cycles/mm. Comparing Figures 33 and 34, the difference in distortion between these test frequencies was pronounced for the second harmonic, especially at 1.0 second applied voltage times. In accordance with greater electric field intensities for 64 cycles/mm, greater initial deposition rates produced greater nonlinearity in deposition vs. image charge level.

For both 64 and 102 cycles/mm, the initial levels of harmonic distortion for both harmonics were larger at the lower electrode spacing. An interaction between electrode spacing and applied voltage time produced differences in the time rate of decrease in harmonic distortions for 64 cycles/mm. The levels of harmonic distortion for 102 cycles/mm remained a consistant percentage higher for the lower electrode spacing, with no significant spacing/time interaction. The increase in distortion levels for the lower electrode spacing appeared inconsistent with postulations for increased nonlinearity at higher electrode spacings.

In terms of electrostatic field spectra, higher electrode spacings were expected to produce greater deposition rates to higher frequency components relative to rates at lower frequency components. Fundamentals at 64 and 102 cycles/mm along with their harmonics, were defined as higher frequency components based on field calculations for the TEP film tested. Relative rates of deposition vs. spatial frequency are not germane to the observed depletion effects for near sinusoidal distribution, and thus the influence of electrode spacing was probably that of absolute field intensity change. In terms of bulk deposition and depletion rates above the film surface, lowering the electrode spacing provided increased particle deposition rates near development initiation. The depletion that occured for sinusoidal imagery appeared to be localized with height above the film surface, as opposed to localized with respect to image component interactions.

Specific electrode spacings and applied voltage times that provided linearity of sinusoidal image transfer were determined from the computed distortion factors. The predominant factor for decreased nonlinearity of sinusoidal image transfer was increased electrodevelopment time. Within 4.3 seconds applied volatge time, the third harmonic distortion factors for 25, 64, and 102 cycles/mm diminished to 3.0% or less. This suggested that third order terms in a nonlinear transfer operator became negligable as electrodevelopment approached completion. Although no consistent trends with time were noted for second order harmonic distortion factors of 25 cycles/mm, significant reductions were noted for the higher fundamentals. Second order distortions reduced to approximately 10% for 64 cycles/mm, and 5% for 102 cycles/mm at 4.3 seconds.

Electrode spacing did not significantly alter the distortion levels at 4.3 seconds applied voltage time. For sinusoidal transfer at 25 cycles/mm, second order distortions were 17. ± 7.% and third order distortions were 2. ± 2.%, with no experimental significance attributed to electrode spacing. For sinusoidal transfer at 64 cycles/mm, second order distortions were 10. ± 1.5% and third order distortions were 1. ± 1.%, with no significant dependence on electrode spacing. For sinusoidal transfer at 102 cycles/mm, second and third order distortions were approximately 5.% and 1.5% with less than 2.% deviation attributed to electrode spacing in each case. Although significant differences occured among second order distortion levels for the different fundamental frequencies, electrode spacing had insignificant effect on distortion levels as development approached completion.

Comparisons of nonlinear transfer for edge distributions in experiment three and sinusoidal distributions in experiment four were necessarily qualitative. The different image distributions were exposed to provide the same average exposure effective exposure levels upon transfer through the sensitometric (H & D) curves. However, the input modulations for the higher spatial frequency components of the edge distribution were inherently lower than those of the same fundamental frequency sinusoidal distributions. Hence, the latent image charge, electrostatic field intensities, and resulting particle deposition rates should have been greater for sinusoidal distributions at higher frequency components. Furthermore, the methods of analysis for nonlinearity were relative, and unique to the image distribution employed.

Analyses for linearity as a function of tested electrodevelopment parameters indicated simularities between transfer effects for edge and sinusoidal distributions. Both edge and sinusoidal distributions exhibited pronounced nonlinearities in effective transfer near development initiation. For edge distributions, difference in relative electrostatic field intensity as a function of spatial frequency produced nonlinear adjacency effects associated with spatially localized depletion above the film surface. As a result, nonlinear response vs. charge level was noted at intermediate frequency components ($20 < f < 40$ cycles/mm). Sinusoidal distributions exhibited nonlinear deposition vs. charge level as a result of bulk depletion of electrodeveloper particles above the film surface. As a result, individual sinusoidal distributions with fundamentals at 25, 64 and 102 cycles/mm exhibited significant harmonic distortions near development initiation.

As development approached completion, both edge and sinusoidal distributions exhibited decreased nonlinearity in effective transfer. This decrease in nonlinearity indicated restored electrodeveloper particle deposition to initially depleted image components. Although decreased, distortions in resulting imagery were not eliminated within 4.3 seconds applied voltage time. At this development time edge distributions exhibited reductions in response as a function input exposure for spatial frequency components greater than 20 cycles/mm. Sinusoidal image transfer at 25, 64, and 102 cycles/mm exhibited significant second order distortions, also associated with reduced response as a function of charge level.

Dependence of nonlinearity on electrode spacing was determined statistically significant for both edge and sinusoidal transfer. Although the basis vector characterizing this relationship explained only 4.9 percent of experimental edge variations, this vector indicated greater temporal adjacency effects for a lower electrode spacing (0.20 mm). The second order harmonic distortion factors for sinusoidal transfer at 64 and 102 cycles/mm were also initially greater for 0.20 mm as opposed to 1.27 mm electrode spacing. These results, although contrary to postulated effects of electrode spacing, indicated increased nonlinearity of transfer at initiation of development for decreased electrode spacing. This dependence of nonlinearity on electrode spacing was unique to the fountain toning apparatus.

V. CONCLUSIONS

The mechanistic effects of exposing wavelength shift on the linearity of exposure/photoconduction transfer remained inconclusive for the film employed. Increased nonlinear image transfer was obtained for a shift to wavelengths of peak film absorption. However, the degree of nonlinearity introduced was not considered sufficient to warrant transfer characterization using a nonlinear operator. In accordance with postulations, the exposing wavelength shift provided insignificant control on linearity of image transfer for the specific film tested.

The influence of electrodevelopment parameters on linearity of edge transfer varied in accordance with the experimental development apparatus. For the continuous electrode apparatus, degree of nonlinear edge transfer was controlled by the interaction between electrode spacing and film platen velocity. Approximations to linear edge transfer were limited to slower film platen velocities for the 1.27 mm electrode spacing. Adjacency effects at short development times (faster film platen velocities) were interpreted as localized nonlinear depletion effects. For this apparatus, the initial amounts of nonlinear adjacency effect and their rate of decrease with increased film platen velocity, decreased with electrode spacing. The lowest spacing exhibited the least dependence of dynamic deposition on spatial frequency, providing approximate linear transfer at all film platen velocities.

For the fountain toner electrodevelopment apparatus, experimental error and analysis limitations precluded accurate assessment of linearity vs. electrode spacing. A transition from adjacency effects to microsensitometry variation was noted for increasing durations of applied voltage to the development electrode. In comparison to results for the continuous electrode apparatus, these results indicated greater adjacency effects near development initiation (1.0 seconds). The gating method employed for the fountain toner apparatus allowed greater control for testing linearity of edge transfer vs. electrodevelopment time. Longer durations of applied electrode voltage produced limited depletion at higher charge levels of high frequency components in the edge distributions.

The edge effects observed at short electrodevelopment times were representative of nonlinear adjacency effects. For the continuous electrode apparatus, certain parameter combinations were found to maintain the inherent linear edge effects associated with electrostatic field distributions. For these cases, however, the magnitude of edge enhancement was considered insignificant for enhanced information extraction of fine image details.

Transfer analyses for sinusoidal images using the fountain toner apparatus, revealed a nonlinear deposition phenomenon for higher spatial frequencies. The harmonic distortion content for 64 and 102 cycles/mm indicated correlations of nonlinear deposition phenomenon with electrode spacing and electrodevelopment time.

Disproportionate deposition vs. charge level at these sinusoidal frequencies would explain observed intermediate and high frequency depletion for extended development of edge distributions. Near development initiation, the nonlinear responses observed for edge and sinusoidal distributions explained different depletion phenomena. As opposed to depletion interactions among image components in edge transfers, electrodevelopment of sinusoidal distributions revealed a bulk nonlinear depletion vs. image charge density.

Both edge and sinusoidal image transfer were significantly nonlinear near development initiation. These nonlinearities prohibited characterization of image transfer using a Modulation Transfer Function (MTF) at short development times. Dissimilar nonlinear electrodevelopment mechanisms were apparent for edge vs. sinusoidal distributions. Specific electrode spacing and electrodevelopment time combinations could not be associated with strict linear transfer for either edge or sinusoidal distributions.

For the longer electrodevelopment times, both edge and sinusoidal responses indicated nonlinear deposition vs. charge at higher spatial frequencies ($f > 40$ cycles/mm). However, the degree of nonlinearity observed in each case would not preclude reasonable approximation for image transfer using a linear operator. Therefore, Modulation Transfer Functions would provide approximate predictions for image responses near development to completion. Variations should be minimal among Modulation Transfer Functions computed for different development electrode spacings at complete development. Considerable differences should be expected for Modulation Transfer Functions when images are developed with different electrodevelopment apparatus.

FOOTNOTES

FOOTNOTES

1. H. E. J. Neugebauer, "Electrostatic Fields of Xerographic Images," *Xerography and Related Processes*, eds. J. H. Dessauer and H. E. Clark, (New York: Focal Press, 1965), pp. 217-223.

2. R. M. Schaffert, ed., *Electrophotography*, (New York: Halstead Press, 1975), pp. 505-511.

3. C. C. Kao, "Electric Field, Transfer, and Spread Functions in Xerographic Image Studies," *Journal of Applied Physics* 44 (April 1973): 1543.

4. J. C. Witte and J. F. Szczepanik, "Application of Transfer Function Methods to the Characterization of Xerographic Development," *Journal of Applied Photographic Engineering* 4 (Spring 1978): 52.

5. H. E. J. Neugebauer, "A Describing Function for the Modulation Transfer of Xerography," *Applied Optics* 4 (April 1965): 453.

6. A. J. Rushing, D. C. Hoesterey, and G. F. Fritz, "Limiting Factors in Electrophotographic Latent Image Resolution," *International Conference on Electrophotography*, 2nd, Society of Photographic Scientists and Engineers, 1969, p. 200.

7. Neugebauer, "A Describing Function for the Modulation Transfer of Xerography," p. 455.

8. Witte and Szczepanik, p. 52.

9. Rushing, Hoesterey, and Fritz, p. 204.

10. E. Ingelstam, "Attempts to Treat Nonlinear Imaging Devices," *Japanese Journal of Applied Physics* 4, Supplement I (1965): 15.

11. P. Eychoff, *System Identification*, (New York: John Wiley & Sons, 1974), pp. 94-130.

12. M. Schetzen, *The Volterra and Wiener Theories of Nonlinear Systems*, (New York: John Wiley & Sons, 1980), pp 39, 80.

13. J. L. Simonds, "Analysis of Nonlinear Photographic Systems," *Photographic Science and Engineering* 9 (September 1965): 294.

14. R. Clay, *Nonlinear Networks and Systems*, (New York: John Wiley & Sons, 1971), p. 108.

15. Ibid., p. 111.

16. R. E. Swing, personal communication.

17. Simonds, "Analysis of Nonlinear Photographic Systems," p. 296.

18. A. Papoulis, *The Fourier Integral and Its Application*, (New York: McGraw Hill, 1962), pp. 82-119.

19. Rushing, Hoesterey, and Fritz, p. 200.

20. Ibid., P. 202.

21. Ibid., p. 200.

22. Ibid., p. 201.

23. R. G. Zech, J. F. Dirks, and L. M. Ralston, "Transparent Electrophotographic Films for Optical Data Storage Applications," *Applied Optics* 16 (June 1977): 1642.

24. Rushing, Hoesterey, and Fritz, p. 204.

25. Kao, p. 1543.

26. Ibid., pp. 1543-1548.

27. Schaffert, p. 479.

28. Ibid., p.498.

29. Ibid., p. 498-500.

30. Kao, p. 1549.

31. Zech, Dirks, and Ralston, p. 1642

32. H. E. J. Neugebauer, "A Describing Function for the Modulation Transfer of Xerography," p. 453.

33. H.-G. Junginger and R. Strunk, "Latent Image Changes During Electrophotographic Development," *Journal of Applied Physics* 47 (July 1976): 3021.

34. H.-G. Junginger and R. Strunk, "Time Dependence of Latent Images in Electrophotographic Development," *Journal of Photographic Science* 25 (1977): 109.

35. R. Kohler, D. Giglberger, and F. Bestenreiner, "Studies on Electrophoretic Developers for Pictorial Electrophotography," *Photographic Science and Engineering* 22 (1978): 218.

36. Ibid., p. 225.

37. H.-G. Junginger, R. F. Schmidt, and R. Strunk, "Experiments on Latent Electrostatic Images and Electrophoretic Development, Comparison with Model Calculations," *Photographic Science and Engineering* 22 (July/August 1978): 213.

38. Kohler, Giglberger, and Bestenreiner, p. 226.

39. Junginger, Schmidt, and Strunk, "Experiments on Latent Electrostatic Images and Electrophoretic Development," p. 221

40. Ibid., p. 216

41. Schaffert, pp. 557-567.

42. Ibid., p. 568.

43. H. A. Pohl, "Nonuniform Field Effects: Dielectrophoresis," *Electrostatics and Its Applications*, ed., A.D. Moore, (New York: John Wiley & Sons, 1973), pp. 336-349.

44. H. A. Pohl, "The Motion and Precipitation of Suspensoids in Divergent Electric Fields," *Journal of Applied Physics* 22 (July 1915): 869.

45. C. Inoue, *Mapping of Fields*, Volume 1, ed., E. Weber, (New York: John Wiley & Sons, 1950), p. 387.

46. Schaffert, p. 568.

47. H. M. Stark and R. S. Menchel, "Kinetics of Electrophoretic Development of Electrostatic Charge Patterns," *Journal of Applied Physics* 41 (June 1970): 2905.

48. Kohler, Giglberger, and Bestenreiner, p. 224.

49. R. P. Lubianez, personal communication.

50. H. G. Junginger, F. F. Schmidt, and R. Strunk, "Experiments on Latent Electrostatic Images and Electrophoretic Development," Photographic Science and Engineering 22 (July/August 1978): 214.

51. Schaffert, pp. 230-233.

52. J. L. Simonds, "Application of Characteristic Vector Analysis to Photographic and Optical Response Data," Optical Society of America 53 (August 1963): 968.

53. R. P. Lubianez and E. B. Bourgeois, "Advanced Electrodeveloper for High Performance TEP Film Applications," Air Force Wright Aeronautical Laboratory Report No. TR-82-1043, January 1982, pp. 9-23.

54. P. I. Bachelder, J. F. Dirks, and G. J. Myers, "Electrophotographic Film Recording and Duplicating Systems," U.S.A.F. Report for Conract F33615-78-C-1628, November 1980, p. 216.

55. J. F. Dirks, personal communication.

56. B. Saunders, "The Mead Electrophotographic Evaluator," Journal of Applied Photographic Engineering 5 (Winter 1979): 26.

57. R. L. Lamberts, "The Production and Use of Variable-Transmittance Sinusoidal Test Objects," Applied Optics 2 (March 1963): 273.

58. M. Born and E. Wolf, Principles of Optics (New York: Pergamon Press, 1964), pp. 480-486.

59. R. Keller, personal communication.

60. "Operation and Maintenance Manual for the ARI Precision Focus Control, Model 301," Aerodyne Research, Inc., Bedford Research Park, Crosby Drive, Bedford, Massachusetts. July 1979. p. 6.

61. R. E. Swing, "Problems of Linear Microdensitometry," U.S.A.F. Report for Contract F33615-71-M-5007, May 1975, pp. 90-96.

62. R. A. Jones, "The Effects of Slit Misalignment on the Microdensitometer Modulation Transfer Function," Photographic Science and Engineering 9 (November 1965): 97.

63. J. Leonard, "Micro-D Analysis of Sine Wave Grating," Report for AFWAL/AARF, Wright-Patterson Air Force Base, Ohio (September 1974), pp. 1-6.

64. N. C. Griswold, "A Study in Reconnaissance Sensor Response with Fourier Analysis Methods," (Thesis, University of Cincinnati, 1971), pp. 55-57.

65. Simonds, "Characteristic Vector Analysis," pp. 969-974.

66. A. D. Rickmers and H. N. Todd, *Statistics*, (New York, McGraw-Hill, 1967), pp. 557-562

67. Ibid, p. 294.

68. Rushing, Hoesterey, and Fritz, p. 203.

69. Kao, pp. 1548-1550.

70. Junginger, Schmidt, and Strunk, "Experiments on Latent Electrostatic Images and Electrophoretic Development," p. 217.

BIBLIOGRAPHY

BIBLIOGRAPHY

Bachelder, Phillip I., Dirks, Johan F., and Meyers, George J. "Electrophotographic Film Applications." Air Force Aeronautical Laboratory Report No. TR-82-1043, 1982.

Born, Max, and Wolf, Emil. Principles of Optics. New York: Macmillan Co., 1964.

Clay, Richard. Nonlinear Networks and Systems. New York: John Wiley & Sons, 1971.

Eychoff, Pieter. System Identification. New York: John Wiley & Sons, 1974.

Griswold, Normand C. "A Study in Reconnaissance Sesnor Response with Fourier Analysis Methods." Thesis, University of Cincinnati, 1971.

Ingelstam, Erik. "Attempts to Treat Nonlinear Imaging Devices." Japanese Journal of Applied Physics 4, Supplement I (1965): 15-22.

Inoue, C. Mapping of Fields. Vol. I. ed. E. Weber. New York: John Wiley & Sons, 1950.

James, Robert A. "The Effect of Slit Misalignment on the Microdensitometer Modulation Transfer Function." Photographic Science and Engineering 9 (November/December 1965): 355-59.

Junginger, H.-G., Schmidt, R. F., and Strunk, R. "Experiments on Latent Electrostatic Images and Electrophoretic Development, Comparison with Model Calculation." Photographic Science and Engineering (July/August 1978): 213-18.

Junginger, H.-G., and Strunk, R. "Latent Image Changes During Electrophotographic Development." Journal of Applied Physics 47 (July 1976): 3021-27.

________. "Time Dependence of Latent Images in Electrophotographic Development." Journal of Photographic Science 25 (1977): 109-14.

Kao, Cheng C. "Electric Field, Transfer, and Spread Functions in Xerographic Image Studies." Journal of Applied Physics 44 (April 1973): 1543-51.

Kohler, R., Giglberger, D., and Bestenreiner, F. "Studies on Electrophoretic Developers for Pictorial Electrophotography." Photographic Science and Engineering 22 (July/August 1978): 218-27.

Lamberts, Robert L. "The Production and Use of Variable-Transmittance Sinusoidal Test Objects." Applied Optics 2 (March 1963): 273-76.

Leonard, James. "Micro-D Analysis of Sine Wave Grating." Report for AFWAL/AARF, Wright-Patterson Air Force Base, Ohio. September 1974.

Lubianez, Ronald P., and Bourgeios, Elizabeth B. "Advanced Electrodeveloper for High Performance TEP Film Applications." Air Force Wright Aeronautical Laboratory Report No. TR-82-1043. November 1980.

Neugebauer, Hans E. J. "Electrostatic Fields of Xerographic Images." Xerography and Related Processes. eds. J. H. Dessauer and H. E. Clark. New York: Focal Press, 1965.

________. "A Describing Function for the Modulation Transfer of Xerography." Applied Optics 4 (April 1965): 943-45.

Papoulis, Athanasios. The Fourier Integral and Its Applications. New York: McGraw-Hill, 1962.

Pohl, Herbert A. "The Motion and Precipitation of Suspensoids in Divergent Electric Fields." Journal of Applied Physics 22 (July 1915): 869-71.

________. "Nonuniform Field Effects: Dielectrophoresis." Electrostatics and Its Applications. ed. A. D. Moore. New York: John Wiley & Sons, 1973.

Rickmers, Albert D., and Todd, Hollis N. Statistics. New York: McGraw-Hill, 1967.

Rushing, A. J., Hoesterey, D. C., and Fritz, G. F. "Limiting Factors in Electrophotographic Latent Image Resolution." International Conference on Electrophotography, 2nd. Society of Photographic Scientists and Engineers, 1969.

Saunders, Burt. "The Mead Electrophotography Evaluator." Journal of Applied Photographic Engineering 5 (Winter 1979): 26-31.

Schaffert, R. M., ed. Electrophotography. New York: Halstead Press, 1975.

Schetzen, Martin. The Volterra and Wiener Theories of Nonlinear Systems. New York: John Wiley & Sons, 1980.

Simonds, J. L. "Analysis of Nonlinear Photographic Systems." Photographic Science and Engineering 9 (September-October 1965): 294-300.

________. "Application of Characteristic Vector Analysis to Photographic and Optical Response Data." Optical Society of America 53 (August 1963): 968-74.

Stark, H. M., and Menchel, R. S. "Kinetics of Electrophoretic Development of Electrostatic Charge Patterns." Journal of Applied Physics 41 (June 1970): 2905-13.

Swing, Richard E. "Problems of Linear Microdensitometry." Report for U.S. Air Force contract no. F33615-71-M-5007, May 1975.

Witte, J. C., and Szczepanik, J. F. "Application of Transfer Function Methods to the Characterization of Xerographic Development." Journal of Applied Photographic Engineering 4 (Spring 1978): 52-56.

Zech, R. G., Dirks, J. F., and Ralston, L. M. "Transparent Electrophotographic Films for Optical Data Storage Applications." Applied Optics 16 (June 1977): 1642-51.

General References

Bestenreiner, Friedrich. "Pictorial Electrophotography." Photographic Science and Engineering 23 (March/April 1979): 93-98.

Brigham, E. Oran. The Fast Fourier Transform. Englewood Cliffs: Prentice Hall, 1974.

Dainty, J. C., and Shaw, R. Image Science. New York: Academic Press, 1974.

Gaskill, Jack D. Linear Systems, Fourier Transforms, and Optics. New York: John Wiley & Sons, 1978.

Gopala, U. V. Rao, Zeman, Gary H., and Fatouros, Panos P. "Xerogadiography and the MTF Concept." Journal of Applied Photographic Engineering 5 (Spring 1979): 78-83.

Halfdamarson, J., and Hauffe, K. "On the Electrokinetic Properties of Positively Charged Toner Dispersions and Electrostatic Image Development." Photographic Science and Engineering 23 (January/February 1979): 27-32.

Jones, Robert A., and Coughlin, John F. "Elimination of Microdensitometer Degredation from Scans of Photographic Images." Applied Optics 5 (September 1966): 1411-14.

Jones, Robert A., and Yeadon, Edward C. "Determination of the Spread Function from Noisy Edge Scans." Photographic Science and Engineering 13 (1969): 200-204.

Lancaster, Peter. Theory of Matrices. New York: Academic Press, 1969.

Lewis, R. B., and Stark, H. M. "High Sensitivity Electrophotographic Development." Current Problems in Electrophotography. ed. W. F. Berg and K. Hauffe. New York: deGruyter Press, 1972.

Neugebauer, H. E. J. "Development Method and Modulation Transfer Function of Xerography." Applied Optics 6 (May 1967): 943-45.

Stechemesser, Reinhold. "Space Charge and Flow in Liquid Electrophotographic Developers." Photographic Science and Engineering 26 (January/February 1982): 27-30.

Stremler, Ferrel G. Introduction to Communication Systems. 2nd ed. London: Addison-Wesley, 1982.

Swing, Richard E. "The Investigation of the Double-Sinusoid Target as a Means for Linearity Testing." Report for National Bureau of Standards, U.S. Department of Commerce, Washington, D.C., December 1974.

APPENDICES

APPENDIX A

Circuit for Gating Voltage Applied to the Development Electrode, Fountain Toning Apparatus

A schematic for the Gating Circuit cited in Section IV.C.1. is given in Figure A1. The circuit is connected to a +5 Volt line in the microprocessor logic of the Mead Electrophotographic Evaluator, and controls switching of high voltage applied to the development electrode. A negative pulse from an LED sensor for film platen position activates the timing circuit. Two NE/SE 555 timing devices (Signetics) are employed as monostable multivibrators to time (1) a delay from LED pulse to high voltage switching, and (2) duration of activated high voltage, respectively. Applied voltage durations are selected in accordance with chosen resistance for the second monostable multivibrator. Capacitors, transistors, and diodes are used in conjuction to filter out noise pulses (microseconds) from the microprocessor logic to the NE/SE 555 devices.

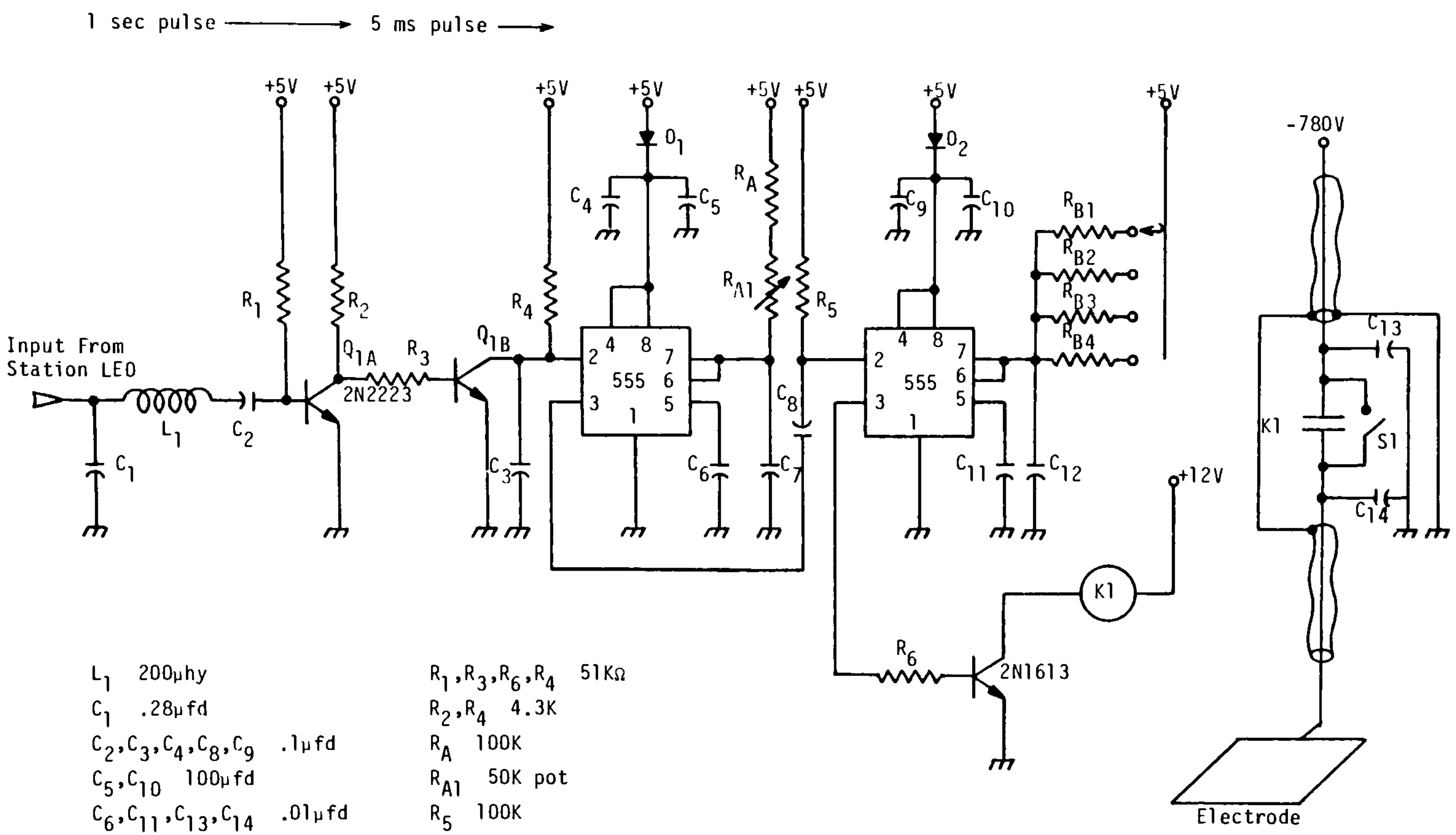

L_1	200μhy
C_1	.28μfd
C_2,C_3,C_4,C_8,C_9	.1μfd
C_5,C_{10}	100μfd
C_6,C_{11},C_{13},C_{14}	.01μfd
C_7,C_{12}	1μfd
D_1,D_2	1N4003

R_1,R_3,R_6,R_4	51KΩ
R_2,R_4	4.3K
R_A	100K
R_{A1}	50K pot
R_5	100K
R_{B1}	3.6 meg + 1 meg pot
R_{B2}	4.3 meg + 1 meg pot
R_{B3}	5.1 meg + 1 meg pot
R_{B4}	7.5 meg + 1 meg pot

Figure A1. Circuit for Gating Voltage Applied to the Development Electrode, Fountain Toning Apparatus.

APPENDIX B

Sensitometric H & D Responses and Edge Response Vectors Measured on Electrophotographic Film Samples of Experiment One.

In this Appendix, Hunter and Driffield (H & D) response curves are illustrated for sensitometric images generated in experiment one; Figures B1 & B2. Effective exposure edge response vectors for experiment one are included in Figures B3 through B6. These vectors are grouped according to Film Platen Velocity and Exposing Wavelength parameter levels.

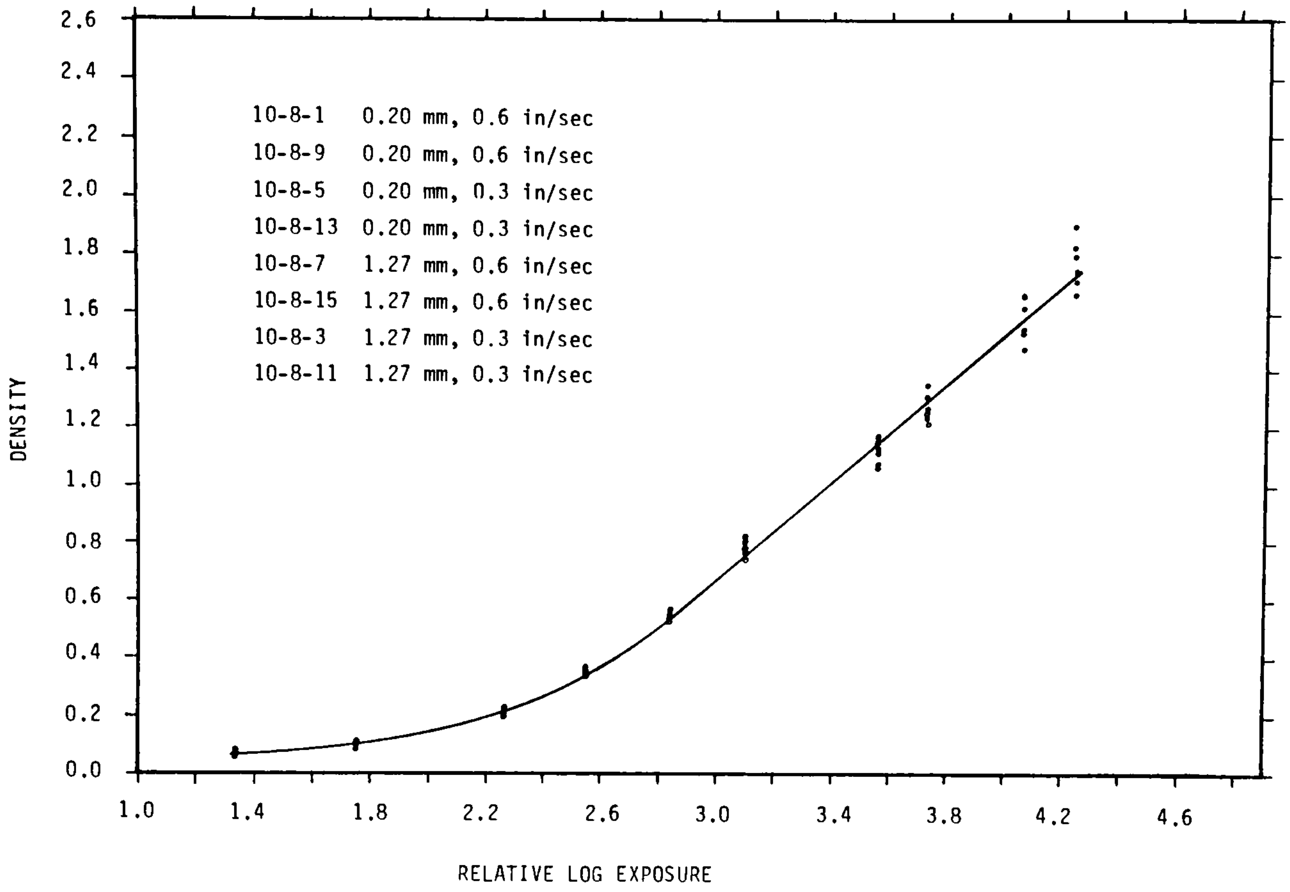

Figure B1. Sensitometric H&D Curves for Experiment One; Exposing Wavelength 440 nm.

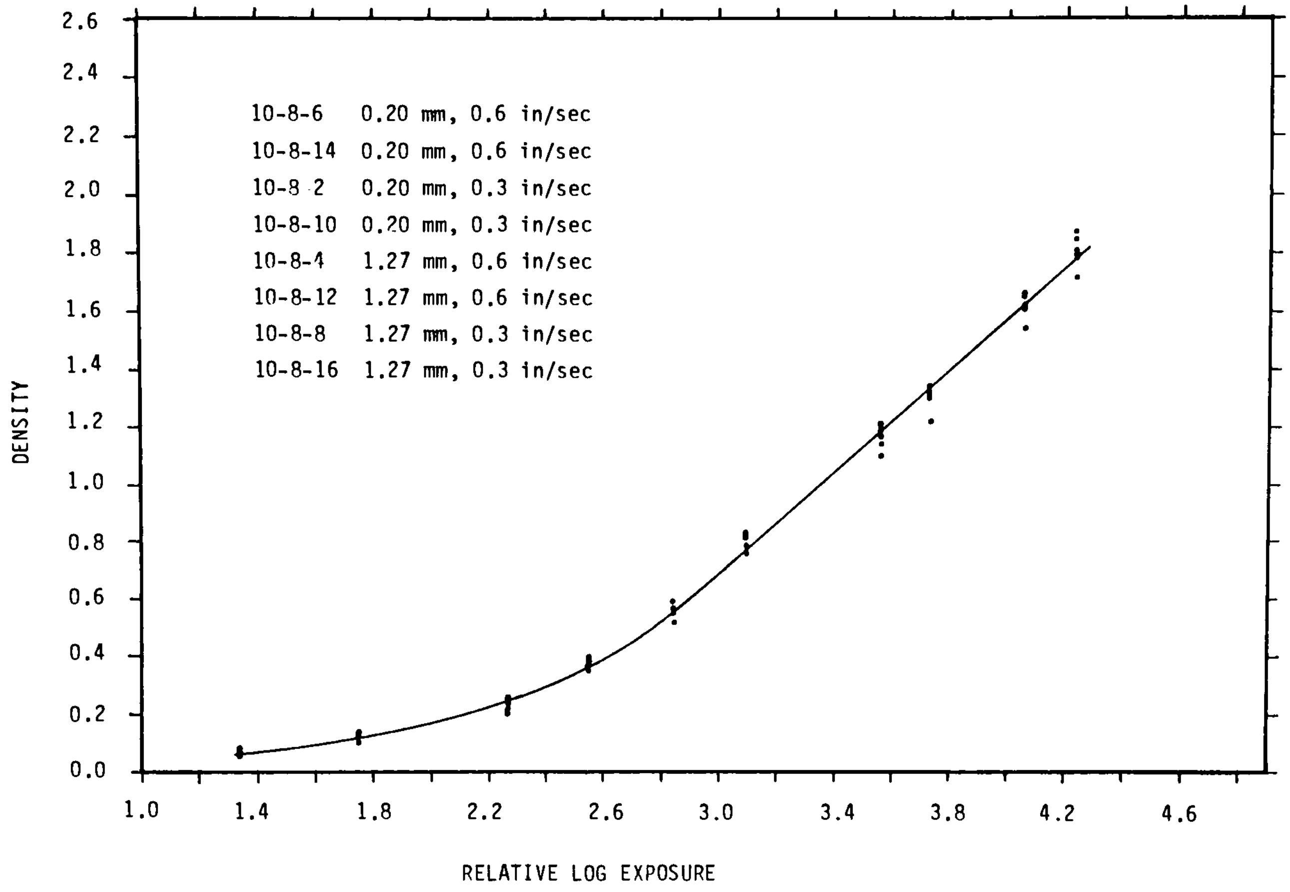

Figure B2. Sensitometric H&D Curves for Experiment One; Exposing Wavelength 500 nm.

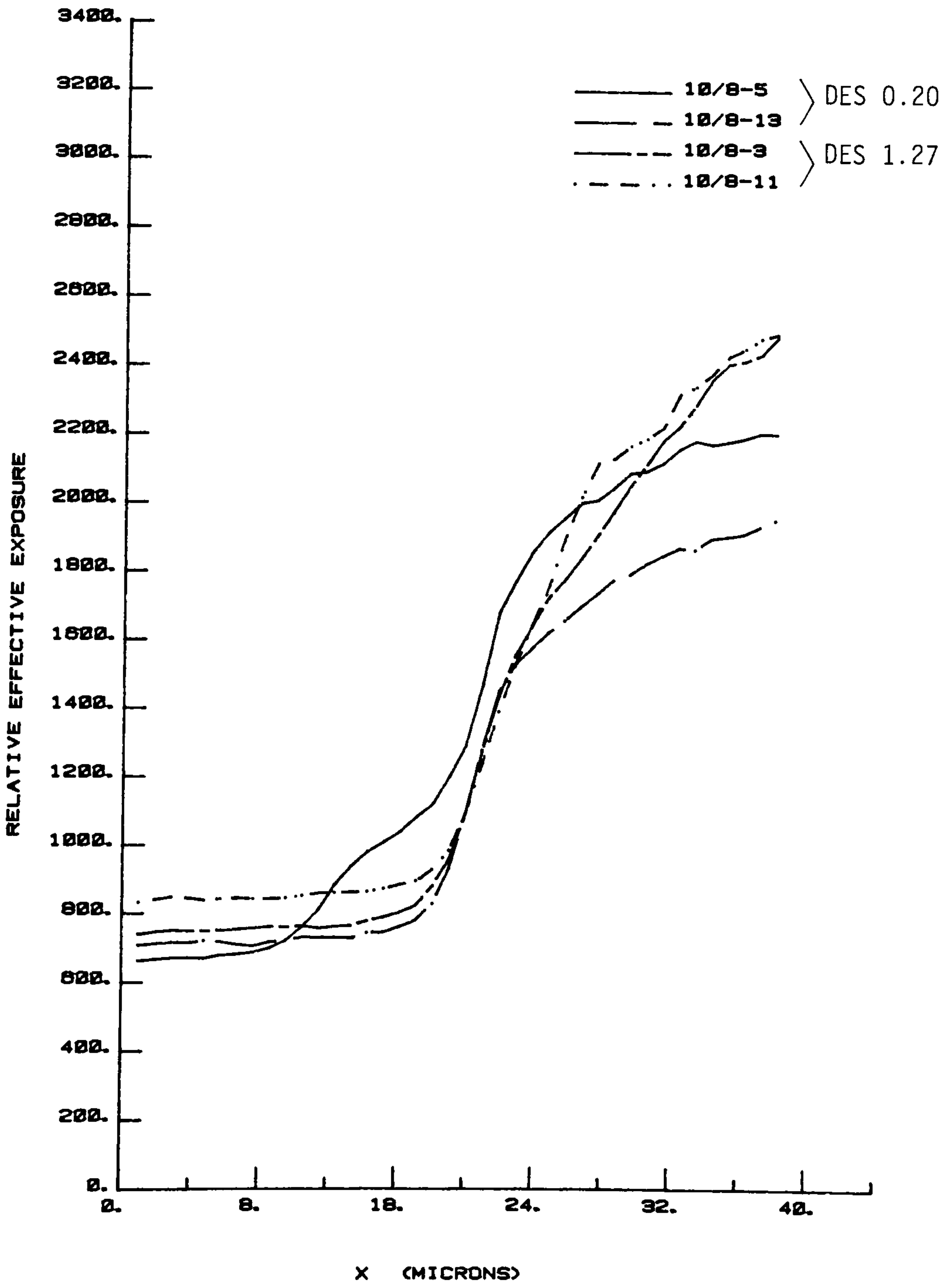

Figure B3. Experiment One Edge Response Vectors; Film Platen Velocity 0.3 in/sec; Exposing Wavelength 440 nm.

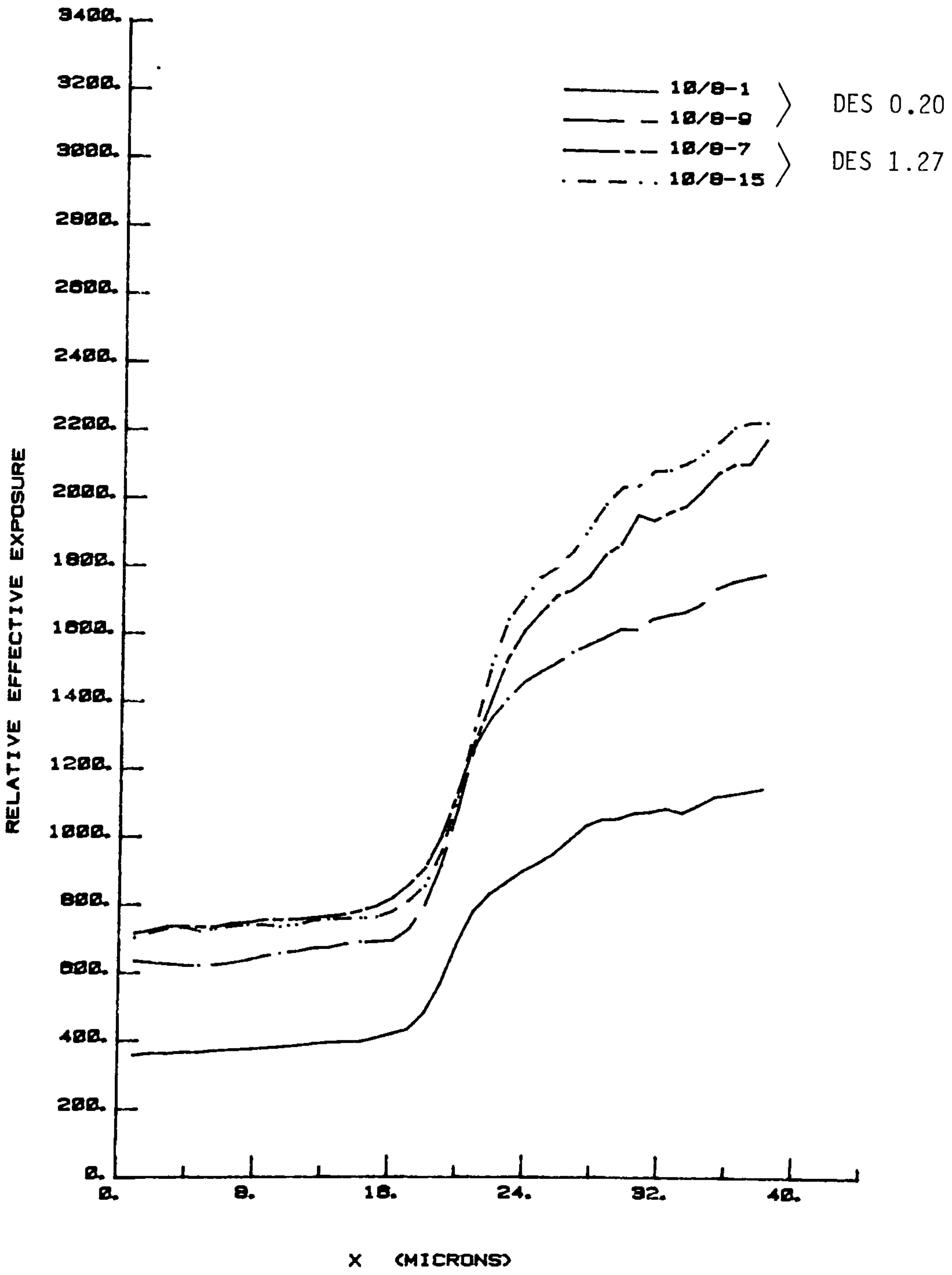

Figure B4. Experiment One Edge Response Vectors; Film Platen Velocity 0.6 in/sec; Exposing Wavelength 440 nm.

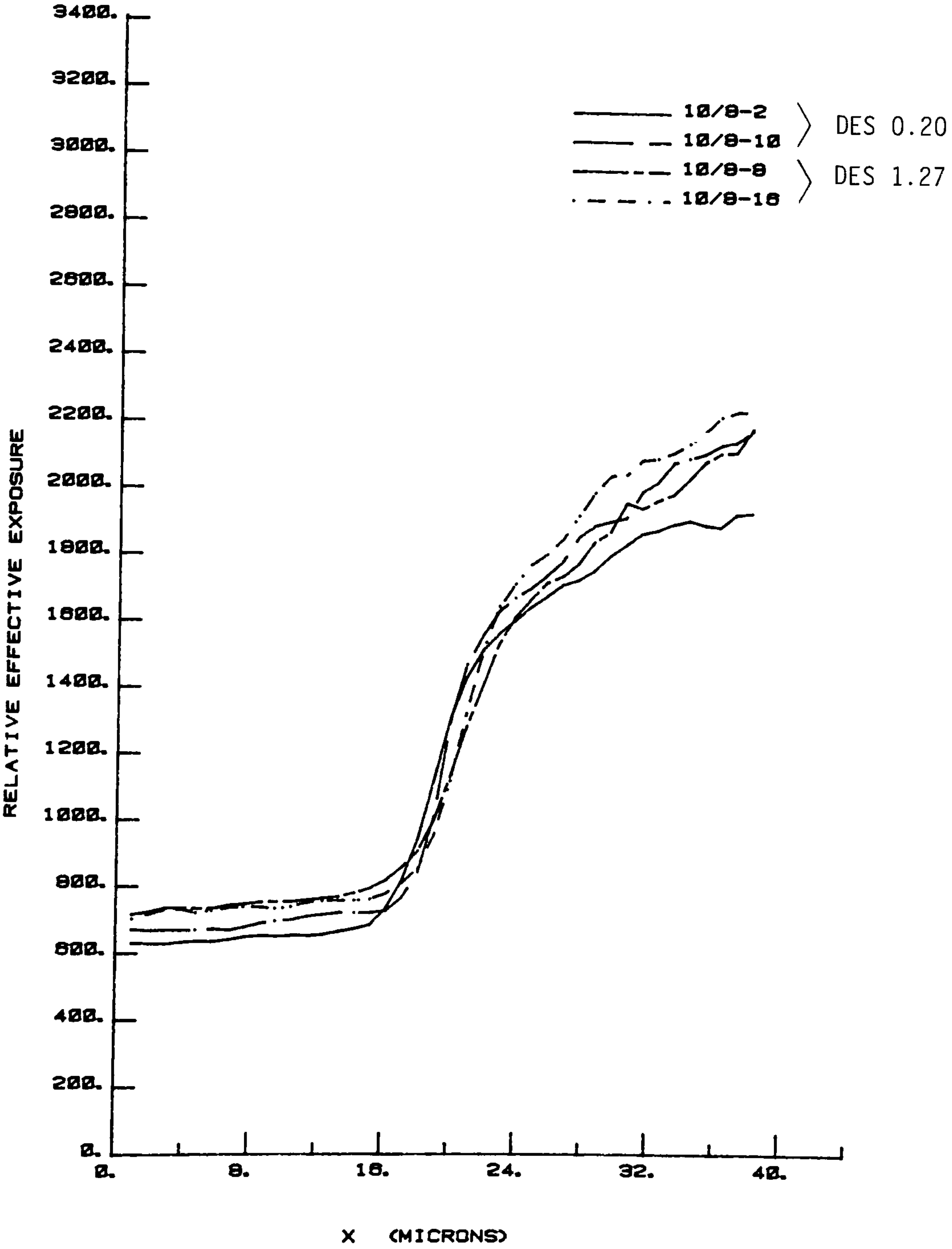

Figure B5. Experiment One Edge Response Vectors; Film Platen Velocity 0.3 in/sec; Exposing Wavelength 500 nm.

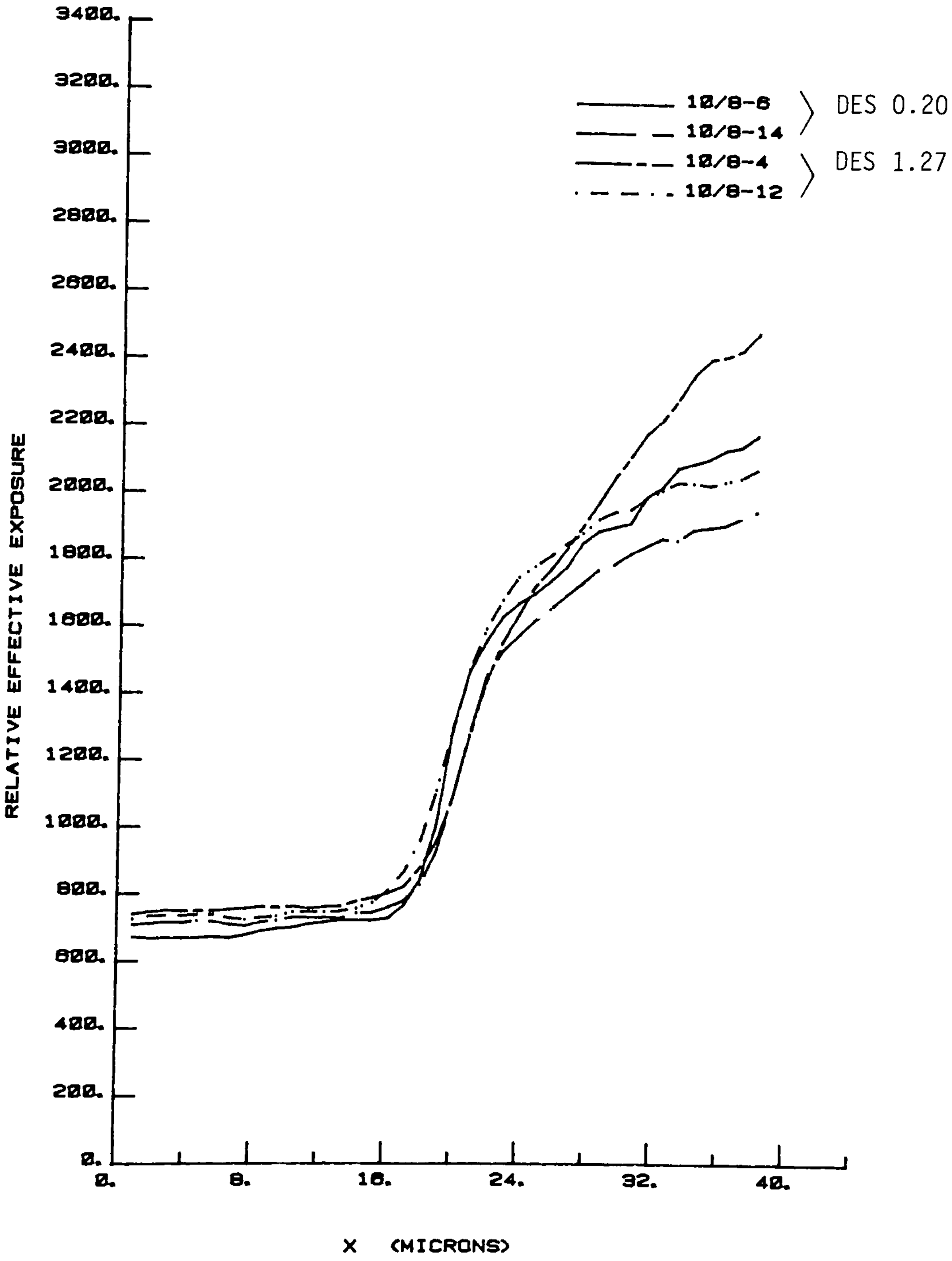

Figure B6. Experiment One Edge Response Vectors; Film Platen Velocity 0.6 in/sec; Exposing Wavelength 500 nm.

APPENDIX C

Sensitometric H & D Responses and Edge Response Vectors Measured on Electrophotographic Film Samples of Experiment Two.

In this Appendix, Hunter and Driffield (H & D) response curves are illustrated for sensitometric images generated in experiment two; Figures C1 - C3. Effective exposure edge response vectors for experiment two are included in Figures C4 through C7. These vectors are grouped according to Film Platen Velocity parameter levels.

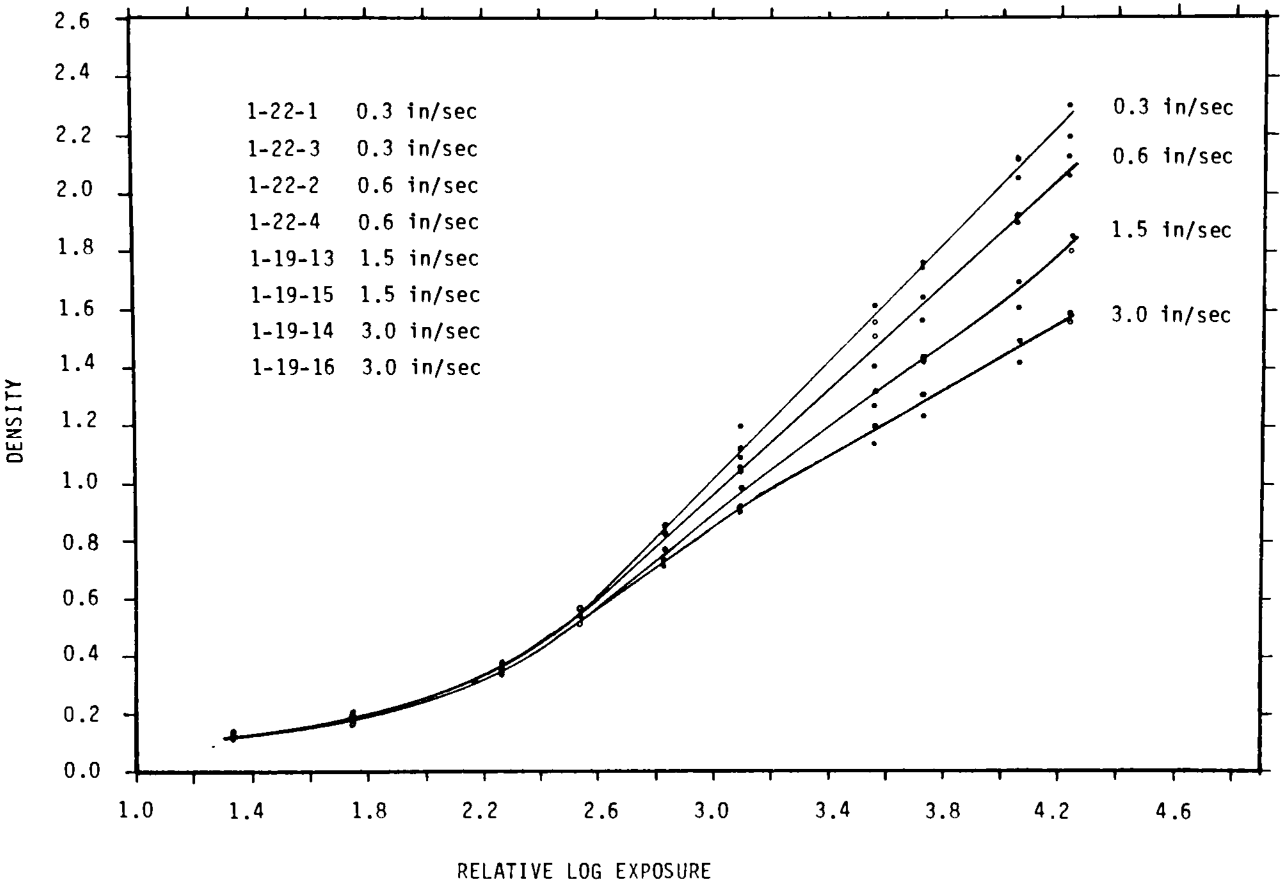

Figure C1. Sensitometric H&D Curves for Experiment Two; Development Electrode Spacing 0.20 mm.

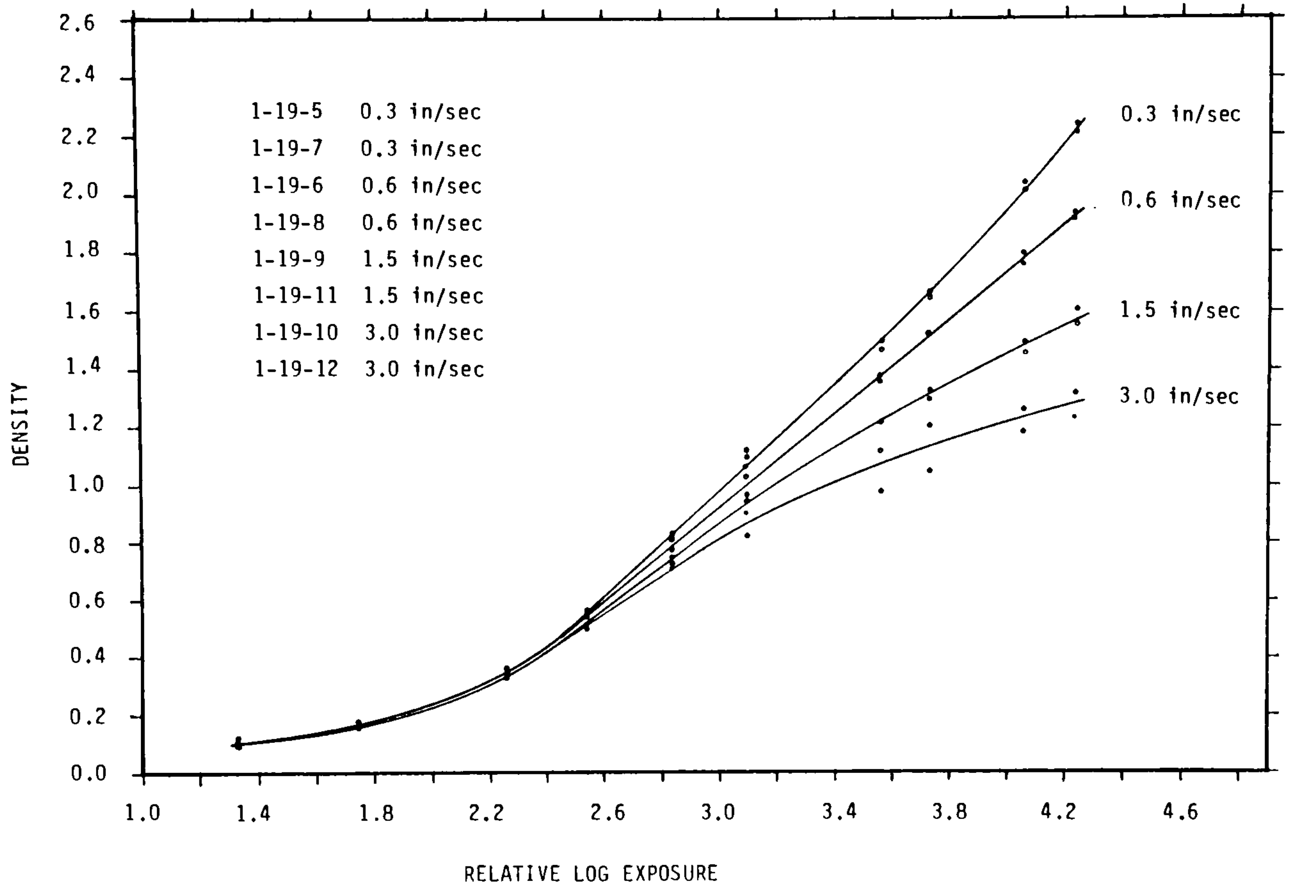

Figure C2. Sensitometric H&D Curves for Experiment Two; Development Electrode Spacing 0.60 mm.

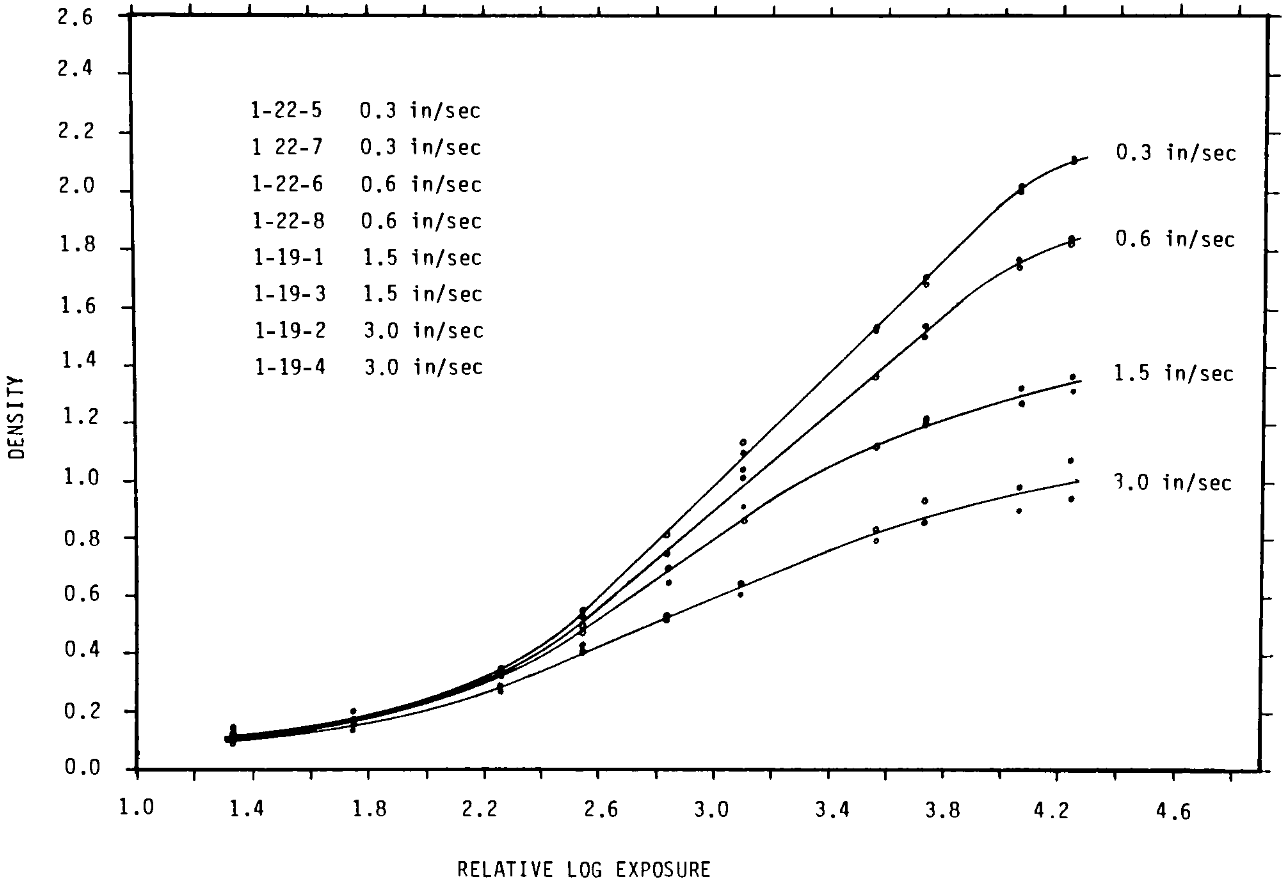

Figure C3. Sensitometric H&D Curves for Experiment Two; Development Electrode Spacing 1.27 mm.

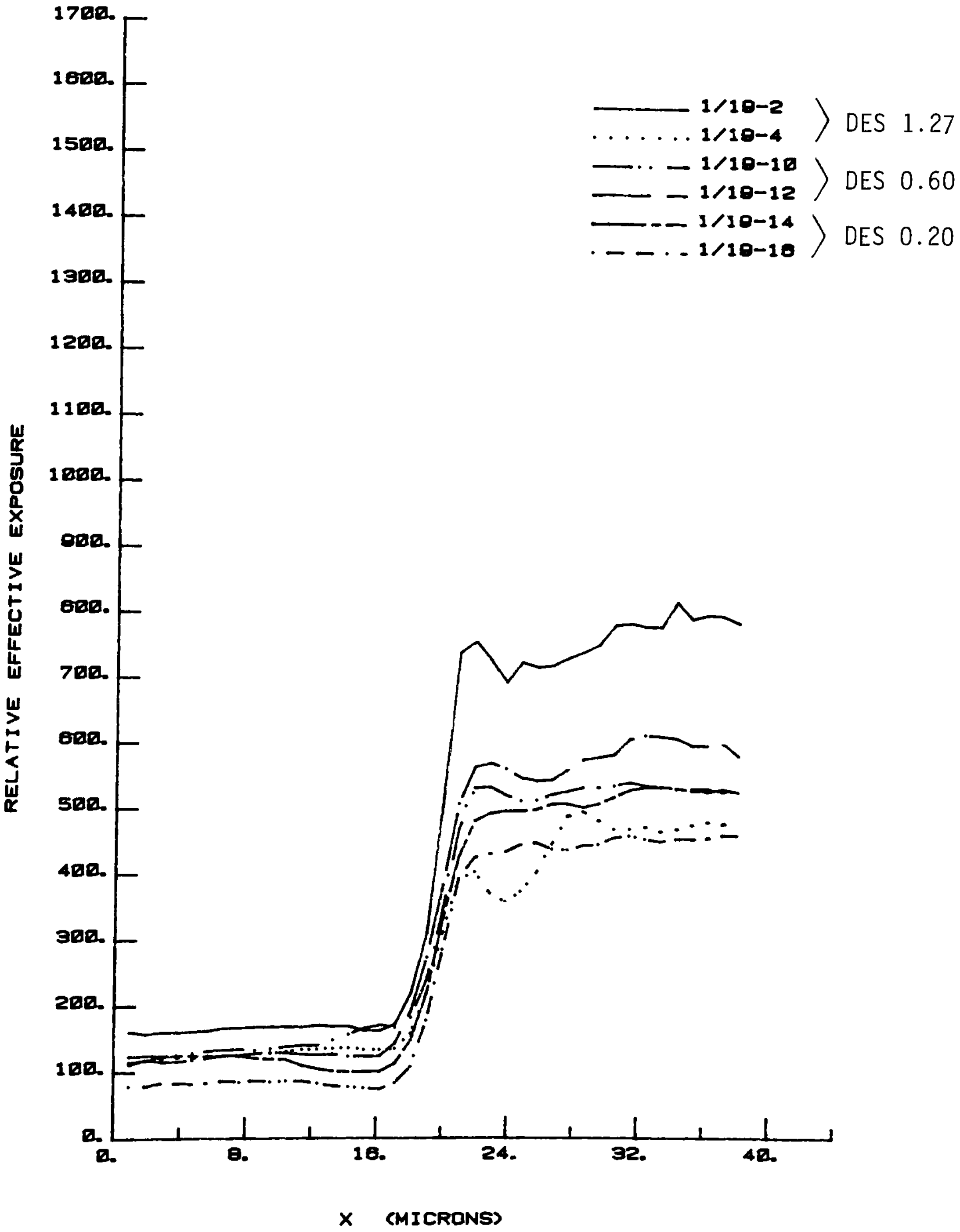

Figure C4. Experiment Two Edge Response Vectors; Film Platen Velocity 3.0 in/sec; Development Electrode Spacing (DES) in millimeters.

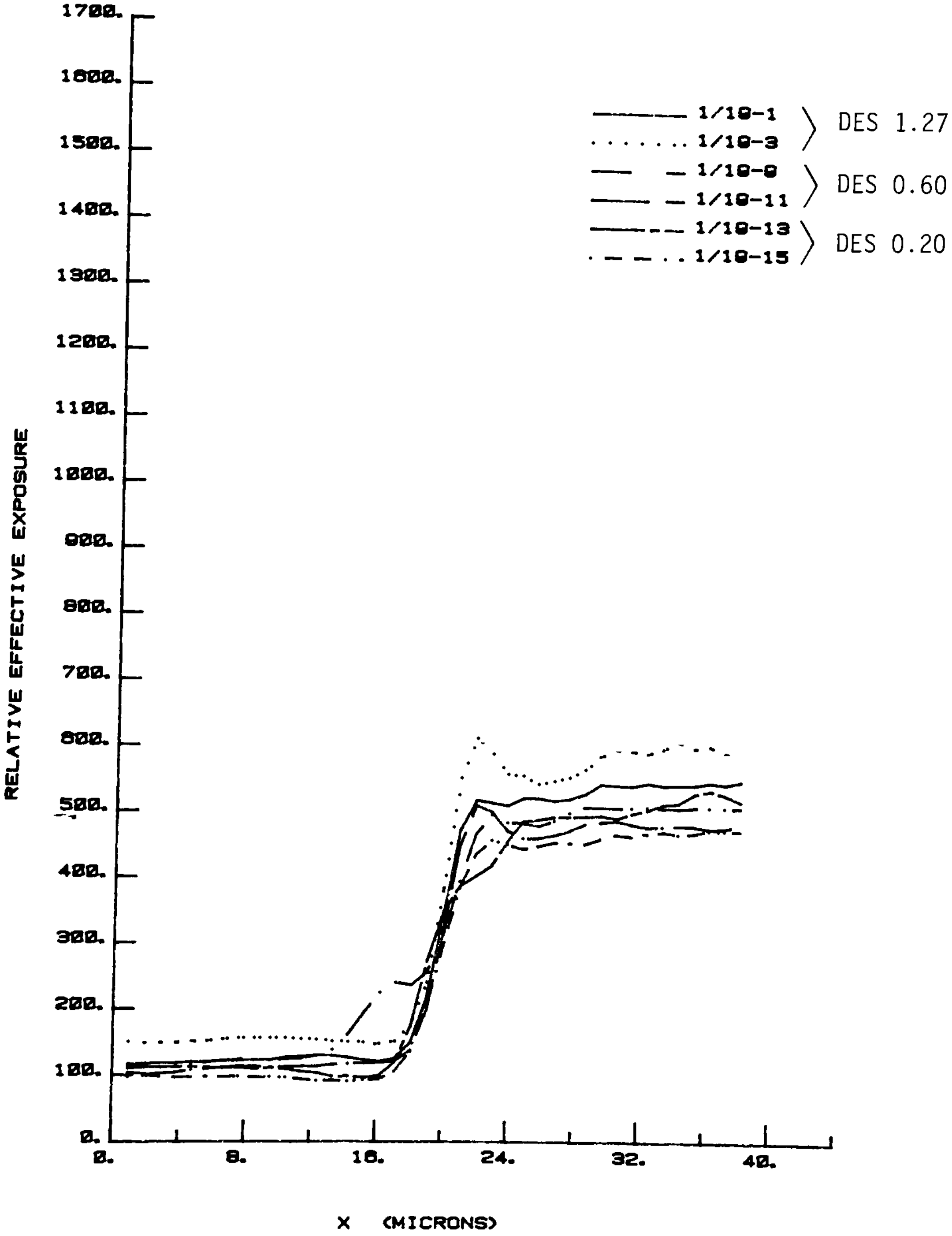

Figure C5. Experiment Two Edge Response Vectors; Film Platen Velocity 1.5 in/sec; Development Electrode Spacing (DES) in millimeters.

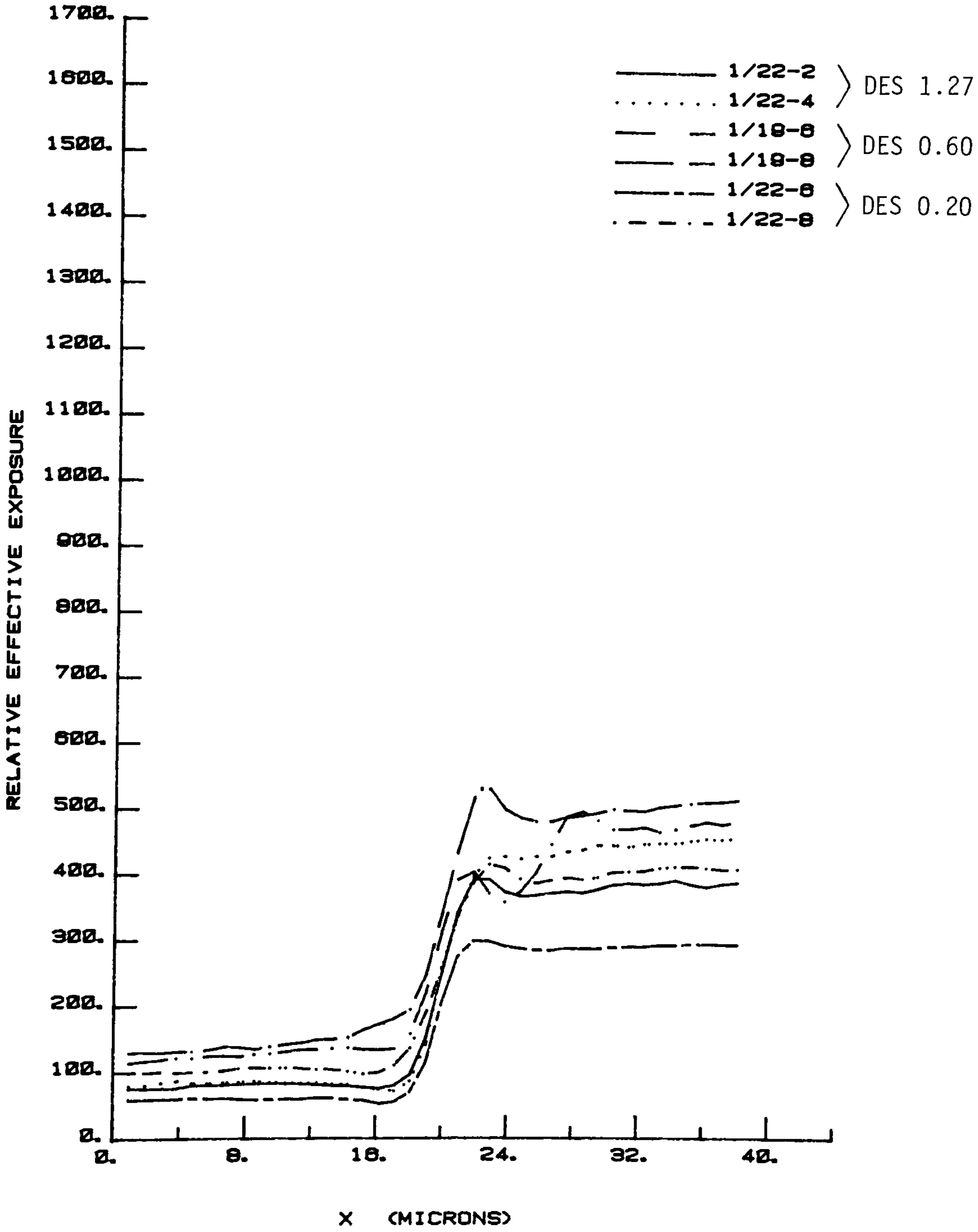

Figure C6. Experiment Two Edge Response Vectors; Film Platen Velocity 0.6 in/sec; Development Electrode Spacing (DES) in millimeters.

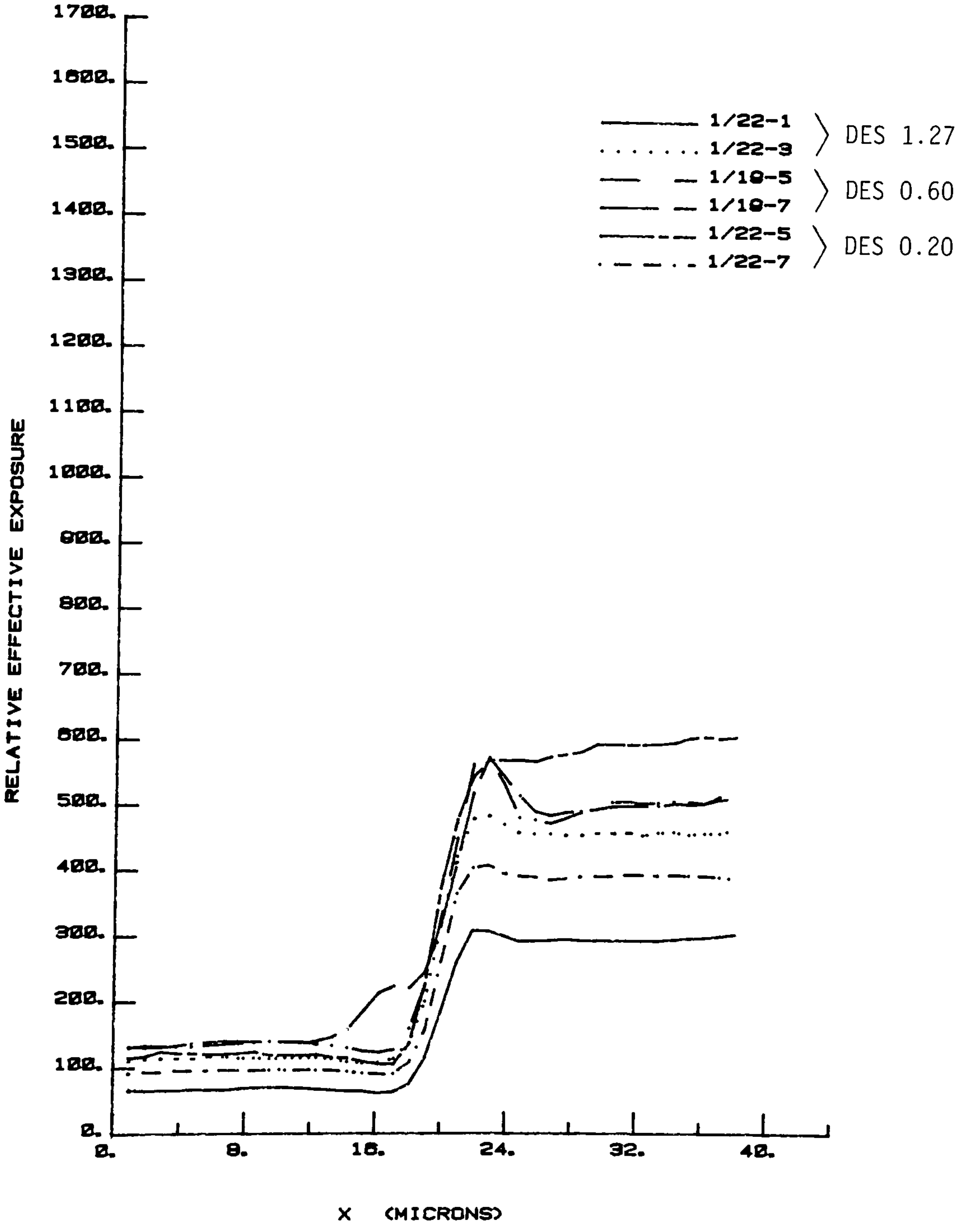

Figure C7. Experiment Two Edge Response Vectors; Film Platen Velocity 0.3 in/sec; Development Electrode Spacing (DES) in millimeters.

APPENDIX D

Sensitometric Responses for Experiments Three and Four; and Edge Response Vectors for Experiment Three, as Measured on Electrophotographic Film Samples.

In this Appendix, Hurter and Driffield (H & D) response curves are illustrated for sensitometric images common to experiments three and four; Figures D1 through D3. Effective exposure edge response vectors for experiment three are included in Figures D4 through D9. These edge response vectors are grouped according to replicates for each experimental treatment.

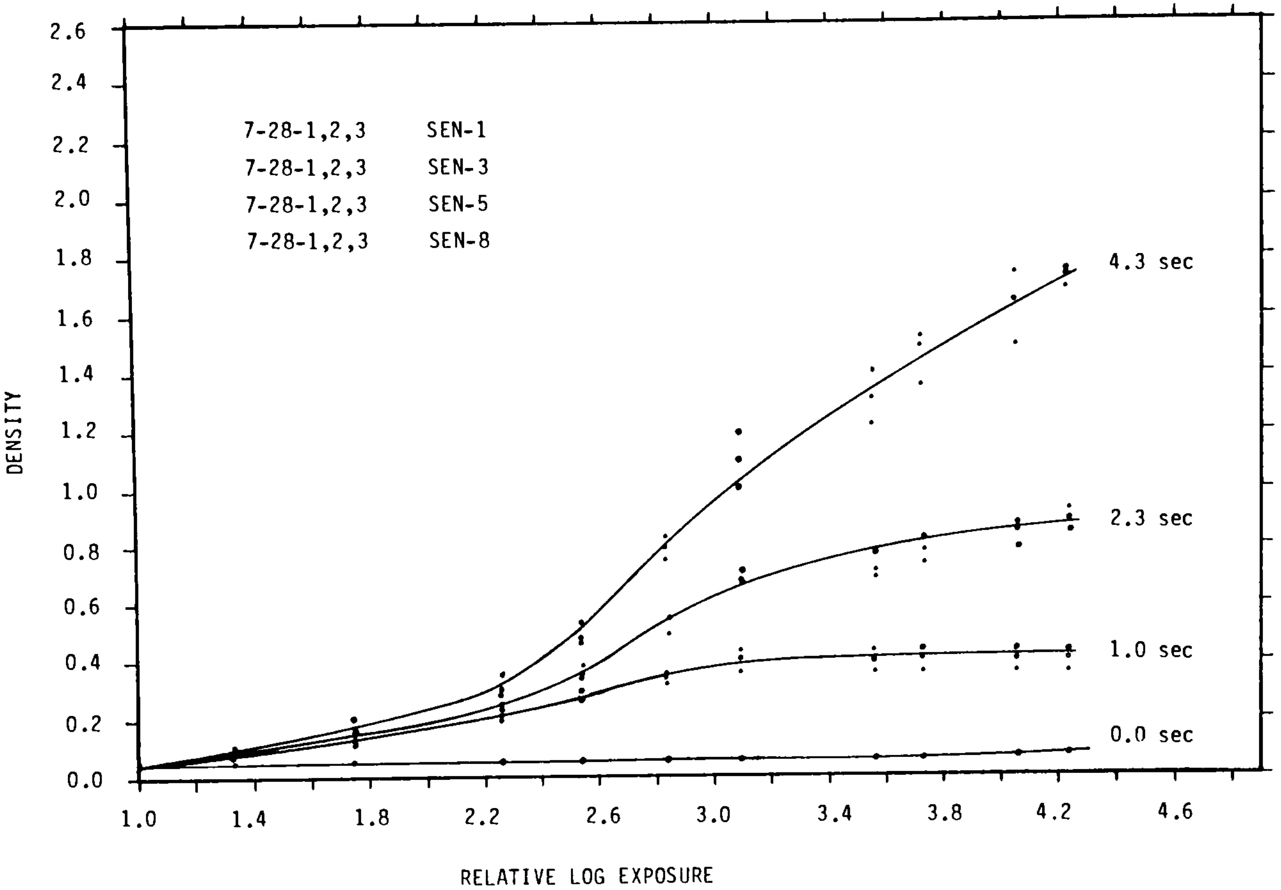

Figure D1. Sensitometric H&D Curves for Experiment Three and Four; Development Electrode Spacing 0.20 mm.

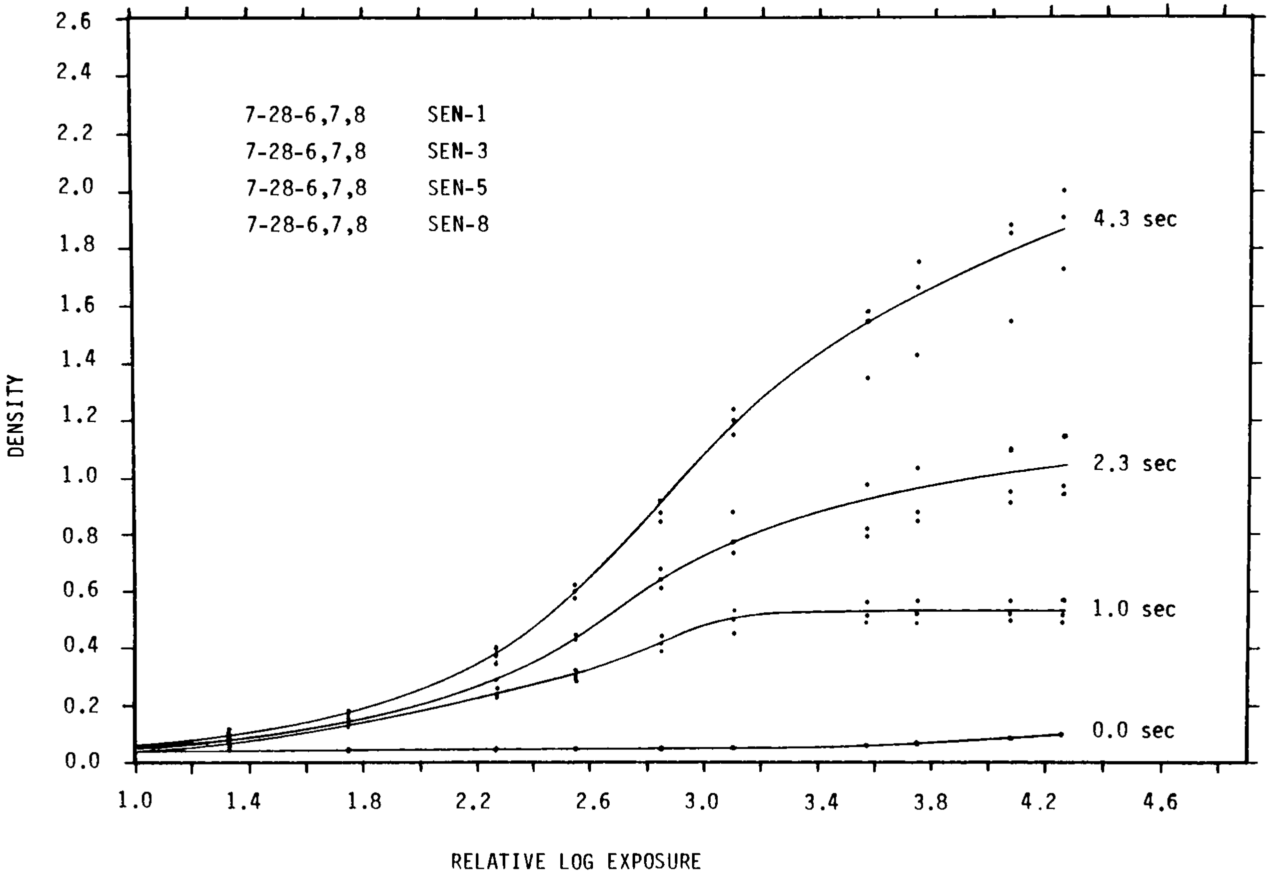

Figure D2. Sensitometric H&D Curves for Experiments Three and Four; Development Electrode Spacing 0.60 mm.

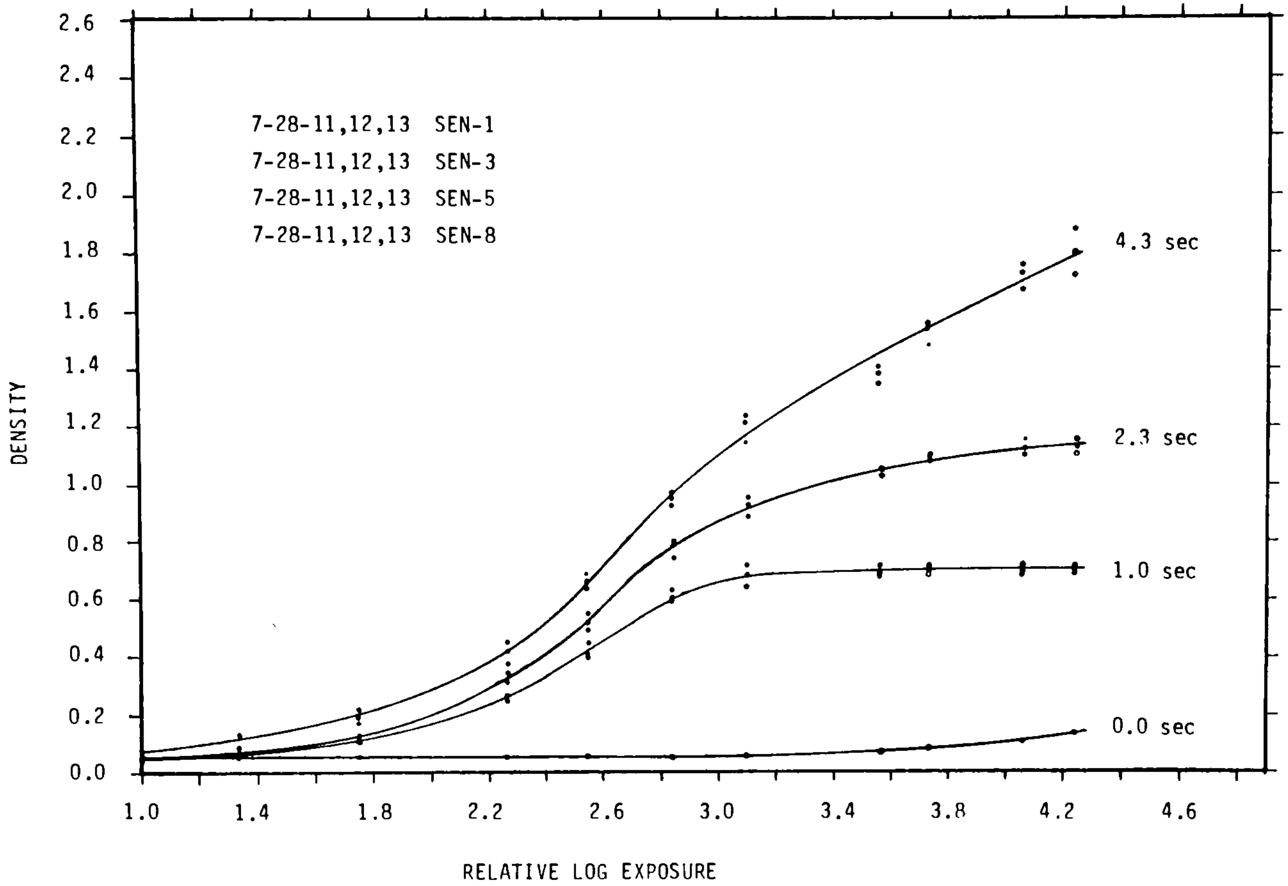

Figure D3. Sensitometric H&D Curves for Experiments Three and Four; Development Electrode Spacing 1.27 mm.

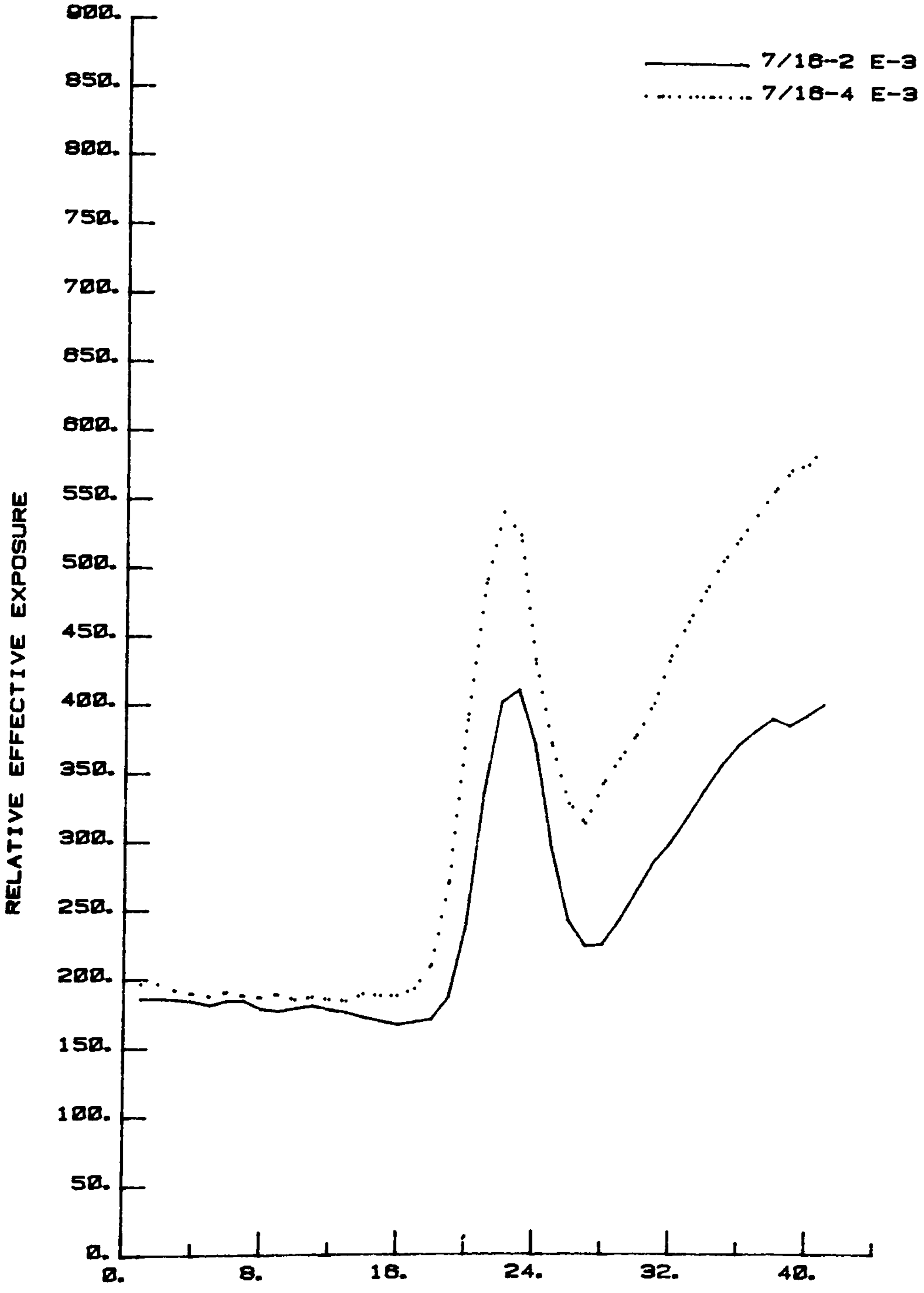

Figure D4. Experiment Three Edge Response Vectors; Applied Voltage Time 1.0 Second; Development Electrode Spacing 0.20 mm.

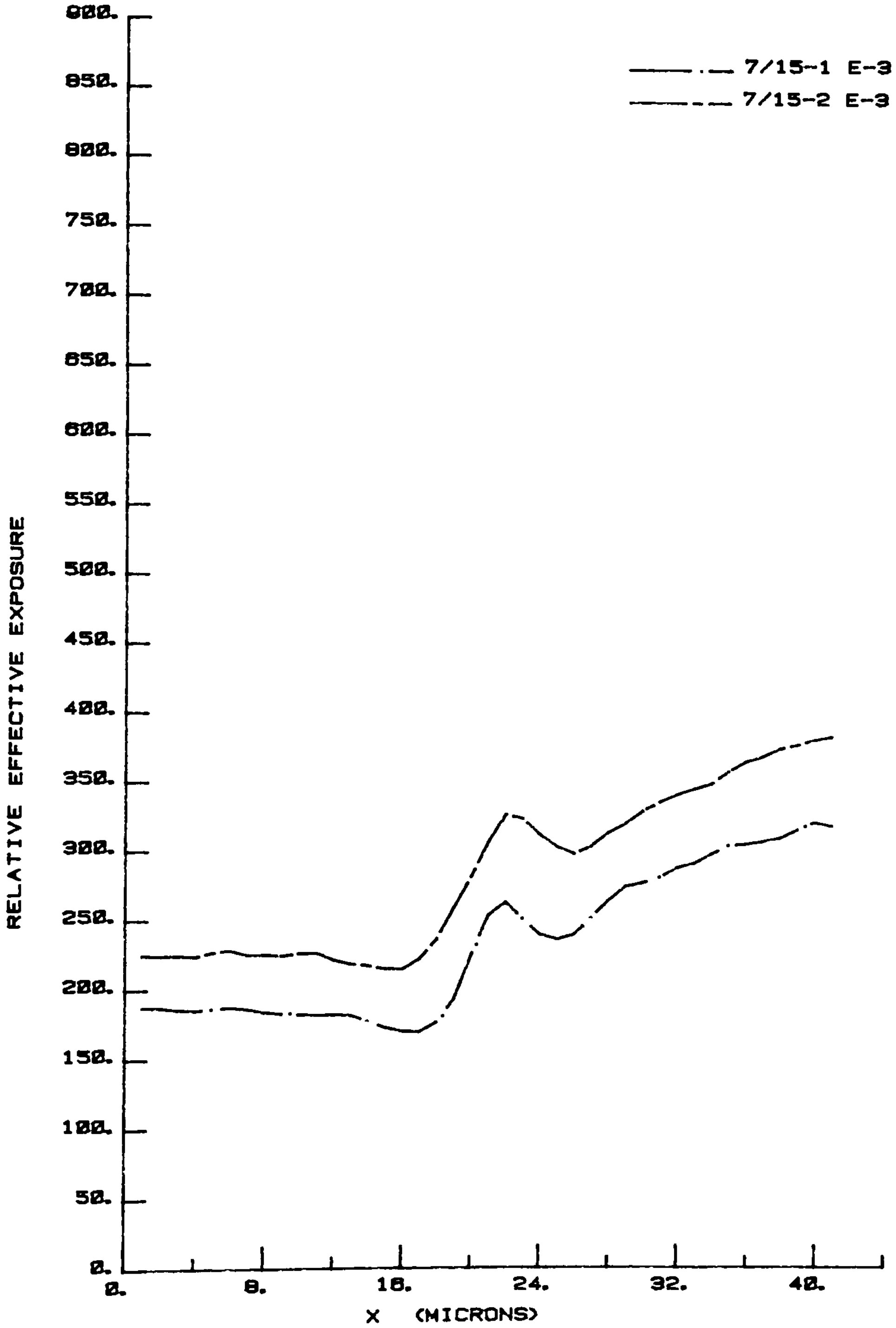

Figure D5. Experiment Three Edge Response Vectors; Applied Voltage Time 1.0 Second; Development Electrode Spacing 1.27 mm.

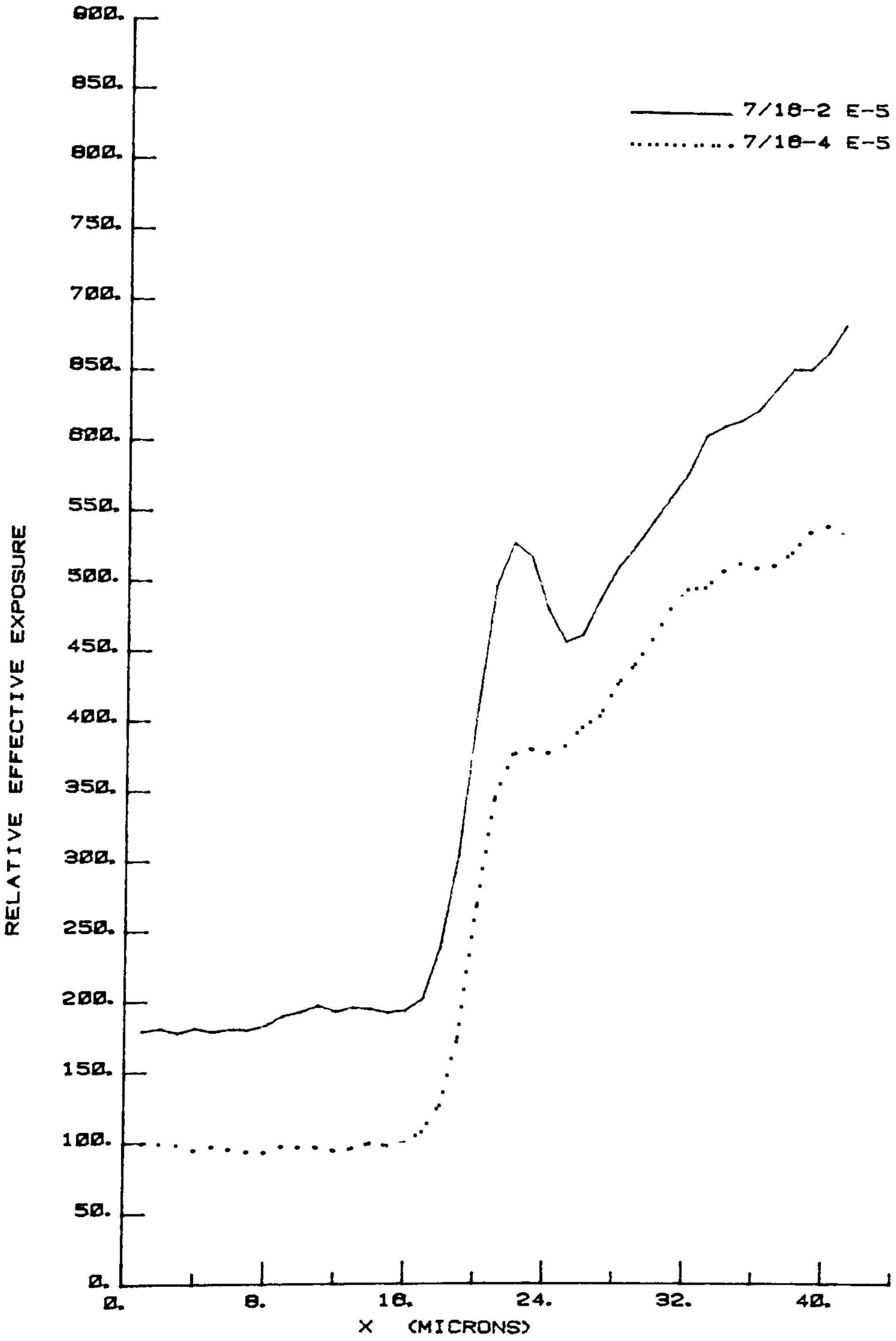

Figure D6. Experiment Three Edge Response Vectors; Applied Voltage Time 2.3 Seconds; Development Electrode Spacing 0.20 mm.

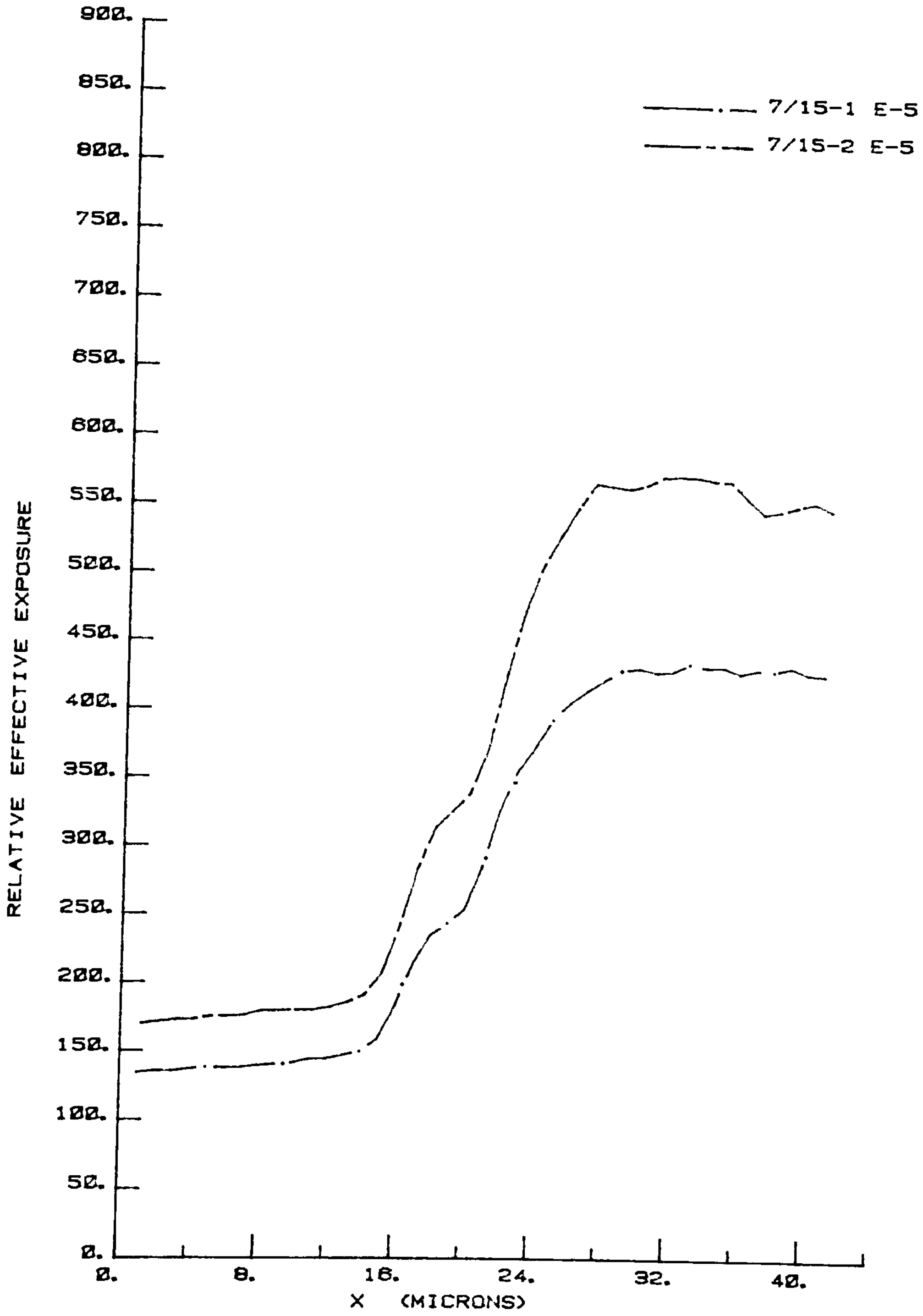

Figure D7. Experiment Three Edge Response Vectors; Applied Voltage Time 2.3 Seconds; Development Electrode Spacing 1.27 mm.

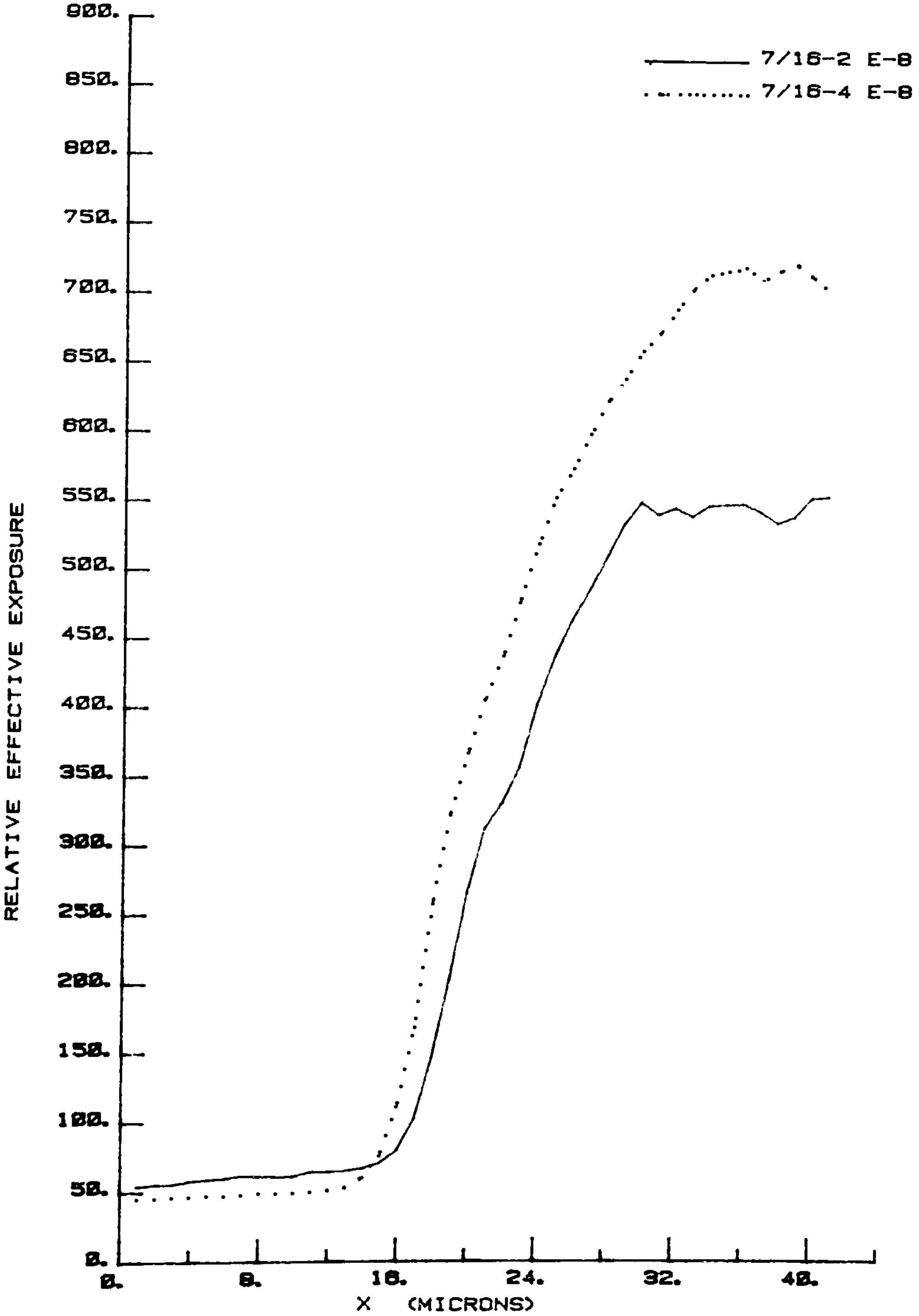

Figure D8. Experiment Three Edge Response Vectors; Applied Voltage Time 4.3 Seconds; Development Electrode Spacing 0.20 mm.

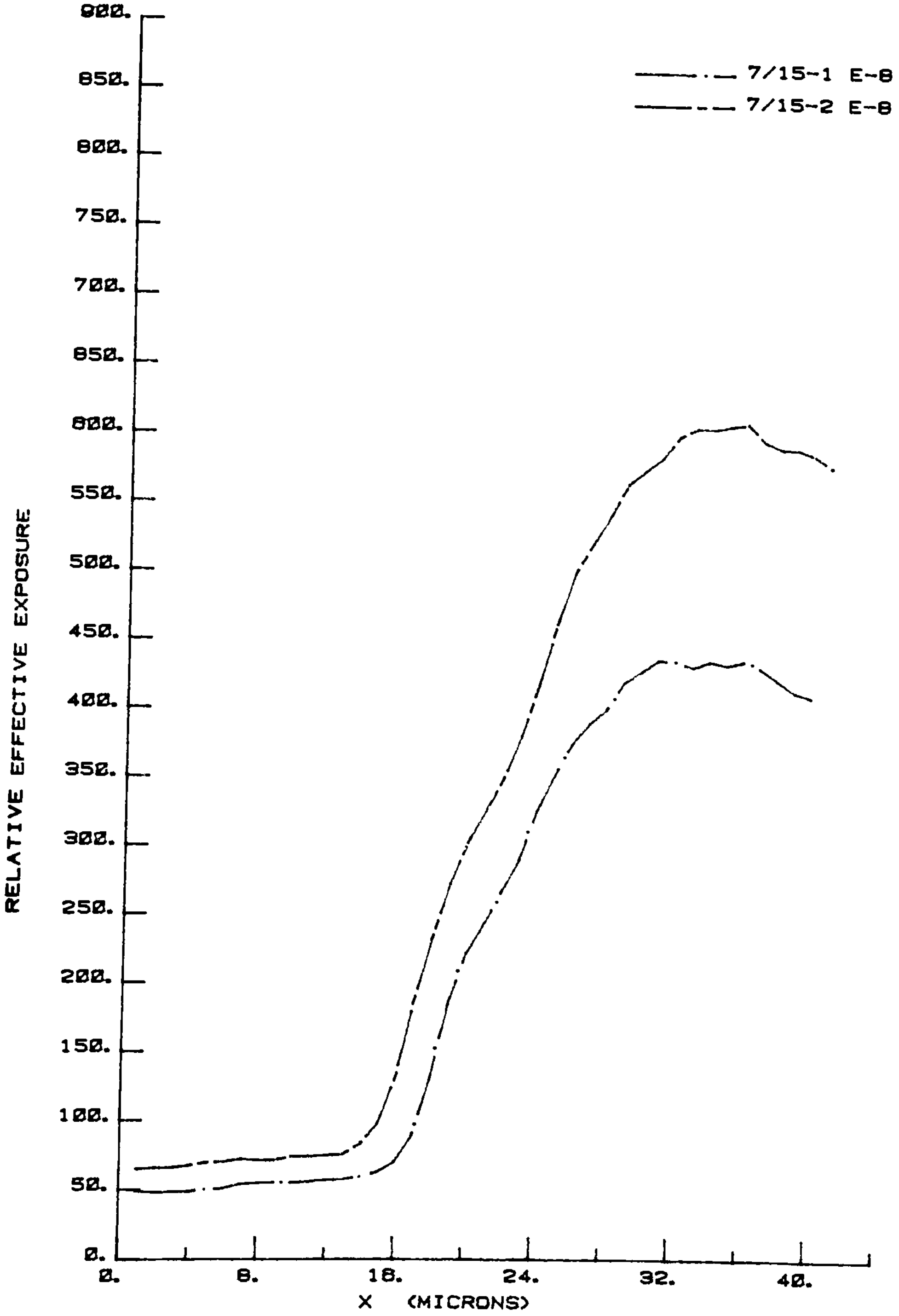

Figure D9. Experiment Three Edge Response Vectors; Applied Voltage Time 4.3 Seconds; Development Electrode Spacing 1.27 mm.

APPENDIX E

Effective Exposure Distributions and Fourier Spectra for Sinusoidal Images on Transparent Electrophotographic Film.

Sinusoidal effective exposure distributions and their corresponding Fourier spectra for images generated in experiment four are illustrated in this Appendix. The Fourier spectra were obtained by application of a Fast Fourier Transform algorithm to an integer number of cycles in the effective exposure distributions. For the three fundamental frequencies tested, the number of cycles, N, included in the F.F.T. computations and the average frequency sampling resolutions, Δf, are as follows:

(a) Fundamental 25 cycles/mm: $N = 5$, $\Delta f = 5.2$ cycles/mm

(b) Fundamental 64 cycles/mm: $N = 8$, $\Delta f = 8.0$ cycles/mm

(c) Fundamental 102 cycles/mm: $N = 8$, $\Delta f = 12.8$ cycles/mm

Figures E1 through E6 show the distributions and Fourier spectra for fundamental 25 cycles/mm. Figures E7 through E12 show the distributions and Fourier spectra for fundamental 64 cycles/mm. Figures E13 through E18 show the distributions and Fourier spectra for fundamental 102 cycles/mm. The modulus values for all Fourier spectra have been normalized to 1.0 at the fundamental frequency.

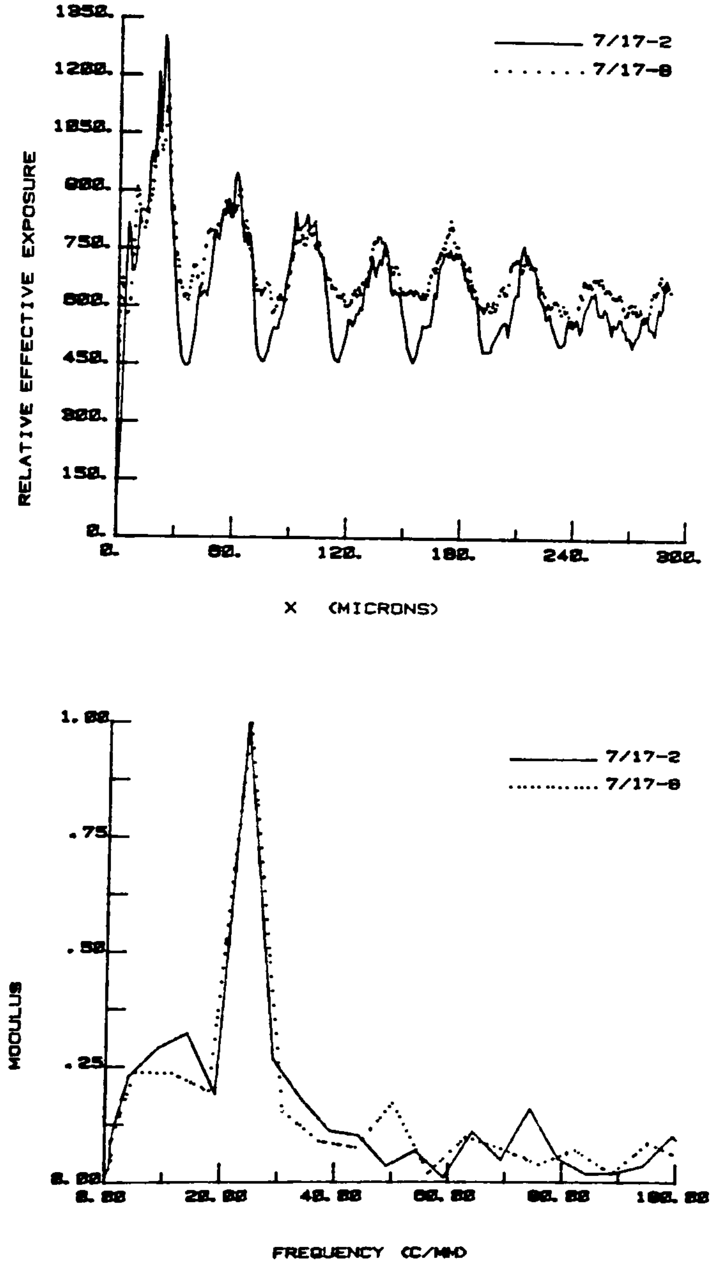

Figure E1. Sinusoidal Effective Exposure Distributions and Fourier Spectra, Fundamental: 25 Cycles/mm; Applied Voltage Time 1.0 Second; Development Electrode Spacing 0.20 mm.

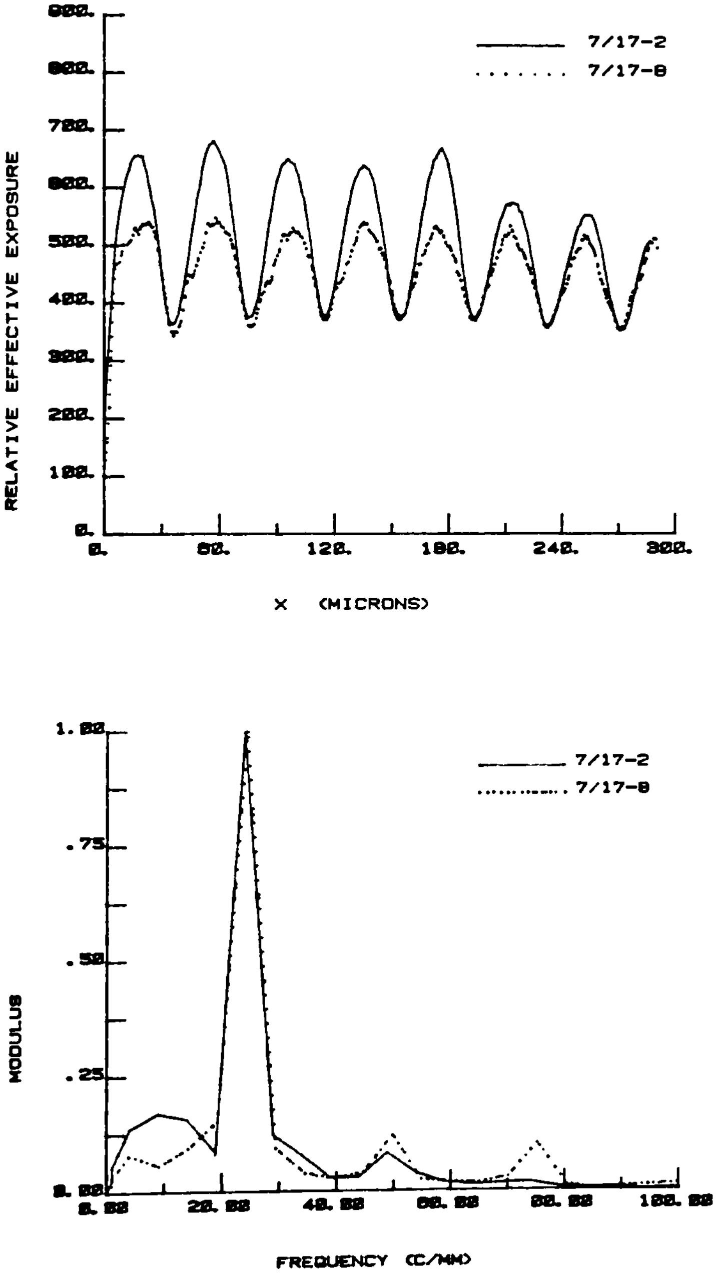

Figure E2. Sinusoidal Effective Exposure Distributions and Fourier Spectra, Fundamental: 25 Cycles/mm; Applied Voltage Time 2.3 Seconds; Development Electrode Spacing 0.20 mm.

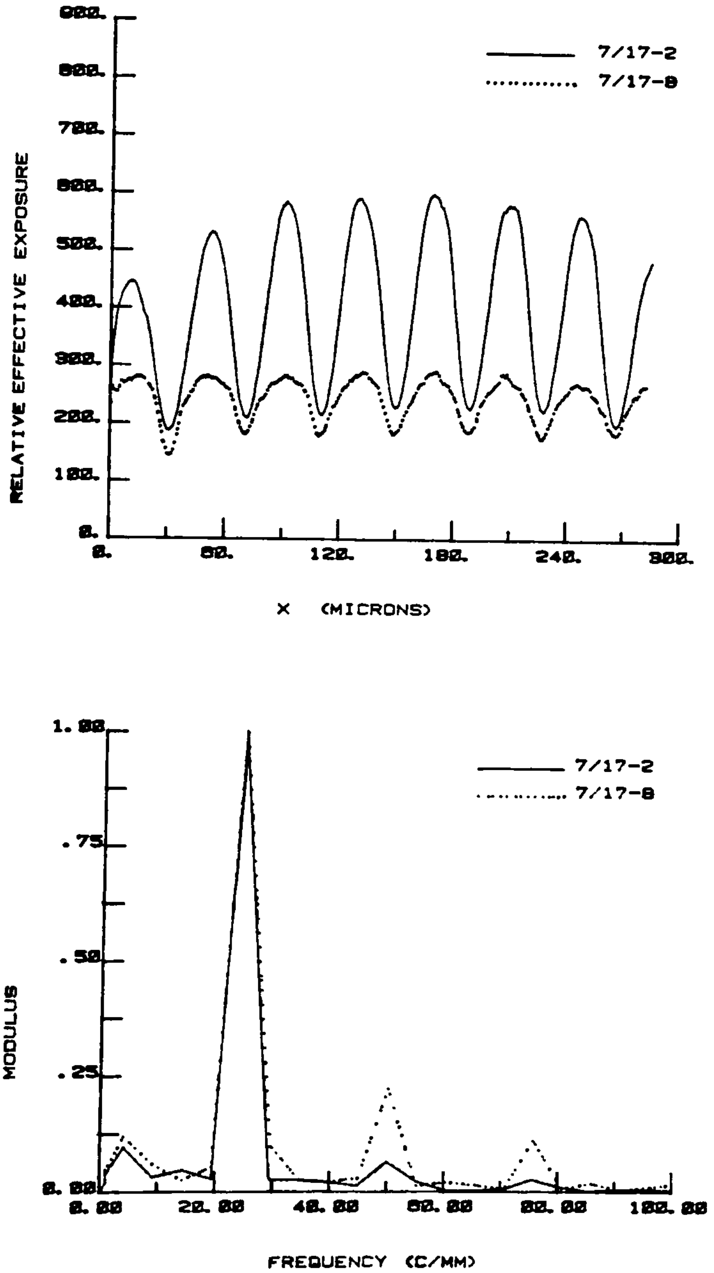

Figure E3. Sinusoidal Effective Exposure Distributions and Fourier Spectra, Fundamental: 25 Cycles/mm; Applied Voltage Time 4.3 Seconds; Development Electrode Spacing 0.20 mm.

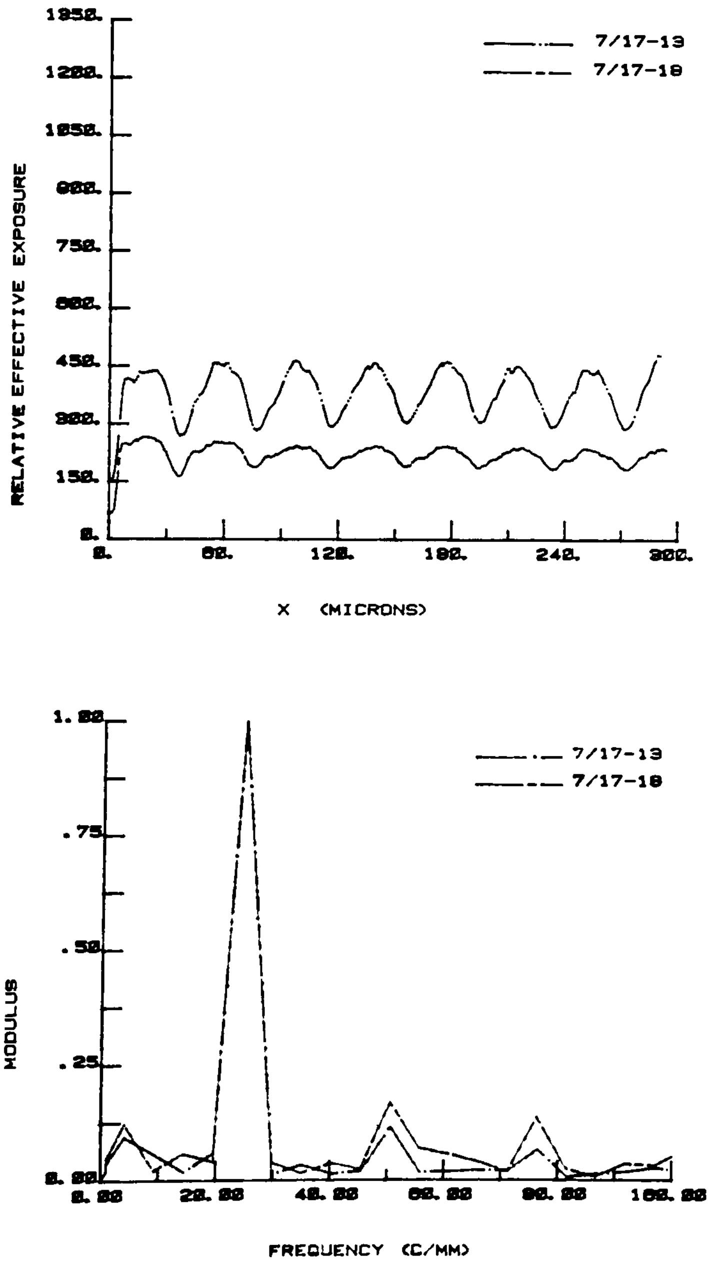

Figure E4. Sinusoidal Effective Exposure Distributions and Fourier Spectra, Fundamental: 25 Cycles/mm; Applied Voltage Time 1.0 Second; Development Electrode Spacing 1.27 mm.

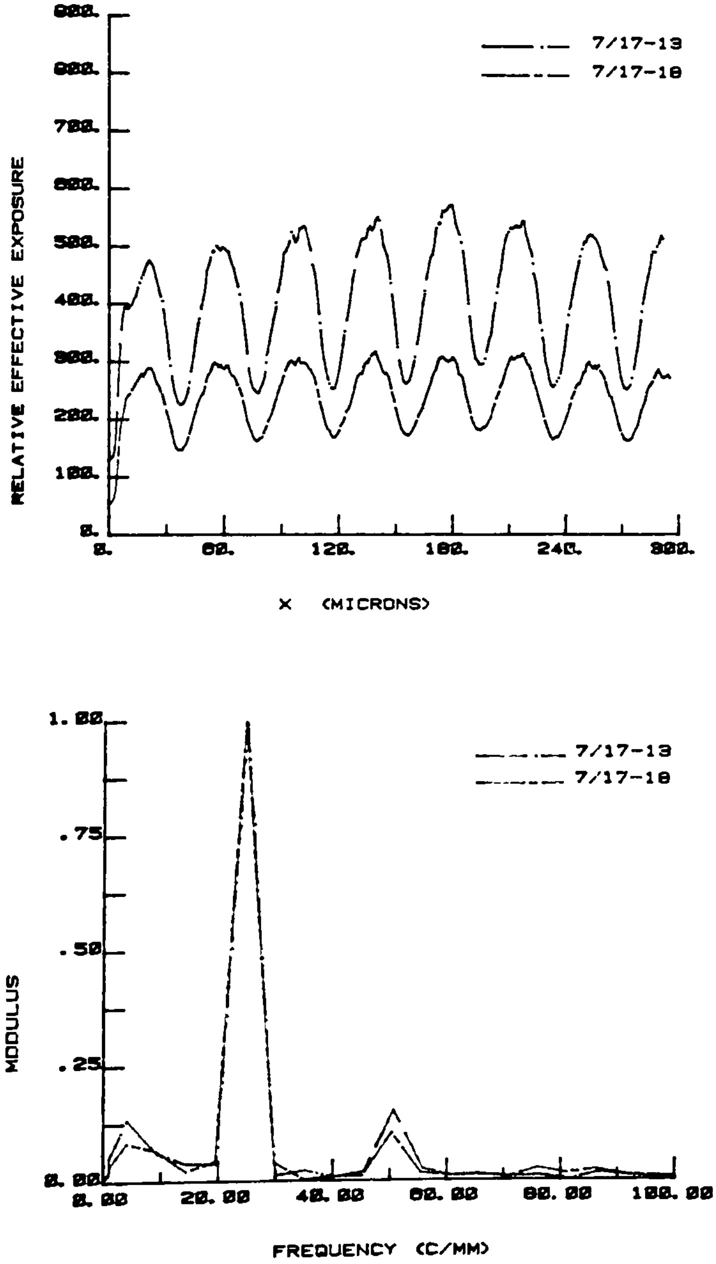

Figure E5. Sinusoidal Effective Exposure Distributions and Fourier Spectra, Fundamental: 25 Cycles/mm; Applied Voltage Time 2.3 Seconds; Development Electrode Spacing 1.27 mm.

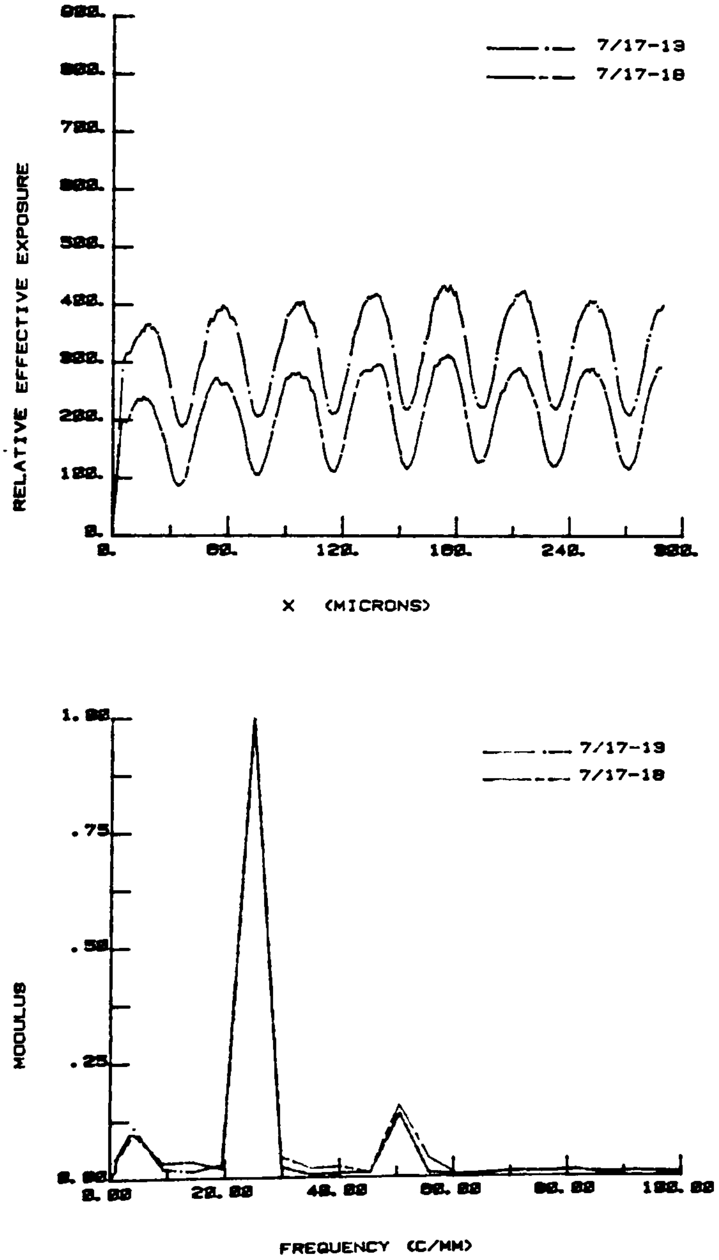

Figure E6. Sinusoidal Effective Exposure Distributions and Fourier Spectra, Fundamental: 25 Cycles/mm; Applied Voltage Time 4.3 Seconds; Development Electrode Spacing 1.27 mm.

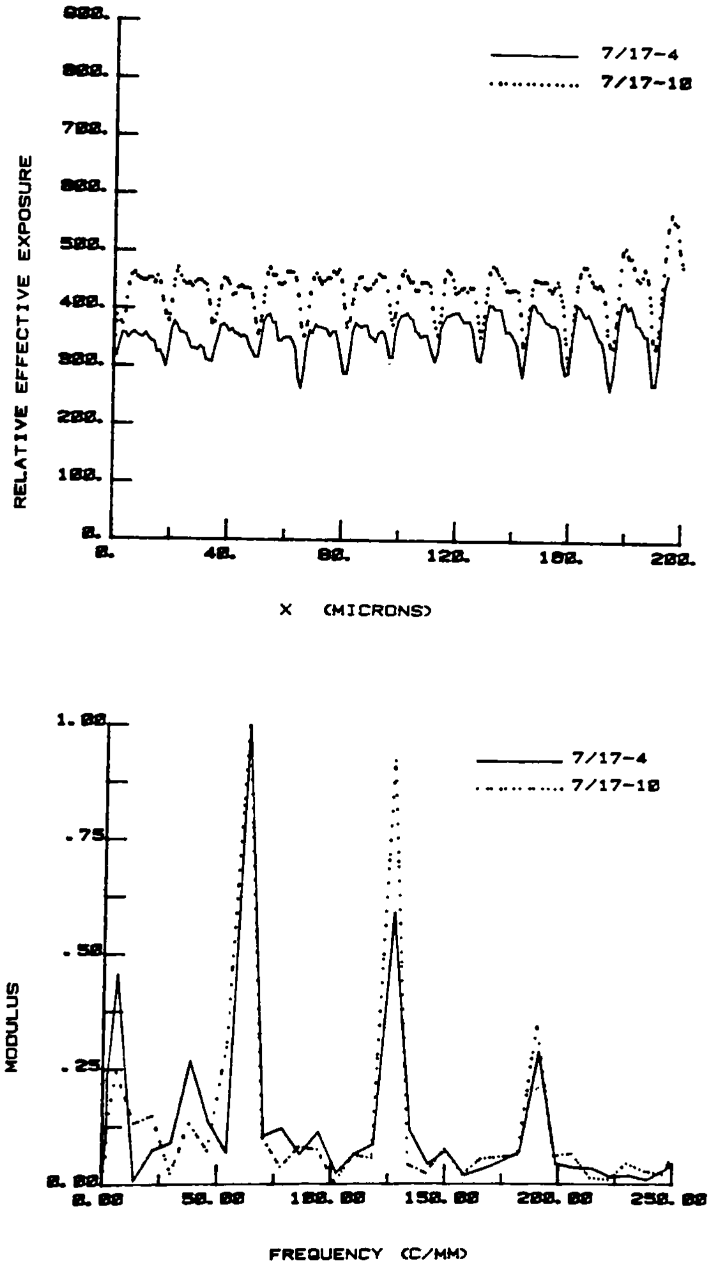

Figure E7. Sinusoidal Effective Exposure Distributions and Fourier Spectra, Fundamental: 64 Cycles/mm; Applied Voltage Time 1.0 Second; Development Electrode Spacing 0.20 mm.

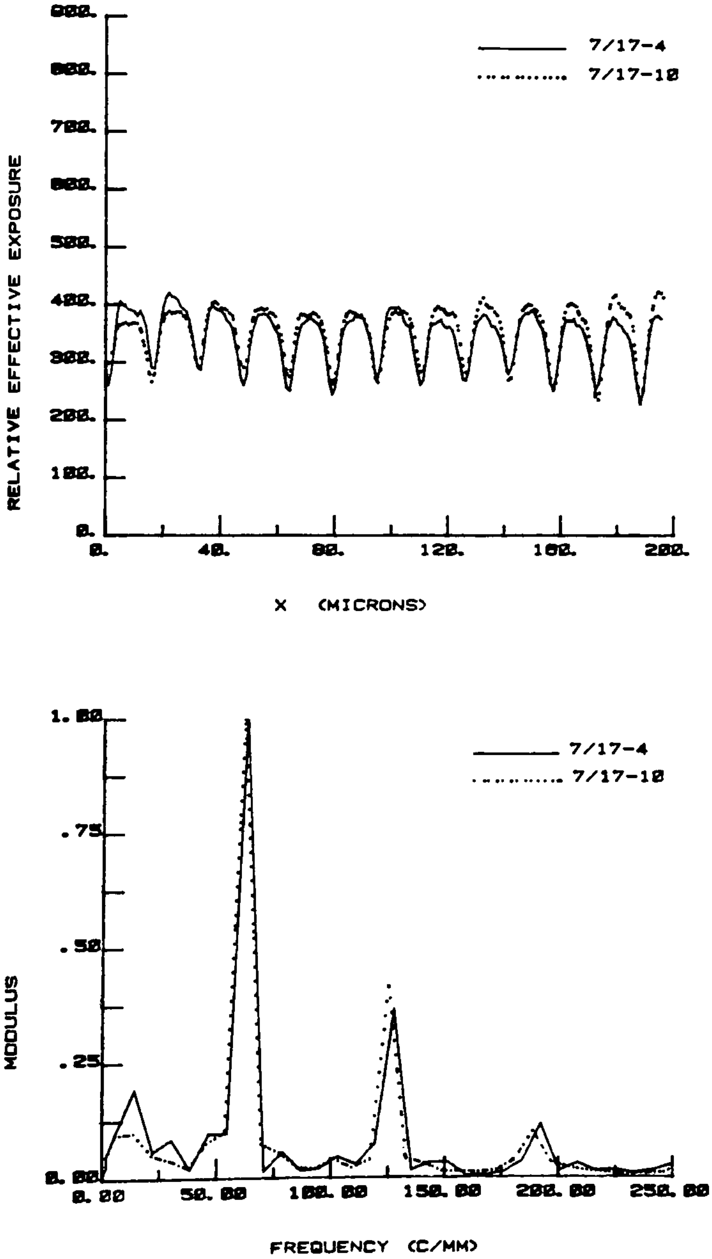

Figure E8. Sinusoidal Effective Exposure Distributions and Fourier Spectra, Fundamental: 64 Cycles/mm; Applied Voltage Time 2.3 Seconds; Development Electrode Spacing 0.20 mm.

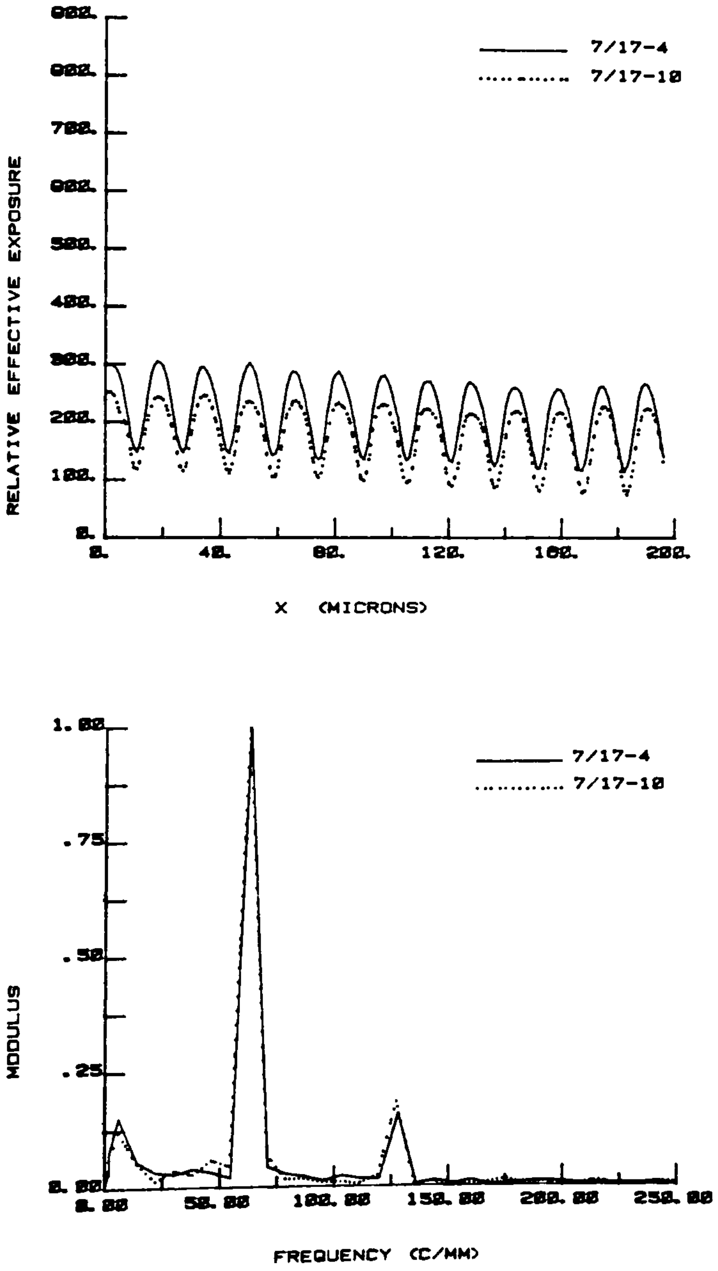

Figure E9. Sinusoidal Effective Exposure Distributions and Fourier Spectra, Fundamental: 64 Cycles/mm; Applied Voltage Time 4.3 Seconds; Development Electrode Spacing 0.20 mm.

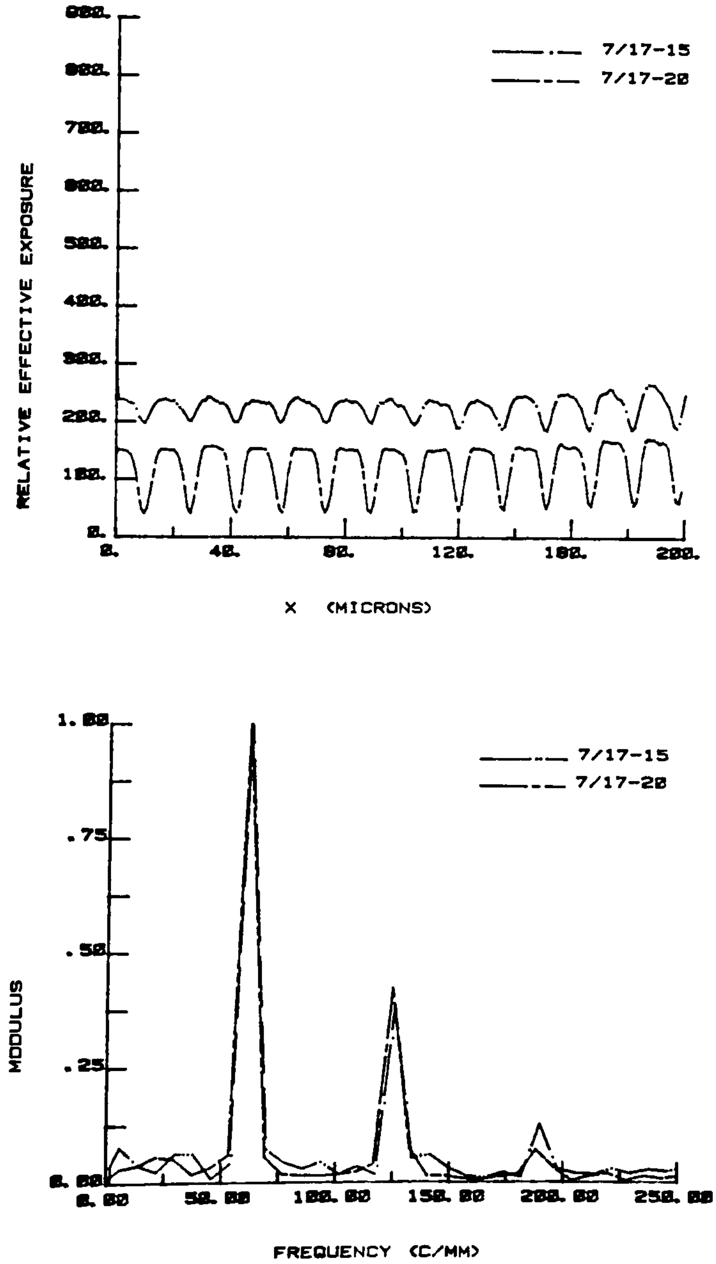

Figure E10. Sinusoidal Effective Exposure Distributions and Fourier Spectra, Fundamental: 64 Cycles/mm; Applied Voltage Time 1.0 Second; Development Electrode Spacing 1.27 mm.

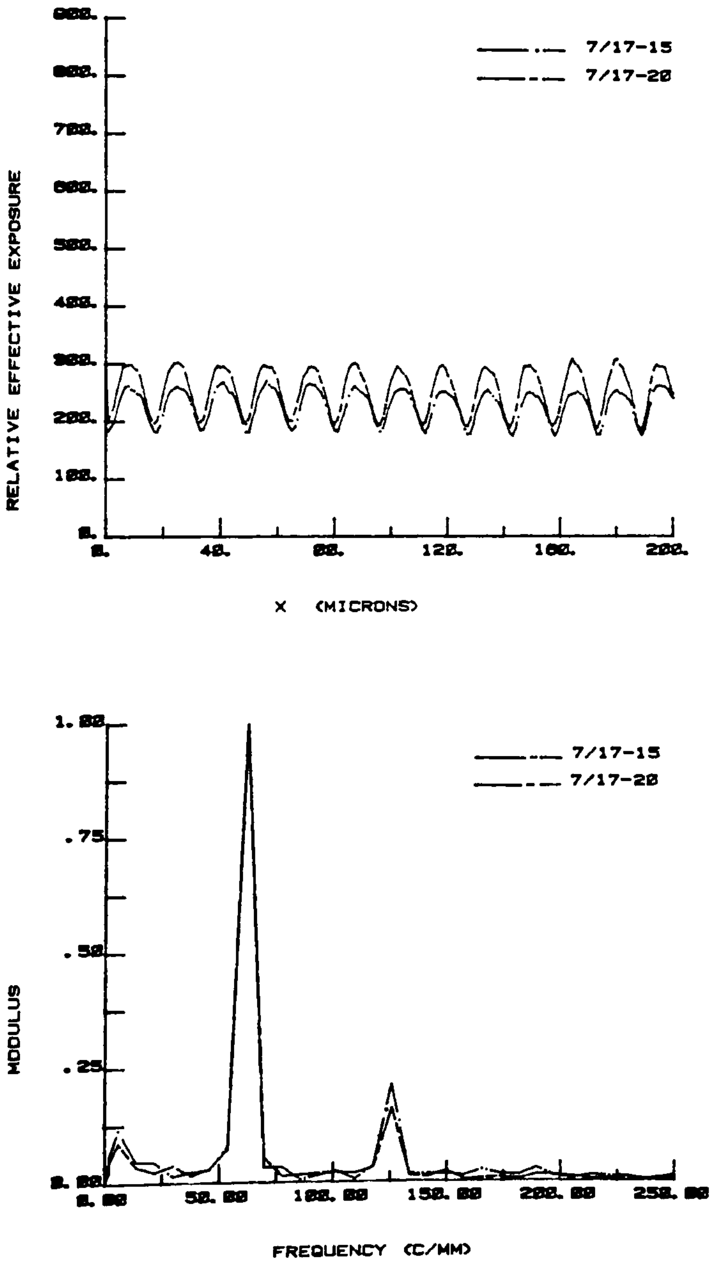

Figure E11. Sinusoidal Effective Exposure Distributions and Fourier Spectra, Fundamental: 64 Cycles/mm; Applied Voltage Time 2.3 Seconds; Development Electrode Spacing 1.27 mm.

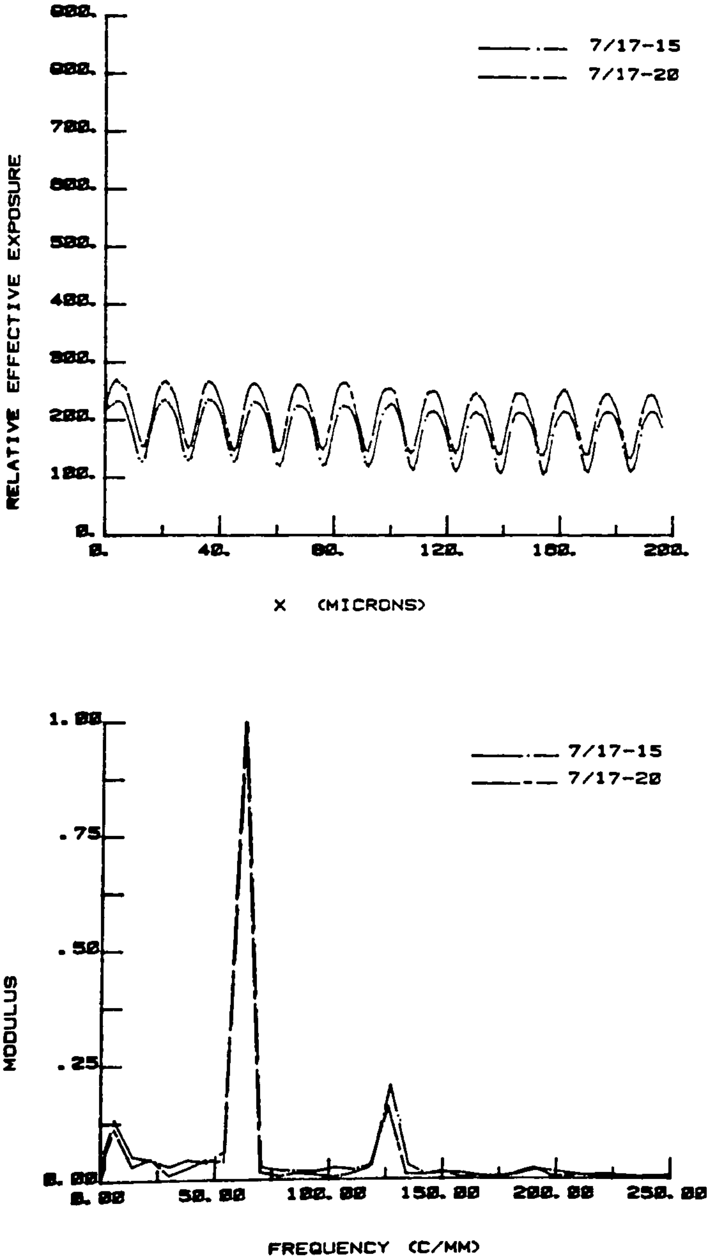

Figure E12. Sinusoidal Effective Exposure Distributions and Fourier Spectra, Fundamental: 64 Cycles/mm; Applied Voltage Time 4.3 Seconds; Development Electrode Spacing 1.27 mm.

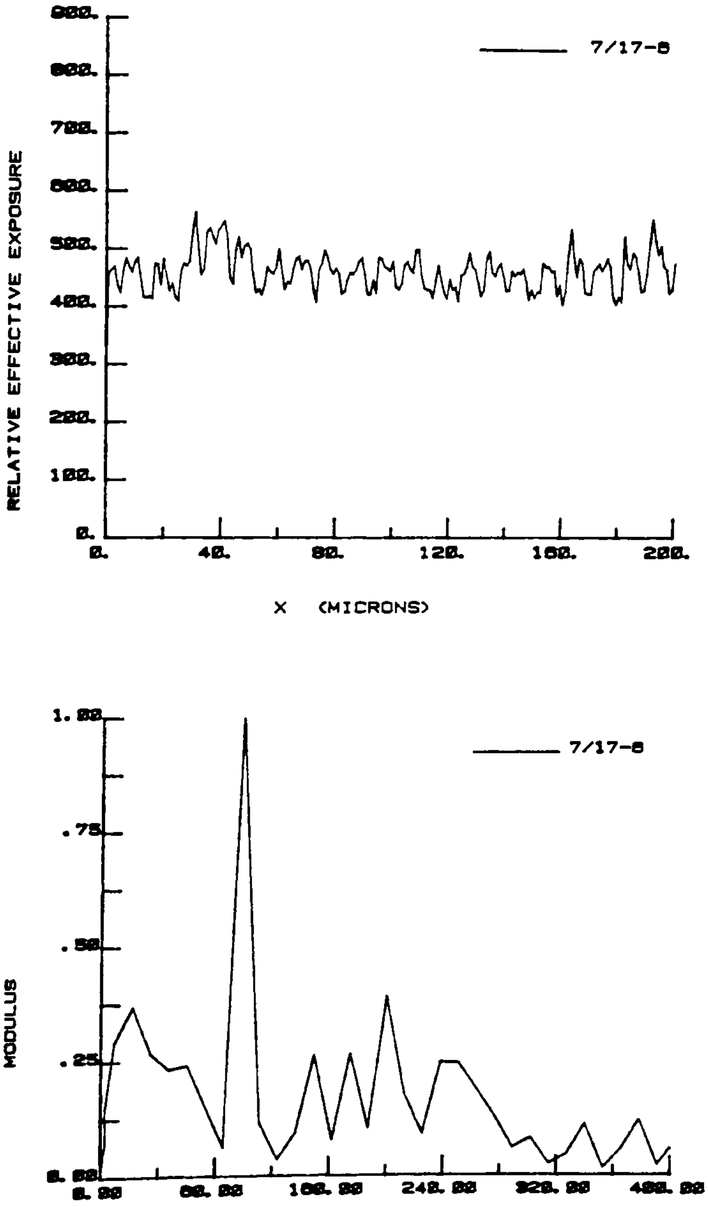

Figure E13. Sinusoidal Effective Exposure Distributions and Fourier Spectra, Fundamental: 102 Cycles/mm; Applied Voltage Time 1.0 Second; Development Electrode Spacing 0.20 mm.

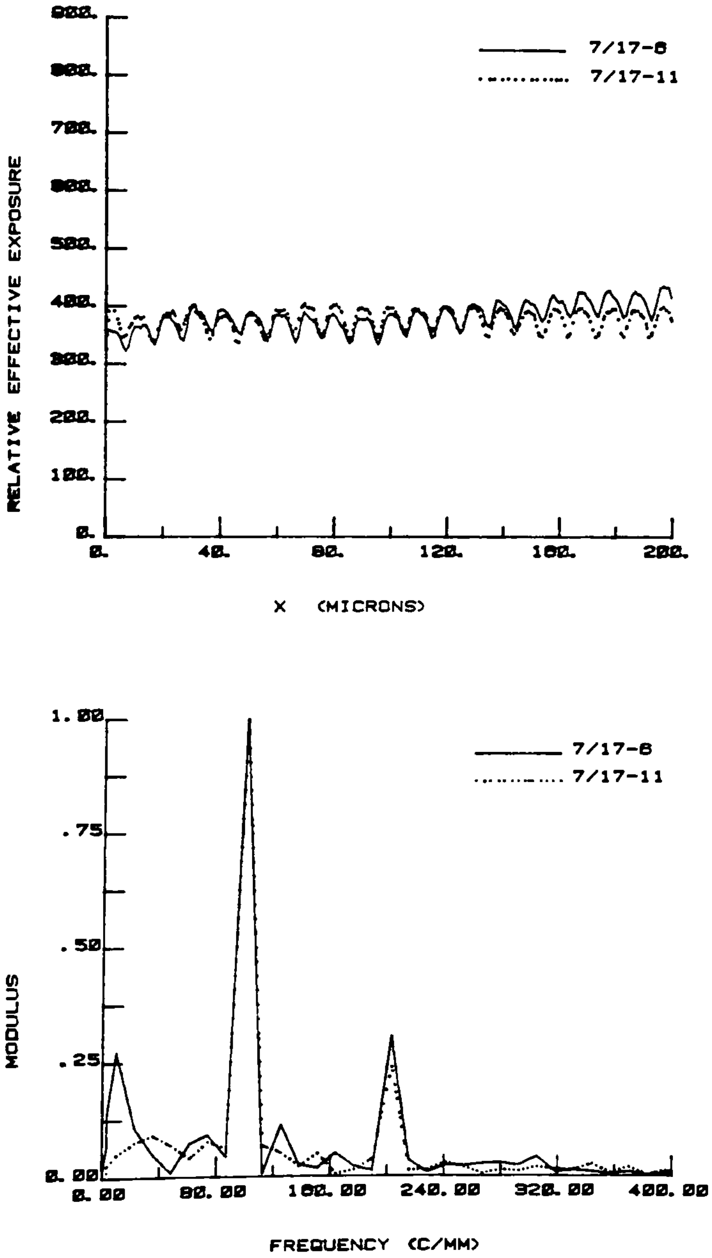

Figure E14. Sinusoidal Effective Exposure Distributions and Fourier Spectra, Fundamental: 102 Cycles/mm; Applied Voltage Time 2.3 Seconds; Development Electrode Spacing 0.20 mm.

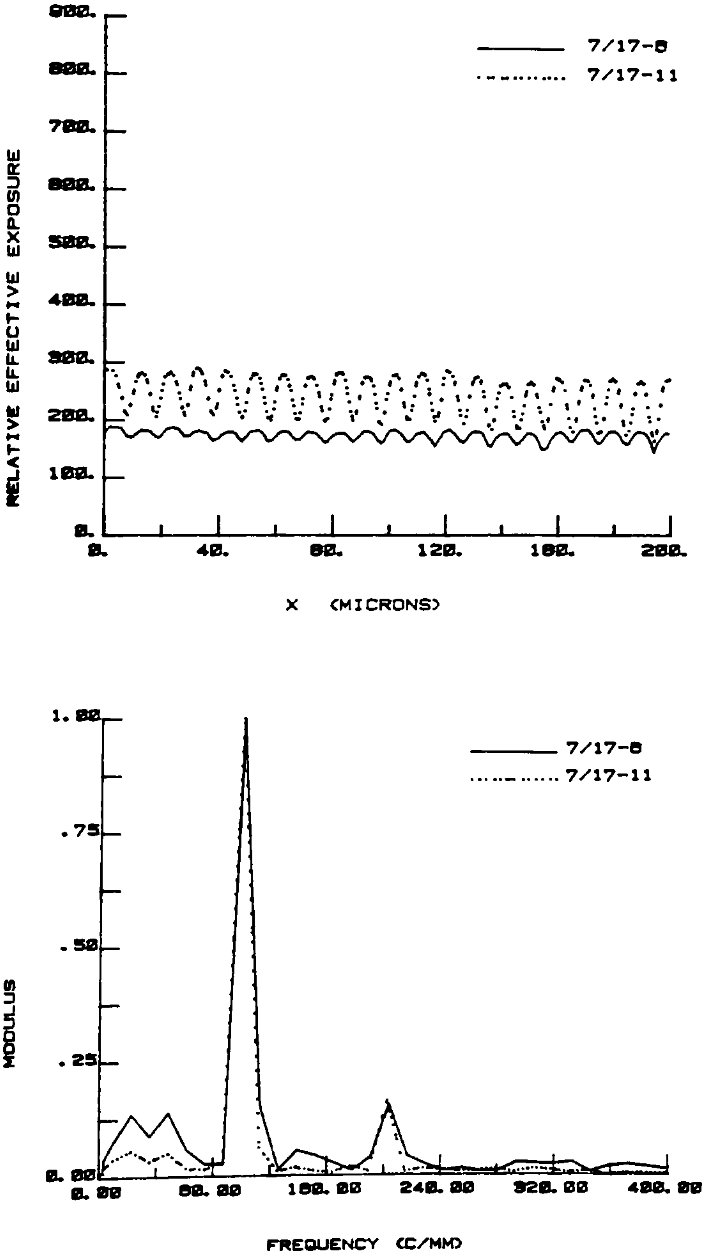

Figure E15. Sinusoidal Effective Exposure Distributions and Fourier Spectra, Fundamental: 102 Cycles/mm; Applied Voltage Time 4.3 Seconds; Development Electrode Spacing 0.20 mm.

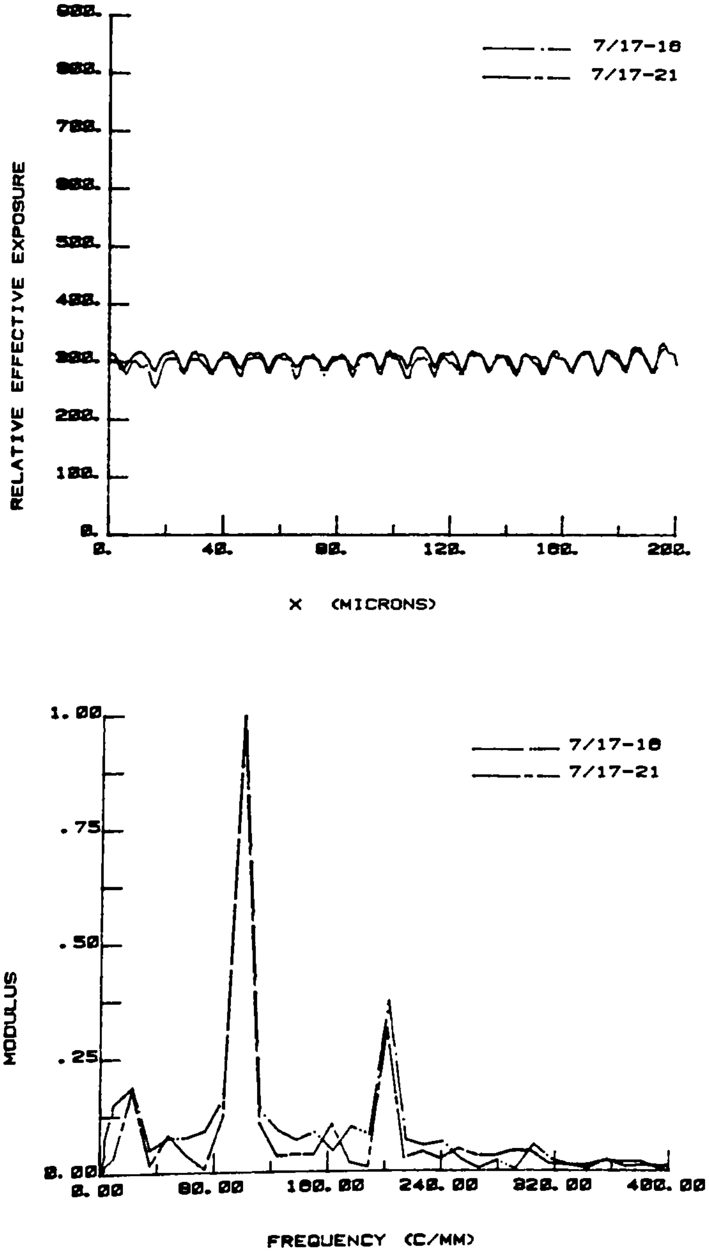

Figure E16. Sinusoidal Effective Exposure Distributions and Fourier Spectra, Fundamental: 102 Cycles/mm; Applied Voltage Time 1.0 Second; Development Electrode Spacing 1.27 mm.

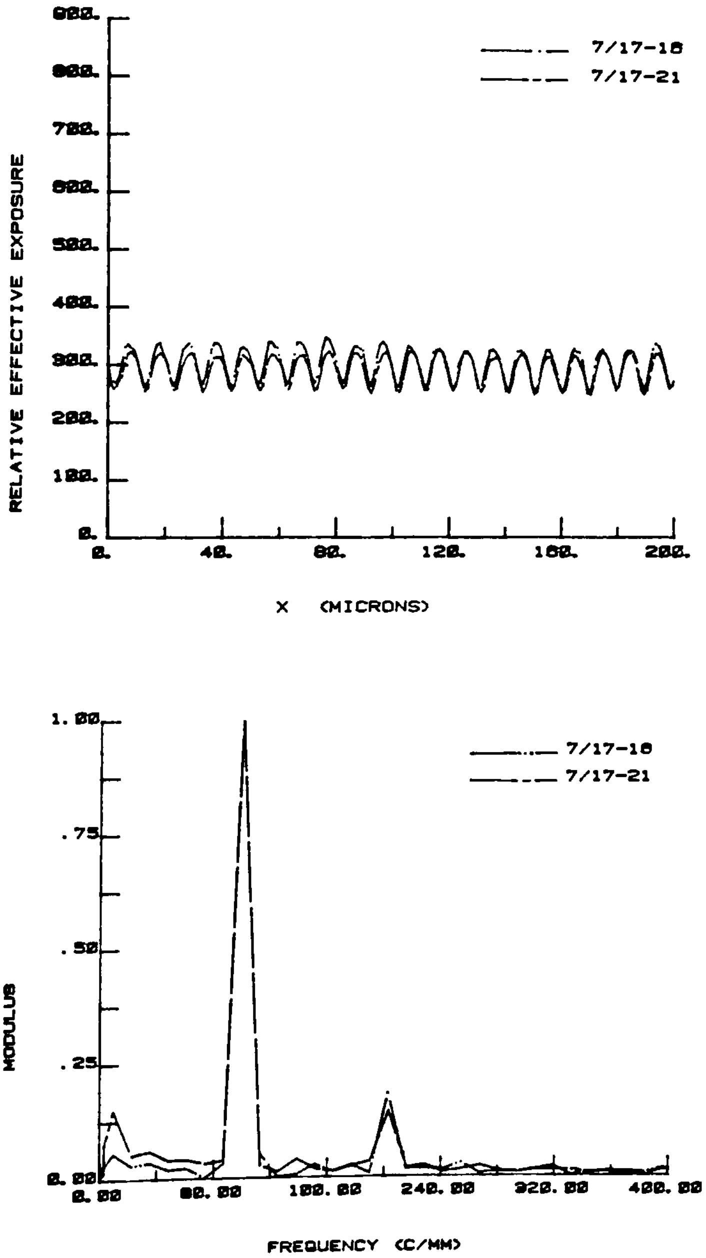

Figure E17. Sinusoidal Effective Exposure Distributions and Fourier Spectra, Fundamental: 102 Cycles/mm; Applied Voltage Time 2.3 Seconds; Development Electrode Spacing 1.27 mm.

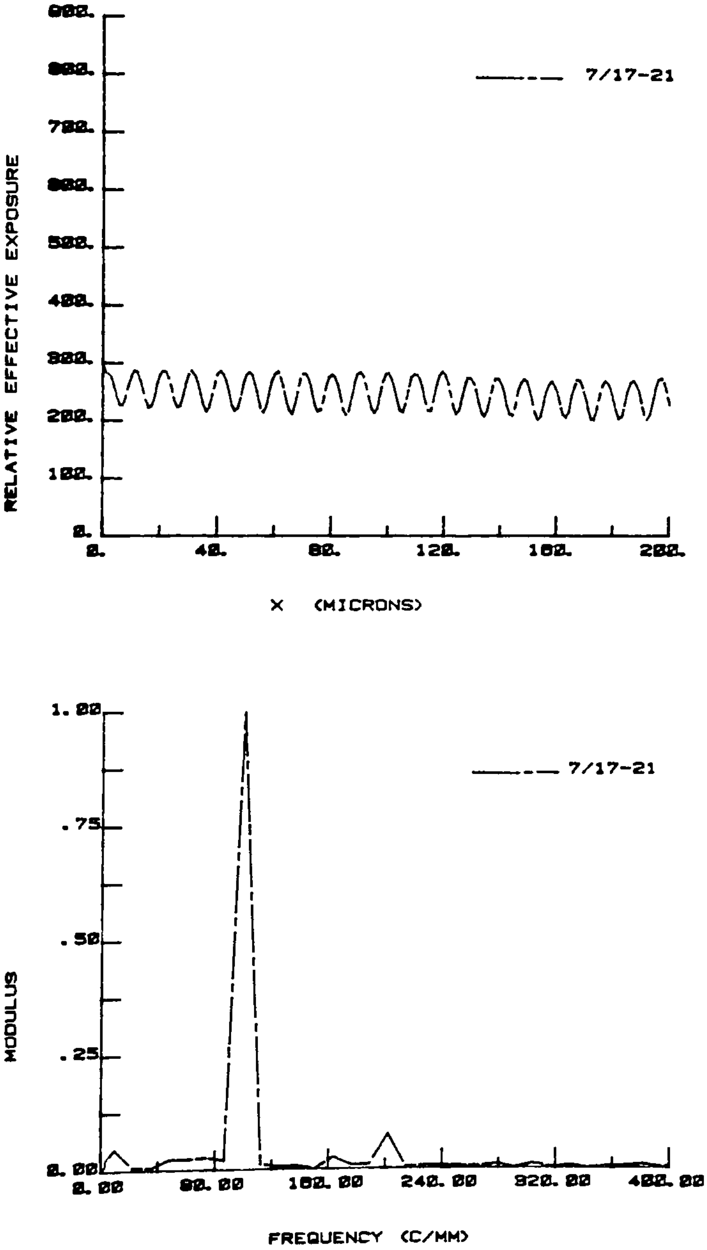

Figure E18. Sinusoidal Effective Exposure Distributions and Fourier Spectra, Fundamental: 102 Cycles/mm; Applied Voltage Time 4.3 Seconds; Development Electrode Spacing 1.27 mm.

VITA

VITA

Lloyd Griffith Clark was born in Moscow, Idaho on January 25, 1957, and he is currently a U.S. Citizen. He attended high school in Basking Ridge, New Jersey, where his parents currently reside. In September of 1975, Mr. Clark enrolled as a freshman in the Physics curriculum at the Rochester Institute of Technology. In September of 1976, he transferred from the Physics to the Photographic Science and Instrumentation curriculum. Mr. Clark alternated studies at the Rochester Institute of Technology, with work at Wright-Patterson Air Force Base starting September of 1977. From June of 1980 he has worked full-time on research and development projects for the Air Force Wright Aeronautical Laboratories near Dayton, Ohio. Research work in these laboratories initially concentrated on evaluation of electrophotographic imaging systems. Recent work has involved digital image processing for remote sensing systems, including photographic, electro-optical, infrared, and radar sensor systems.